Studies on Fringing Field Impedance Spectroscopy as a Tool for the Evaluation of Underwater Encapsulants

Thesis submitted to

COCHIN UNIVERSITY OF SCIENCE AND TECHNOLOGY
KOCHI – 682022, KERALA, INDIA

in partial fulfillment of the requirements for the award of the degree of

DOCTOR OF PHILOSOPHY

IN

FACULTY OF TECHNOLOGY

BY

THOMAS K A

NAVAL PHYSICAL & OCEANOGRAPHIC LABORATORY
KOCHI-682021

CERTIFICATE

This is to certify that the Ph.D. Thesis entitled "**Studies on fringing field impedance spectroscopy as a tool for the evaluation of underwater encapsulants**" submitted by **Shri. Thomas K. A.** in partial fulfilment of the requirements for the award of the degree of Doctor of Philosophy, to the Cochin University of Science and Technology, Kochi-22, is an authentic record of the bonafide research work carried out by him under my supervision and guidance at Naval Physical and Oceanographic Laboratory, Kochi, India. The results embodied in this thesis or parts of it have not been presented for the award of any other degree from any other institution.

I further certify that all the relevant corrections and modifications suggested by the audience during pre-synopsis seminar and recommended by the Doctoral Committee have been incorporated in the thesis.

Dr. Reji John
Supervising Guide
Scientist 'G'
Naval Physical & Oceanographic Laboratory
Defence Research & Development Organisation
Government of India, Ministry of Defence
Kochi-682021
Kerala, India

Kochi-21
20 Oct 2017

DECLARATION

I do hereby declare that the PhD thesis entitled "**Studies on fringing field impedance spectroscopy as a tool for the evaluation of underwater encapsulants**" is an authentic record of original research work carried out by me under the supervision of Dr. Reji John, Scientist G, Naval Physical and Oceanographic Laboratory, Kochi in partial fulfilment of the requirements for the award of the degree of Doctor of Philosophy and that no part of this work has been submitted previously anywhere for the award of any degree.

Kochi-21

20 Oct 2017

Thomas K. A.

ACKNOWLEDGEMENTS

CONTENTS

6. Chapter-6:Electrochemical Impedance Spectroscopy

7. Chapter-7:Estimation of Water Uptake

ABSTRACT

Underwater encapsulants are thick coatings that are widely used to protect underwater sensors and structures against water ingress. Materials used for the encapsulation of underwater sensors such as electro-acoustic transducers of SONAR (Sound Navigation And Ranging) system need to have adequate electrical insulation resistance in wet conditions. Regular monitoring of water ingress and electrical resistance of encapsulants is very important to ensure reliability of the transducer system. The present method to assess the reliability of the transducer is by measuring the electrical resistance between the output of the electrical leads. It is advantageous if it is possible to measure the water uptake and electrical degradation of the encapsulant in a non-destructive manner so that health of the transducer can be monitored.

Electrochemical impedance spectroscopy (EISY) is a widely accepted technique for determining the degradation of coatings. Water uptake and electrical degradation in the coating immersed in saline water, can be estimated by this technique. However, EISY is a laboratory technique and it is not suitable for the field evaluation of coatings for many reasons. In this context, fringing field impedance spectroscopy (FFISY) is developed as a non destructive tool for monitoring the water uptake and electrical degradation of underwater encapsulants. The water uptake and electrical degradation of different encapsulant systems were measured by FFISY and compared with EISY in this thesis work.

A fringing electric field (FEF) sensor is essential for employing FFISY technique. Analytical studies were carried out to understand the effect of sensor electrode

configuration on the sensitivity and measuring depth (penetration depth) of the sensor. Several types of FEF sensors with varying sensor area, penetration depth, electrode width and gap were fabricated for the validation of theoretical results.

Two types of FEF sensors were selected for measuring fringing field impedance spectra (FFIS) of typical encapsulants of thickness varies from 100 μm to 2 mm. Initially, FFISY measurements were done on encapsulants that were cast over the sensor. Encapsulants cast over the sensor provide an ideal condition for the FFIS measurement due to the intact contact between sensor and test encapsulant sample. Commercial underwater encapsulant material of polyurethane (PU), epoxy and polychloroprene (CR) were used as encapsulants in this study. PU encapsulants loaded with different fillers such as powders of polyaniline, carbon black and nano silica were also selected for the FFISY measurements.

The changes in the FFIS of encapsulants exposed to 3.5 wt % aqueous NaCl (which simulate the salt content of sea water), were measured at regular intervals. The capacitance and the electrical resistance of the encapsulants were estimated by fitting the FFIS in the appropriate equivalent electrical circuit. The water uptake and electrical degradation were estimated from the increase in capacitance and decrease in electrical resistance respectively. The water uptake-time and electrical degradation profiles were compared with that of EISY. Water uptake values were also compared with the values from gravimetry. Encapsulant electrical resistance obtained from FFIS was correlated with materials of known electrical resistivity.

A prototype hand held probe fitted with FEF sensor was developed to measure FFIS of encapsulants in the field. Encapsulant test samples were prepared for this

purpose. A measuring circuit was implemented and validated with standard impedance analyzer circuit to make the system portable.

The water uptake and percentage of electrical degradation of encapsulants estimated by FFISY are comparable with that of EISY. It can be concluded that FFISY can be used as a non-destructive technique for monitoring the water uptake and electrical degradation of encapsulants. **An Indian patent application No.201711004301 dated 30 March 2017, is filed for this invention**.

Also, the application of FEF sensor for monitoring the curing process of thermoset resins is included as a part of thesis work.

LIST OF ABBREVIATIONS

FFISY	Fringing Field Impedance Spectroscopy
EISY	Electrochemical Impedance spectroscopy
FFIS	Fringing Field Impedance Spectra
EIS	Electrochemical Impedance spectra
FEF sensor	Fringing Electric Field Sensor
PU	Polyurethane
CR	Polychloroprene
PD	Penetration Depth
ASIC	Application Specific Integrated Circuit
PCB	Printed circuit Board
PEN	Polyethylene Napthalate
PANi	Polyaniline

LIST OF FIGURES

Figure No   **Page No**

LIST OF TABLES

CHAPTER – 1

1.1. Introduction

Thick coatings which are used for underwater applications are called 'underwater encapsulants'. Underwater encapsulants are widely used to protect underwater sensors such as electro-acoustic transducers of SONAR (Sound Navigation And Ranging) system. SONAR system makes uses of sound waves for the classification and ranging of underwater objects in sea such as submarines in defence applications. All marine vessels and majority of fishing boats are equipped with SONAR system which helps them to find the availability of fish and depth of water bodies [1].

Materials used for the encapsulation of underwater electro-acoustic transducers need to have adequate electrical insulation characteristics in wet conditions. Retention of electrical resistance under prolonged water submergence in harsh ocean condition, is an essential requirement for underwater encapsulating materials. Encapsulants are thicker (>100 μm) than conventional coatings to ensure good water barrier properties and electrical resistance (insulation resistance) [2].

It is to be noted that no polymeric coating is a perfect barrier to water and with time water and ions diffuse through the coating [3]. Water barrier property and retention of electrical properties are interrelated. The water uptake in the coating in service brings down the electrical resistivity of the material and this will reduce the performance of the coating [4]. Regular monitoring of water uptake and electrical resistance during service is very essential as part of a maintenance procedure to improve the reliability of a system. The existing monitoring technique measures the electrical resistivity of the encapsulated transducer by measuring the electrical resistance between the output and input of the encapsulated transducer. The measured decrease in electrical resistance of the encapsulated transducer can be due to many reasons which include electrical shorting in the active transduction material, failure of encapsulant due to water ingress etc. It will be very difficult to find out the actual cause of electrical failure from many probable factors [2].

Failure of encapsulant is the main factor for transducer failure as it is the outer layer of transducer that protects the active electrical elements from water ingress in harsh sea environment. Hence it is important to have a technique to monitor electrical resistance of the encapsulants separately.

Electrochemical impedance spectroscopy (EISY) is a widely used laboratory technique for determining water uptake and electrical degradation of coating in real time. In EISY, electrochemical impedance spectrum of the coating will be measured periodically in salt water. The change in capacitance and electrical resistance (called pore resistance in EISY) of the coating will be determined by fitting the measured electrochemical impedance spectra (EIS) to a suitable equivalent circuit. The efficiency of a polymeric coating as a water barrier material can be assessed by monitoring its capacitance change due to water uptake. The retention of electrical insulation can be estimated by monitoring its pore resistance [4, 5].

However, EISY is a laboratory technique and not suitable as a non destructive method for the field evaluation of encapsulants due to its own experimental limitations; (1) it requires an electrical connection to the underneath metal substrate and (2) it requires an electrolyte in a confined volume [5].

In this context, fringing field impedance spectroscopy (FFISY) is selected for the measurement of electrical degradation and water uptake of underwater encapsulants. Even though FFISY has used in many applications such as the determination of moisture and additives content in the paper pulp industry [6-8], it has not used for the application of coating or encapsulant evaluation. FFISY can be developed as a non-destructive technique for monitoring water uptake and electrical degradation of underwater encapsulants by measuring fringing field impedance spectra (FFIS) periodically similar to EISY. Hence the main objective of the thesis work is to develop FFISY as a tool for the evaluation of encapsulants used for underwater applications.

It is quite logical to validate the values obtained from FFIS with that of widely accepted EISY as both have similar method of estimating water uptake and electrical degradation. The electrical resistance and capacitance of encapsulants measured by FFISY were compared with EISY in similar conditions (3.5 wt % NaCl) and materials.

1.2. Objectives

The objectives of the present work are to study FFISY as a tool for monitoring water uptake and electrical degradation of encapsulants used for underwater applications. In order to achieve this, following goals were set.

i) Development of FEF sensors to measure the fringing field impedance spectra of underwater encapsulants.

ii) Measure and analyze the fringing field impedance spectrum of encapsulant materials (polyurethane, polychloroprene and epoxy) of thickness varying from 100 μm to 2000 μm, immersed in 3.5 wt% NaCl aqueous solution for a period of two months at room temperature (27± 1° C).

iii) Measure and analyze the electrochemical impedance spectra of encapsulants (polyurethane, polychloroprene and epoxy) of different thickness varying from 100 μm to 2000 μm immersed in 3.5 wt% NaCl aqueous solution for a period of two months at room temperature (27± 1° C).

iv) Determine the water uptake by the encapsulants from the increase in encapsulant capacitance obtained from FFIS and compare the results with that of EIS.

v) Determine the electrical degradation profile of encapsulant from the decrease in encapsulant resistance obtained from FFIS and compare the results with that of EIS.

vi) Compare the estimated water uptake and electrical degradation of the encapsulants with that obtained from gravimetry and standard electrical resistivity measurements.

vii) Develop a prototype of portable FFISY system for encapsulants which consists of a probe carrying the FEF sensor and a measuring circuit. Validate the system by comparing the results with that of EISY.

viii) Protect the intellectual property right of the developed FFISY system by applying for patent.

1.3. Structure of thesis

Chapter -1: Introduction

Introduction, objective of the research work and structure of thesis are given in this chapter.

Chapter -2: Literature Survey

Underwater encapsulants are used for the protection of acoustic transducers and other underwater systems from water ingress. Materials used for underwater encapsulants should retain its electrical insulation during its service in sea water. Different techniques used for the measurement of water uptake and electrical resistance of coatings are listed in this chapter. Even though water uptake can be measured by many techniques, capacitance method is the easiest and most popular for the online monitoring of water ingress. EISY estimates capacitance and pore resistance in a single experiment by measuring the EIS and fitting it to an appropriate equivalent circuit.

This chapter gives details about EISY and how it utilized for monitoring the water uptake and coating degradation of the encapsulant. However, EISY is a laboratory technique and not suitable for the field evaluation of encapsulants due to its own experimental limitations. FFISY is another impedance spectroscopic technique, is discussed in detail in this chapter.

Chapter-3: Experimental: Materials and Methods

The chapter describes about the encapsulant materials used for the study; PU, CR, epoxy and PU encapsulants loaded with carbon black, nano silica and polyaniline (PANi). Impedance analyser and electrochemical workstation were used to measure the FFIS and EIS respectively. The chapter also describes about the methods of sample preparation for FFISY and EISY. All the experiments were carried out at controlled temperature (27±1 ℃) and humidity (45±1 RH). Determination of encapsulant resistance and capacitance from impedance spectra by equivalent circuit approach is described in this chapter.

Chapter-4: Development of Fringing Electric Field Sensor

Chapter describes about the development of FEF sensor. Analytical modelling technique was used to study the effect of sensor geometrical parameters such as electrode width, gap between electrodes, thickness of electrode and substrate material on the sensor output. Based on the results, FEF sensors with different electrode width and gap were fabricated. FEF sensors with penetration depth (PD) 460 μm (Type I sensors) were used to measure FFIS of thin encapsulants and FEF sensors with PD 2 mm (Type II sensors) were used to measure FFIS of thick encapsulants.

Chapter-5: Fringing Field Impedance Spectroscopy

The developed FEF sensor was used to measure the FFIS of PU, CR, epoxy encapsulants and PU encapsulant loaded with fillers, exposed to 3.5 wt % NaCl solution. A controlled study was carried out by measuring FFIS of encapsulant casted on the sensor. FFIS of thin and thick encapsulants were measured for two months.

Chapter-6: Electrochemical Impedance Spectroscopy

EIS of PU and PU filled encapsulants, CR and epoxy encapsulants were measured in 3.5 wt % NaCl aqueous solution for same material and thickness as used in FFISY. The EIS were measured at regular intervals for two months.

Chapter-7: Estimation of Water Uptake

The water uptake was estimated from the increase in encapsulant capacitance obtained from FFISY and EISY using Brasher Kingsbury model. Also, the water uptake estimated from FFIS and EIS were compared with that of gravimetry.

Chapter-8: Estimation of Electrical Degradation

The electrical degradation of the encapsulant exposed to 3.5 wt % NaCl aqueous solutions was estimated from the decrease in electrical resistance of the encapsulant obtained from FFISY and EISY. The degradation percentage at any instant of time was calculated knowing the electrical resistance of unexposed

encapsulant and the instant value. The degradation profile of PU, CR, epoxy and PU encapsulants loaded with fillers were estimated.

Chapter-9: Development of a Portable FFIS Measuring System

A probe named 'impedance probe' was developed to measure the FFIS of encapsulants. A probe housing was designed and fabricated to carry the sensor. The Type - I FEF sensor with enhanced area was used for making impedance probe. The sensor was passivated to get a flat surface and it ensures intimate contact between sensor and the encapsulant. The sensor was calibrated with and without passivation in dielectric liquids with known dielectric constants. .

An application-specific measuring circuit (ASIC) was implemented to measure FFIS. The circuit was validated with a standard impedance analyzer.

CR and PU encapsulants in sheet form were soaked in saline water for a period of two months. FFIS of encapsulant samples were measured continuously for two months by the impedance probe. Water uptake and electrical degradation of encapsulant samples were calculated from the increase in capacitance and decrease in electrical degradation obtained from FFIS and compared with that of EISY.

Chapter-10: Summary and Suggestions for Future Studies

The summary and suggestions for future work are given in this chapter. FFISY can be used as a non-destructive technique for monitoring water uptake and electrical degradation of encapsulants. A few suggestions are given for future studies at the end of this chapter.

CHAPTER – 2

LITERATURE REVIEW

2.1. Overview

SONAR (Sound Navigation And Ranging) is a technique used for detecting and ranging underwater targets in ocean environment, similar to Radio Detection and Ranging (RADAR) used for detecting aerial targets [9]. Sound waves propagate long distances in the ocean enabling long range detection of underwater targets. The basic element of the SONAR system is the electro acoustic transducer which are used for transmitting and receiving acoustic signal. Before underwater usage, these electro acoustic transducers are required to be encapsulated with an acoustically transparent material and named as underwater encapsulants. Commercial polymeric materials developed for underwater encapsulants are based on polychloroprene, castable polyurethane and epoxy considering different operating frequency and depth of operation of transducers [1].

Underwater encapsulants are thicker (>100 µm) than conventional coatings to ensure good water barrier properties and electrical resistivity [2]. Underwater encapsulants protect the electro-acoustic transducers from physical damage and water ingress, while allowing the passage of acoustical energy without significant reflection, loss or distortion etc [1]. Fig.1 is a cross section of a typical encapsulated underwater transducer used in SONAR system.

Materials used for the encapsulation of underwater electro-acoustic transducers should have adequate electrical insulation characteristics in wet conditions [9]. Retention of electrical resistance under prolonged water submergence in harsh ocean condition, is an essential requirement for underwater encapsulating materials [1]. The water uptake by the encapsulant in service, brings down the electrical resistivity of the material and this will reduce the performance of the transducer.

Water uptake and retention of electrical resistance are interrelated [11]. It is to be noticed that no polymeric coating is a perfect water barrier so that with time,

water and ions diffuse through the encapsulant [3]. Hence, in situ monitoring of water uptake and electrical resistance of the encapsulant is essential as a part of a health monitoring procedure to improve the reliability of the transducer. Different techniques were reported for the measurement of water uptake and electrical resistance of encapsulants. They are discussed in the following subsections.
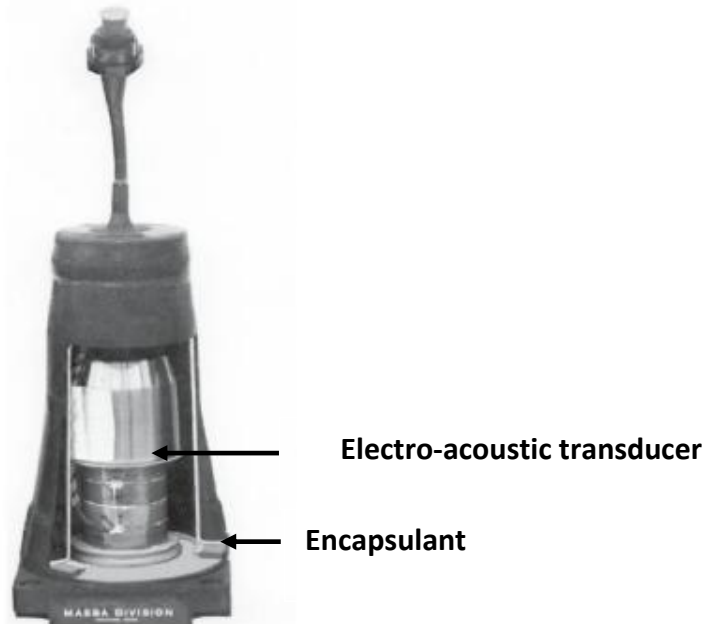
Fig.1. Photograph of cross-section of a transducer [1]

2.2. Methods of measuring water uptake by the encapsulants

The most direct way to determine the water uptake by encapsulant is by weight measurements [10-12], either as weight gain during absorption or as weight loss during drying. Other possible techniques include thermo gravimetric analysis (TGA) [13, 14], differential scanning calorimetry (DSC) [15, 16], microbalance oscillator sensor [17], Fourier transform infrared spectroscopy (FTIR) [18, 19] and capacitance measurements [20-23]. Among these, capacitance measurement technique stands out as the best by its simplicity and convenience [24]. Water ingress can be monitored by the capacitance technique in real time being an electrical measurement.

2.2.1. Water uptake estimation by capacitance measurement

Capacitance measurements are very sensitive to water ingress in the coating. Capacitance of a coating (C) is directly proportional to the relative dielectric

constant of the coating (ε) and to the area (A) of the capacitor (the surface area of the coating), and inversely proportional to the coating thickness (d):

$$C = \frac{\varepsilon \varepsilon_0 \, A}{d} \qquad (1)$$

The constant 'ε_0' represents the dielectric constant of free space, (8:854 x 10^{-14} F/cm). The dielectric constant of polymers is typically in the range 3–8, and for water it is 78.3 at 25°C and hence the water uptake by the coating lead to a rise in the mixed dielectric constant. This results in a higher capacitance for the coating.

Brasher and Kingsbury proposed a model to estimate the water content or uptake from the increase in capacitance of a coating [10]:

$$\emptyset = \frac{K \log \left(\frac{C_t}{C_0}\right)}{\log (\varepsilon_w)} \qquad (2)$$

In this equation, C_t and C_0 represent the capacitance at an instant time and the capacitance of the "dry" coating, respectively. ε_w is the dielectric constant of water and $\emptyset$ is the water content, expressed as the volume fraction in the coating. K accounts for the increase of volume due to swelling of the coating and it should not exceed 1.25. However, K is always taken as one which corresponds to a constant volume in the cases of commercial water barrier coatings.

Eq. (2) was in fact derived from a formula proposed by Hartshorn et al. [25] for a mixed dielectric constant, εr:

$$\varepsilon_r = \varepsilon_{coating}^{(V_{Coating}\ /V)} \varepsilon_{water}^{(V_{water}\ /V)} \varepsilon_{air}^{(V_{air}\ /V)} \qquad (3)$$

Where V is the total volume and $V_{coating}$, V_{water}, V_{air} are respective volumes of coating, water and air.

Brasher and Kingsbury followed certain assumptions in selecting and applying the above formula [10]:

a) The measured capacitance values are related to the coating only and are not affected by the resistance or capacitance of the solution in which the coated panels are immersed.

b) The change in capacitance of the coating is entirely due to the permeation of water into the film.

c) The permittivity of the absorbed water is constant and equal to 78.5 at 25°C.

d) The swelling of the coating can be ignored or if necessary corrections can be made as shown in the equation as K factor.

e) The distribution of water within the coating is random and uniform. Water distribution can be in columns perpendicular to the surface or in parallel to the surface. It is assumed that random distribution is the most likely one and lies between the perpendicular and parallel distribution.

f) No polar solvent is present in the coating.

Brasher and Kingsbury (B-K) observed that their equation gave comparable values of water uptake with that of gravimetry especially in thin varnish coatings. Coatings with pigments and pores showed higher water uptake than gravimetry and interpreted the discrepancy by the non uniform distribution water in the coating. Water distribution as columns perpendicular to the surface gives higher water uptake value than gravimetric technique. A work by Lindqvist [27] revealed a fairly good agreement of the B–K equation with gravimetric tests made on several types of coatings. It seems however that the degree of deviation from gravimetric value depended greatly on the composition of the coating [26].

The models from Castela-Simões [28,29], Bellucci -Nicodemo [30] and J.M. Sykes [31] were also proposed to estimate water content from capacitance. In many cases even the values from these equations were significantly above those from gravimetry. In spite of various limitations, B-K equation is the most widely used technique today to estimate the water uptake in coatings. It has been shown that this method is valid for comparing the water barrier effect of different formulations over the same experimental conditions and coating thicknesses. This equation has been used widely in the last few decades to describe the water uptake of coatings [112-113].

2.3. Methods of measuring electrical resistance of encapsulants

As mentioned earlier, the retention of electrical resistance of encapsulants is very essential in wet conditions for the long life of transducer. Hence, the electrical resistance of the encapsulated transducer will be monitored during fabrication and integration of transducer into the SONAR system. Electrical resistance is measured by measuring the DC resistance between two defined points of the encapsulated transducer at a specific voltage. There are chances that, electrical resistance degrades quickly in wet conditions due to the moulding defects in the encapsulant. These defects provide low insulation resistance which acts as a path for leakage current to ground and finally leads to the failure of transducer. The current technique measures the electrical resistance of the encapsulated system as a whole and hence will not provide any information about local defects [2].

EISY is used widely for the estimation of electrical degradation of coating and could be assessed by the drop in coating resistance during immersion in sodium chloride solution [32]. Conventional electrical resistivity meter or four probe conductivity meter were also used for the measurement of electrical resistance of coating [33, 34]. However, they are not suitable for the in situ measurement of electrical resistance changes.

It is to be noticed that the measurement of capacitance and electrical resistance of the coating requires different techniques. But, it is possible to measure both resistance and capacitance of a coating in a single experiment by impedance spectroscopy.

2.4. Impedance spectroscopy

Impedance spectroscopy is a powerful technique for the characterization of electro-chemical systems [35-39]. The fundamental approach of the impedance spectroscopy is to apply a small amplitude sinusoidal current (or voltage) excitation to the system under the steady-state and measure the voltage (or current) response. The frequency of the input voltage is varied and corresponding amplitude of the current is measured in each case. The ratio of applied voltage to measured current is the impedance of the system (Z=E/I) and the impedances over a wide frequency range give a spectrum. The impedance spectrum and the phase angle between the

voltage and current provide information about the processes with different kinetics that may occur in the system under study [42, 43].

The measured impedance spectra is fitted to the impedance spectra of an equivalent electrical circuit that represent the system. The values of the electrical components in the equivalent circuit give values of different parameters of the system.

Impedance data is typically presented either in the Bode plot or Nyquist plot. The Bode Plot consists of two graphs: one with the phase of the impedance (φ) on the Y-axis and the logarithmic frequency on the X-axis, the other one is plot of the log of the magnitude of the impedance on the Y-axis and the logarithmic frequency on the X-axis as described in Fig.2. This format is preferred by many investigators because the impedance of the system can be obtained for each frequency values and phase angle data is often very sensitive to changes in the surface.
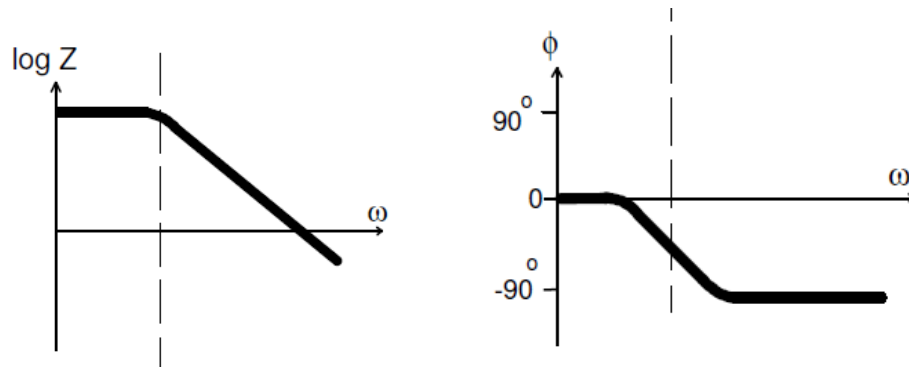
Fig.2. A Bode plot representation of impedance spectrum [3].
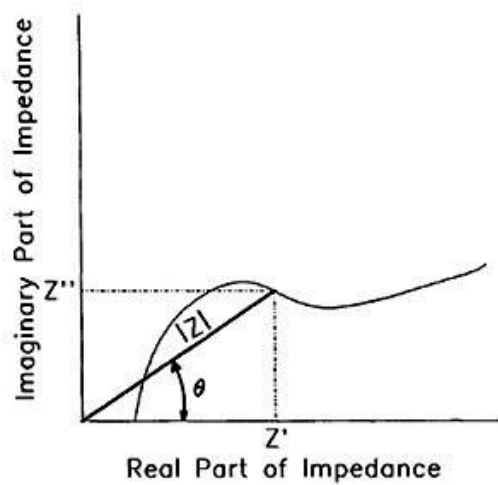
Fig. 3. A Nyquist plot representation of impedance spectrum [24].

The Nyquist plot, is a graphical representation where the X-axis represents the real part (Z') and the Y-axis represents the imaginary part (Z'') of the impedance (Fig.3). In Fig.3, the IZI is the modulus of impedance and θ is the phase angle between voltage and current.

2.4.1. Electrochemical impedance spectroscopy

The application of impedance spectroscopy to electrochemical studies is evolved as electrochemical impedance spectroscopy (EISY). When working with electrochemical systems, this perturbation is normally an AC voltage of small amplitude (typically 5–20 mV peak-to-peak) for frequency ranging typically from 10 mHz to 100 kHz [43]. Experimental impedance data of an electrochemical cell can be easily fitted to an equivalent circuit model mainly comprising resistors and capacitors. EISY is widely used for the study of coatings. Coating resistance, coating capacitance, onset of corrosion of underneath metal etc. can be determined from the measured electrochemical impedance spectrum.

Fig. 4 shows the Bode plot of an insulated polymer-coated metal in contact with an electrolyte solution. Upon initial exposure to an electrolyte, a high performance coating with excellent barrier properties will act as an almost-perfect capacitor. The Bode plot shows a straight line of slope –1 with high impedance at low frequency and a phase angle of –90° throughout the entire frequency range, characteristic of a pure capacitor. The capacitance value is dependent on the thickness of the coating and its dielectric constant. It can be modeled by a resistance, the electrolyte resistance (R), in series with a capacitance, coating capacitance (C) (Fig.5).
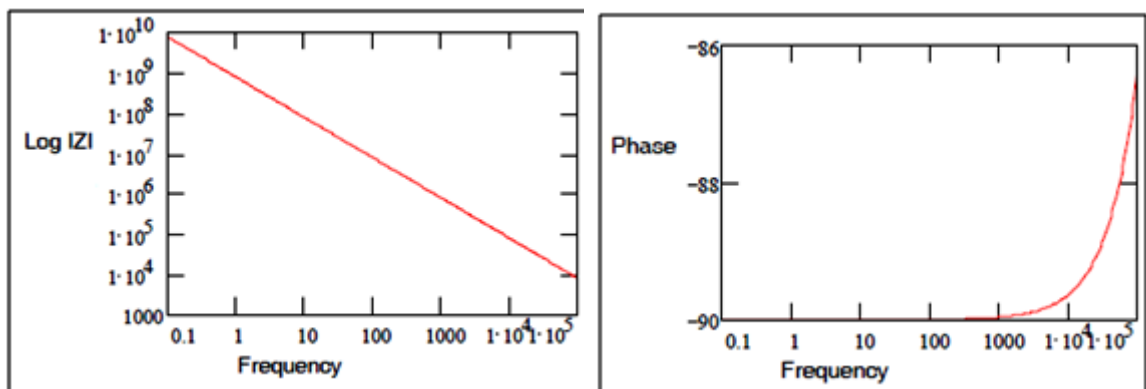
Fig.4. Bode plot of an insulating polymeric coating [117]
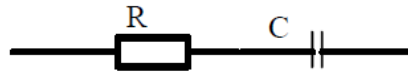
Fig.5 .Equivalent circuit of an insulating polymeric coating [117]

The capacitance is related to the magnitude of the impedance (|Z|) by

$$|Z| = \frac{1}{(2\pi f C_{Coating})} \qquad (4)$$

'f' is the frequency of the applied AC voltage [53].

At some undefined later time, the electrolytes ingress in to the coating and a measurable 'pore resistance' now comes into play. The pore resistance is the resistance offered by the conductive path created by the electrolyte filled micro channels in the coating. Even at this stage, the coating is intact and performs as a good water barrier coating. Fig.6 represents the Bode plot of this stage.
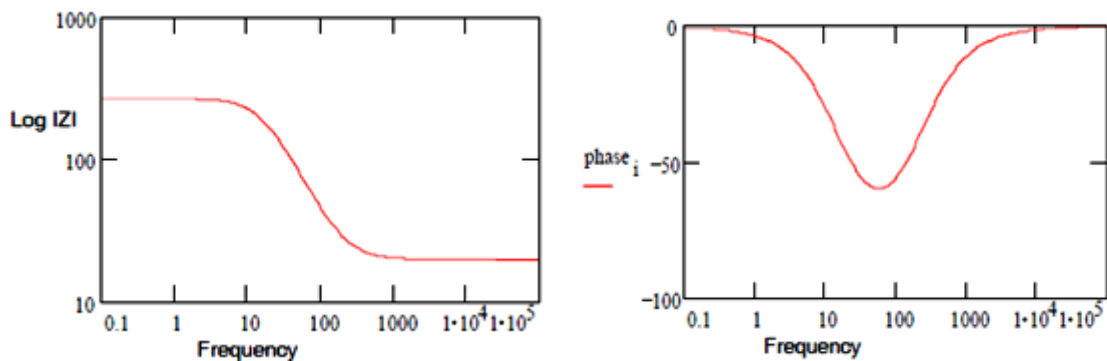
Fig.6. Bode plot of a polymeric coating with absorbed water [117]

The horizontal section of the line at lower frequencies in Bode magnitude plot (Fig.6) is the indication of water ingress in the coating, characteristic of this phenomenon. The magnitude of the impedance at this lower frequency region generally decreases with time until the film is saturated with electrolyte. The equivalent circuit of coating which represents this stage is shown in Fig. 7.

Coating capacitance (C_C) and Pore resistance (R_P) or coating resistance are in parallel. In practice, a pore resistance (R_P) in parallel with Cc normally appears and accounts for initial conductive pathways across the polymer ascribed to small defects in the coating [45,49]. The horizontal section of the line at lower frequencies in Bode magnitude plot (Fig.6) is the indication of a resistive path
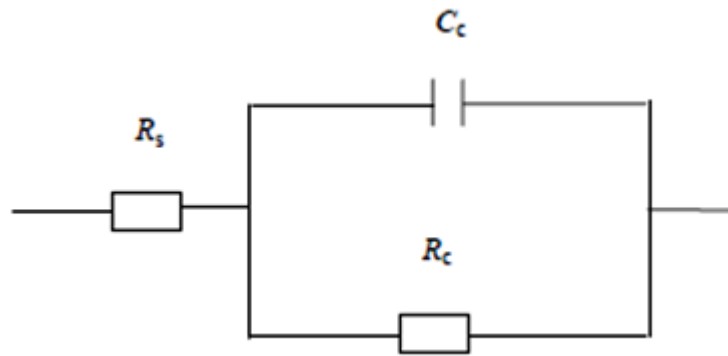
Fig 7: Equivalent circuit of coating after water uptake [117]

formation in the coating. At this region phase angle tends to 0° phase angle which is characteristic of a pure resistor. The magnitude of the impedance at this lower frequency region generally decreases with time until the coating is saturated with electrolyte [117].

2.4.1.1. Monitoring degradation of organic coating by EISY

As discussed in the previous section, EISY has extensively used for the evaluation of organic coatings such as paints and varnishes [45-49, 116-118]. EISY can quantitatively determine both resistances and capacitances changes in the coating in a single experiment.

Degradation of organic coating can be monitored by measuring the EIS at regular intervals of time. Fig. 8 show the Bode plot of an epoxy coating with different time of exposition to 3 % NaCl solution [135]. Upon initial exposure to an electrolyte, a coating with excellent barrier properties will act as an almost-perfect capacitor. The Bode plot shows a straight line of slope –1 with high impedance at low frequency and a phase angle of 90° throughout the entire frequency range, characteristic of a pure capacitor. The capacitance value is dependent on the thickness of the coating and its dielectric constant. The impedance spectra of thick coatings (encapsulants) have this type of patterns [119]. As the water ingress into the coating, the electrical resistance decreases and capacitance increases. The data from the initial period of immersion give quantitative information about the water barrier properties and electrical properties of encapsulants [109].
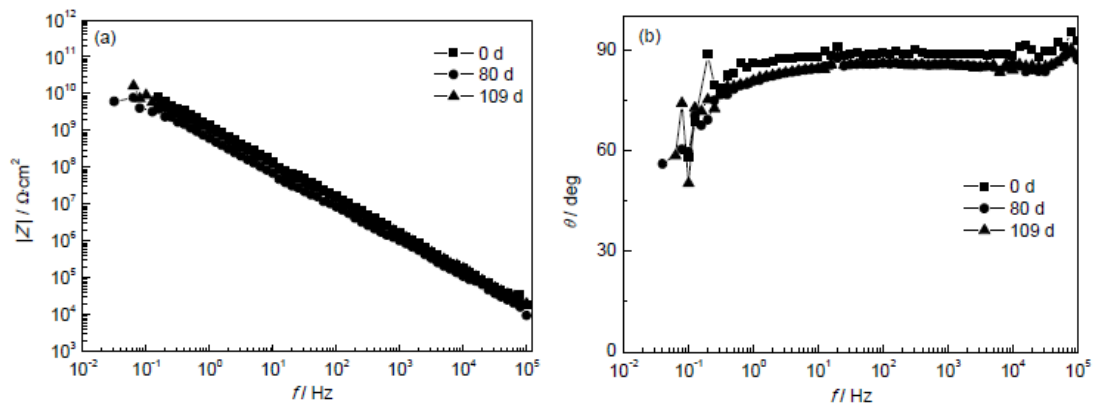
Fig 8: Bode plot of a polymeric coating with different time of exposition to 3 % NaCl solution [135]

2.4.1.2. Water uptake-time profile in polymer coatings

The water uptake-time profile of polymeric coatings can be determined by monitoring the changes in its capacitance. Water transport in polymers is generally categorized into Fickian and Non-Fickian. Fickian diffusion in polymers is an ideal case of water transport, corresponding to free diffusion of penetrant without interference of polymer chain rearrangement - i.e., structural relaxation [53-56]. Fig.9 is a typical plot for the so called Fickian absorption kinetics measured by capacitance.
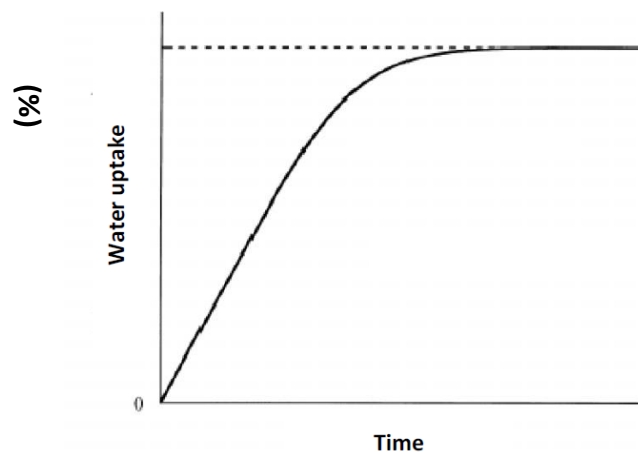
Fig.9. Typical Fickian water uptake curve of coating [56]

2.4.1.3. Measurement set up of EISY

The conventional method of EISY measurement is a three electrode technique in which a test electrolyte reservoir attached either temporarily or permanently onto a horizontally positioned coated flat plate substrate (Fig.10). The electrolyte is filled in the glass tube. Various types of platinum metal meshes

positioned parallel to the coating surface have been employed as counter electrodes. The coated metal or bare metal acts as the working electrode. Any of several conventional reference electrodes could be added into the electrolyte.
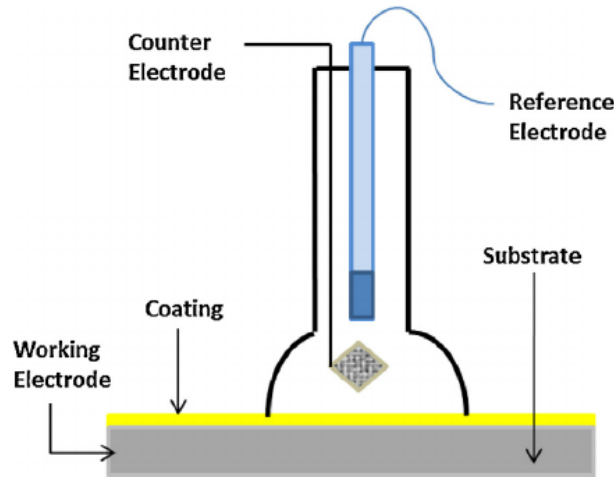
Fig.10: Experimental set up for EISY [135]

2.4.1.4. Limitation of EISY as a field evaluation technique

EISY is a reliable laboratory technique for the in situ monitoring of capacitance and resistance changes in the coating during water ingress. Nevertheless, it is not convenient as a field measurement technique due to several limitations which include a required electrical connection to the metal substrate which results in local coating destruction. Another limitation is the required lengthy electrical connection to the substrate from the power source which could create noisy data and inaccurate readings. Another problem with traditional EISY is that due to the electrolyte solution in the container, only horizontal surfaces can be tested. The attempts to modify traditional EISY experimental set up for field measurements are not very successful [59-64].

2.4.2. Fringing field impedance spectroscopy

Fringing field impedance spectroscopy (FFISY) is a technique in which a fringing electric field sensor (FEF sensor) is employed to measure the fringing field impedance spectrum (FFIS) of test material. FFISY is used in many applications such as the determination of moisture in the paper pulp and agriculture commodities [6-8].

2.4.2.1. Fringing electric field sensor

FEF sensor have interdigitated lectrodes as shown in Fig.11. On applying potential across the electrode, electric field originates from one electrode, penetrates the material under test (MUT) and reaches the second electrode. The resultant current is related to the electrical and dielectric properties of the MUT, such as electrical resistance and capacitance.
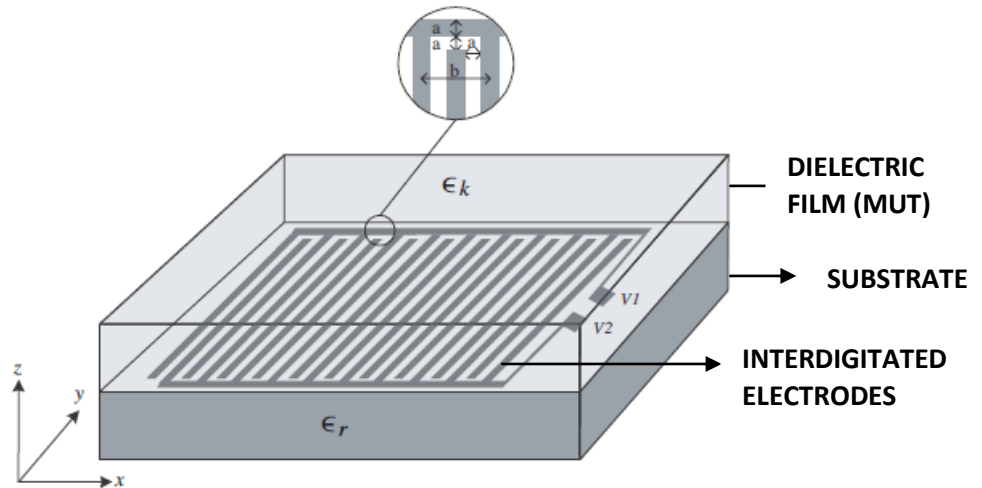
Fig.11.Interdigitated electrodes in FEF sensor [69]

FEF sensors are widely used for non-destructive measurements of electric and dielectric properties of materials [40, 50, 65-68]. In many of these applications, FEF sensors are used as a fringing field capacitor. Abu-Abed et al. [69] calculated the unit cell capacitance of an interdigitated electrode with an infinite thick liquid crystal film as the dielectric material. As shown in Fig.11, the interdigitated pattern consists of two latticed electrodes in the xy plane, each electrode consists of N fingers. Each finger has a width '**a**' and the space between any two adjacent fingers is also set to '**a**'. The spatial distance of the periodic interdigitated cell is called a unit cell which could be defined as the distance between the centre lines of the adjacent fingers belonging to the same electrode.

By applying different potentials on the interdigitated electrodes, V1 and V2, the generated electric field travels from one electrode, penetrating the MUT, as well as the substrate underneath the electrodes, to the other electrode. The capacitance measured between the electrodes depends on the dielectric constants of the substrate and the dielectric film (MUT). Fringing capacitance between the

interdigitated electrodes depends on electrode's width, **a**, where transverse capacitance depends on the electrode's thickness, **t** and the distance between the adjacent electrodes. The unit cell capacitance (C_{uc}) of an interdigitated electrode with an infinite thick liquid crystal film as the dielectric material,

$$C_{uc} = \varepsilon_0(\varepsilon_r + \varepsilon_k)\frac{K\left(\sqrt{1-\left(\frac{a}{b}\right)^2}\right)}{K\left(\frac{a}{b}\right)} + 2\varepsilon_0\varepsilon_k\frac{t}{a} \quad (5)$$

where ε_0 is the dielectric constant in the free space, ε_0 = 8.8542 × 10^{-12} F/m. ε_r and ε_k are the dielectric constants of the substrate and the dielectric film, respectively. $K(\cdot)$ is the complete elliptic integral of the first kind. By making full use of symmetry and neglecting the capacitances of the edges, the total capacitance of the interdigitated capacitor is calculated by

$$C_{TOTAL} = C_{uc}(N-1)L \qquad (6)$$

where **N** is the number of unit cells in the capacitor and **L** is the length of the electrode fingers.

Changes in the dielectric and electric properties of materials will affect the distribution of these field and accordingly sensor output changes apart from the geometrical configuration of the sensor electrodes.

2.4.2.2. Equivalent circuit of a fringing electric field sensor

Fig.12 is the representation of a unit cell of a FEF sensor used for the measurement of biological fluid properties. The lower half plane contains the capacitance through the oxide C_{ox} and the capacitance C going to the conductive Si substrate. C_{ox} and C are the parasitic capacitance which can be subtracted from the total capacitance.
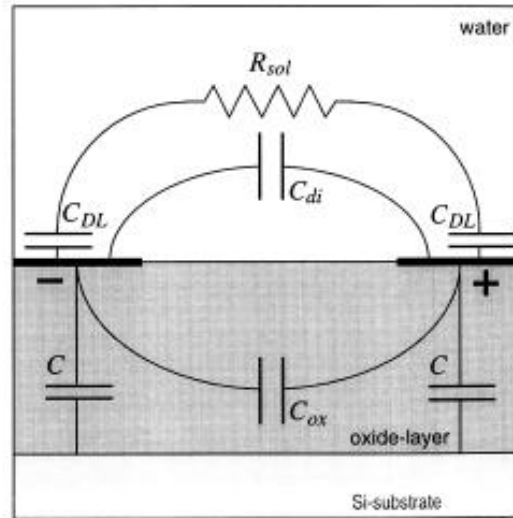
Fig. 12: An equivalent circuit of fringing field impedance sensor in aqueous medium [51].

The upper half plane contains two paths: the dielectric capacitance C_{di} of the water, and the path containing the resistance of the solution R_{sol} in series with the double layer capacitances C_{dl} at the electrodes [51].

2.4.2.3. Penetration depth of a fringing electric field sensor

Penetration depth (PD) of an FEF sensor is the depth up to which the electric field from the sensor can penetrate into the encapsulant. In other words, PD is a measure of how quickly the electric field intensity decreases as the distance from the sensor increases [114]. PD vary depends on the width of the electrode (w) and gap between electrodes (s). PD of a sensor is approximately equal to the sum of 's' and 'w' [115].

2.4.2.4. Cell constant of a fringing electric field sensor

Cell constant is a unique number of an FEF sensor or interdigitated electrode and it depends entirely on the geometry of the sensor [70]. The resistance (R_{coat}) of the encapsulant is related to its   resistivity (ρ_{coat}) by the cell constant K_{Cell} as described by:

$$R_{coat} = K_{cell} \ \rho_{coat} \qquad (7)$$

K_{cell} can be theoretically calculated by the following equation [70],

$$K_{cell} = \frac{1}{L(N-1)} \frac{2K(k)}{K[(1-k^2)^{1/2}]} \qquad (8)$$

Where K is the incomplete elliptic integral

$$K(k) = \int_0^1 \frac{dt}{\left[\left(1-t^2\right)\left(1-k^2t^2\right)\right]^{3/2}} \qquad (9)$$

and where the modulus,

$$k = \cos\left(\frac{\pi}{2} \frac{w}{w+s}\right) \qquad (10)$$

In the preceding equations, N is the number of fingers (electrodes), S the finger spacing, W the finger width and L the finger length. The function K(k) is the incomplete elliptic integral of the first kind.

2.5. Underwater encapsulant materials

Materials for the encapsulation of electro-acoustic transducers of SONAR systems should have a number of desirable properties: (1) density and sound speed match with seawater (that determines characteristic acoustic impedance); (2) Poisson's ratio near 0.50; (3) low shear storage modulus and high shear loss tangent; (4) moderately low water absorption and water permeability. Over the years, different types of polyurethane (PU), rubbers and epoxies were developed for the application of underwater encapsulation [77].

PU and epoxy resins are easy to use as they can be cast at room temperature. Over the past 20 years, a number of commercial   polyurethanes from different manufacturers have been used as encapsulants by Naval laboratories and Naval contractors [78, 79].   Polyurethane is a polymer composed of a chain of organic units joined by carbamate (urethane) links. Polyurethane polymers are traditionally and most commonly formed by reacting a di- or polyisocyanate with

a polyol. Both the isocyanate and polyol were used to make polyurethanes which contain on an average two or more functional group per molecule [79].

Rubber especially polychloroprene rubber (CR) is extensively used for the encapsulation of underwater electro acoustic transducers. Better balance of properties like, seawater resistance, weathering resistance, bonding with metal, amenability to build in desired static and dynamic mechanical properties favour CR over other rubbers for this application [80].

Rapid advances in epoxy technology have led to the development of a range of specially formulated systems for use in high humidity and underwater applications. Unique moisture insensitive hardeners and curing agents have overcome the inability of conventional epoxies to cure in such environments. These compounds offer easy application, long shelf life, excellent adhesion and durability. These systems have been successfully employed for repair, maintenance and underwater assembly being cost efficient and environmental friendly [57].

2.6. Scope of the work

The scope of the study is to develop a non destructive field evaluation system for underwater encapsulants based on FFISY. The water uptake and electrical degradation can be measured in the field without disturbing the encapsulated system.

Fig.13. Schematic of the fringing electric field impedance probe with measuring circuit with a typical encapsulated transducer.

Ideally, the field evaluation system comprises of a hand held probe carrying the FEF sensor and a portable measuring circuit (Fig.13). The FFISY has unique advantages in the evaluation of encapsulants such as (1) it is a non-destructive technique and (2) it does not require any electrolyte for impedance measurement and hence convenient for field measurement.

CHAPTER – 3

Experimental: Materials and Methods

3.1. Introduction

This chapter gives details on the encapsulation materials, preparation of test specimens and the measurement instruments employed for this work.

3.2. Encapsulation materials

In the work, three typical underwater encapsulant materials were used; a ether polyol based polyurethane (PU), a special grade polychloroprene (CR) and epoxy. Three different fillers (powdered PANi, powdered carbon black and nano silica) were selected for incorporating into the PU matrix to measure the FFIS of filler loaded PU in 3.5 wt % NaCl aqueous solution. Epoxy encapsulant which was undergone thermal oxidation for two months was also used for the study. Since the intention was the comparison between water uptake and electrical degradation percentage estimated by FFISY and EISY for the same encapsulant material and thickness, attempt was not made to synthesis new materials other than using commercial materials.

3.2.1. Polyurethane

A polyurethane-three part system consists of isocyanate, ether polyol and chain extender from M/s Ezecast, Pune, India was selected as one of the encapsulant materials. The chemical name of the components were given below with percentage composition.

Ezecast 201 (polypropylene glycol isocyanate+ Toluene diisocyanate):   1

Ezecast 202 (polyether polyol + amine):   1

Ezecast 101: (polypropylene glycol +amine) :   0.3

The above composition of Ezecast PU has viscosity 3000 cP and has 12 min pot life. The resin has an isocyanate content 6.8% and cures completely in 48 hours at room temperature ($27 \pm 1°$ C). The curing was ensured by analysing the –NCO peak (2260 cm^{-1}) of the sample using infra red spectra.

3.2.2. Polychloroprene

Neoprene W grade of polychloroprene, obtained from Dupont was used in this study. The rubber compound preparation involves mixing CR with compounding ingredients as per the recipe given in Table 1.

Table: 1 Compounding ingredients of polychloroprene

Ingredients	Quantity (phr)
Neoprene –W	100
Stearic acid	1
Antidegradant (Vulcanox HS)	1
Carbon Black (FEF N550)	25
Talc	50
Precipitated calcium carbonate	20
Processing oil	10
Red lead	13
Dibenzothiazyl disulphide	1.5
Ethylene thiourea	1

The compound preparation method conforms to ASTM D-3182 in which following general method has been adopted. Ingredients were weighed out on the basis of parts (by weight) per 100g rubber (phr). The compounding recipe for the sample preparation is given in table 1.

A laboratory model mixing mill has been used for mixing rubber with compounding ingredients (Fig.14). Cure characteristics of the compound have been measured as per ASTM-D-2084 using Monsanto Rheometer R-l00 before moulding. Optimum cure time for compound was 90 min at 150^0C.

Fig.14 .Two roll mill for rubber mixing

3.2.3. Epoxy

Araldite AY 103 resin and Aradur HY 951 hardener obtained from Huntsman was used for the study in the ratio of 1:1.3. Araldite AY 103 is a Bisphenol-A diglycidyl ether polymer and Aradur HY 951 is a low viscosity aliphatic amine [1,2-Ethanediamine, N,N'-bis(2-aminoethyl)-Triethylenetetramine]. The mixture has a viscosity 2500 cP at 27° C and cures in 48 hours at room temperature (27 ± 1° C). Curing characteristic of the epoxy resin was studied from its curing exotherm measured by differential scanning calorimetry.

Epoxy encapsulant was subjected to thermal oxidation by exposing the sample at 70° C in an air oven for two months, before immersing the sample in NaCl aqueous solution. Studies have been reported on the thermal oxidation of epoxy polymer [133,134] and it is reported that thermal oxidation of Bisphenol-A diglycidyl ether based epoxy leads to carbonyl and amide formation with subsequent chain scission [133]. Glass transition temperatures (Tg) of the polymer decreases and sol fraction increases due to thermal oxidation [134]. After thermal oxidation, the polymer is expected to absorb more water due to the formation of degradation products of hydrophilic nature. The intention of pre-ageing was to obtain a high level of degradation in a short time when immersed in salt water. A sample having large percentage of degradation is good for comparing two techniques to conclude the results in a short time. These encapsulants which were undergone thermal oxidation are named as 'aged encapsulant' in this work to differentiate them from non aged (fresh) epoxy encapsulants.

3.3. Fillers for encapsulants

Three types of fillers in PU were selected ; powdered polyaniline (PANi), nano silica and powdered carbon black. PANi was used as antifouling fillers in underwater encapsulants [109] and nano silica for improving the water barrier properties of the encapsulant [110]. Carbon black is the most popular filler used in rubber to enhance the mechanical properties [102].

3.3.1. Polyaniline (PANi)

Emeraldine salt is the most stable form of PANi and it was synthesized by conventional oxidative chemical polymerization method. In a typical synthesis,
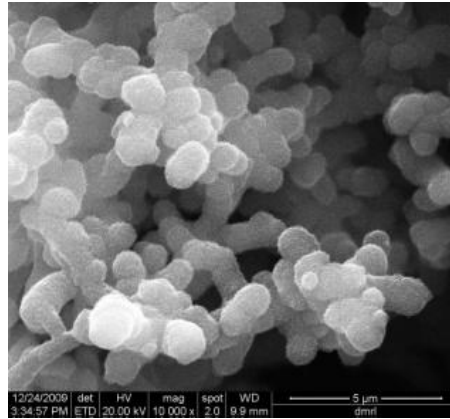
Fig.15. SEM of synthesised PANi (10000 x magnification)

0.1 mol aniline was dissolved in 600 mL 1M HCl pre-cooled to 5° C. A solution of 0.025 mol ammonium persulphate was added drop wise to aniline solution with vigorous stirring. The resulting mixture was stirred for 6 hrs, filtered and dried under dynamic vacuum. The synthesized PANi has an average particle size 10 μm (Fig.15).

3.3.2. Nano silica

Nano silica from Sigma Aldrich (CAS No. 7631-86-9) was used as the filler and has an average particle size 12 nm. The specific surface area of nano silica is 175-225 m^2/g (BET) with 99.8% purity.

3.3.3. Carbon black

Fast Extrusion Furnace (FEF) carbon black from Phillips Carbon Black Ltd, Kochi, was used for the study. The ASTM designation for FEF carbon black is N-550. The physical properties of FEF carbon black used in this study are listed below;

Particle Dia (nm)   : 47

Iodine No.   : 42

Structure (cm^3DBP/100g) : 120

3.3.4. Mixing of fillers in resin

The incorporation of fillers in encapsulant resin was carried out by mixing the fillers in the resin by ultrasonication technique. Fillers were weighed accurately (± 0.01mg) and were mixed with the polyol in a beaker and the mixture was sonicated for 1 hour in the ultrasonic homogenizer (Model No. PS 500 from Orchid

Scientifics & Innovatives India Pvt Ltd) (Fig.16). The resin with fillers was then mixed with isocyanate part in the ultrasonic homogenizer for 5 minutes and immediately coated over the metal substrate by spin coating.

Fig.16. ultrasonic homogenizer

3.4. 1000 DUV Mask Aligner for sensor fabrication

The single side mask aligner system with UV exposure unit, is a table top configuration and has 1000 Watts intensity controlling power supply (make :Mark, USA). It can accommodate up to 6" wafer for lithography. The unit has adjustable vacuum contact and proximity printing capability with a resolution of ± 1 μm. The unit also has split field TV alignment systems, single field zoom and high magnification microscopes. The unit is used for all the lithographic processes for patterning the micron sized features on the flexible as well as silicon substrates (Fig. 17). The unit is used for fabricating FEF sensors on copper clad printer circuit board (PCB).
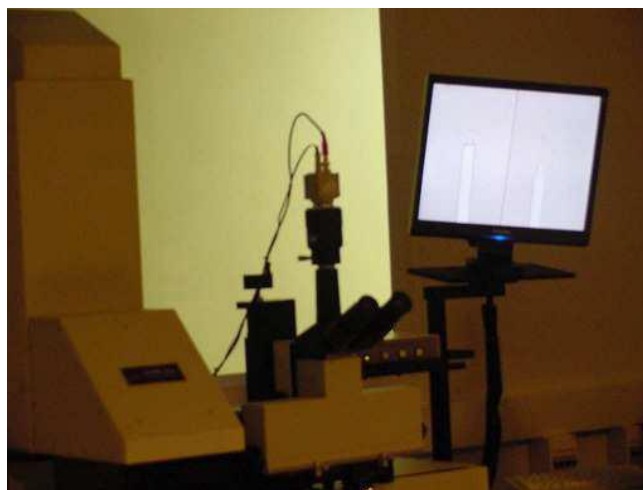
Fig. 17. Mask aligner employed for sensor fabrication

3.5. Preparation of test samples

3.5.1. Preparation of test samples for FFISY

Fringing field impedance spectra of PU and epoxy encapsulants were recorded using two different types of test samples. First type was the cast encapsulant over FEF sensors and the second type was the encapsulant in sheet form. The purpose of two types of test sample is discussed in 'measurement section'. Five samples were prepared for each study.

3.5.1.1. Preparation of encapsulant cast FEF sensor

The sensor patterned PCBs were encapsulated by PU and epoxy resin. Each PCB has five different sensors and a copper pad of area 10x10 mm^2 at the centre. The copper pad was used to measure the coating thickness by thickness gauge. Electrical leads having 8 cm length were taken from each sensor contact pads. The surface of the PCB were cleaned with acetone and placed over a programmable spin coater (Fig.18). Air bubbles were removed from the resin by applying vacuum in a vacuum desiccator (Fig. 19) for 10 minutes before pouring over the PCB.

Fig 18: Programmable spin coater, Fig.19. Vacuum pump with desiccator

The thickness of the coating was controlled by varying the spin speed of the coating. The thickness of PU encapsulant test samples and the corresponding spin coater parameters are given in the Table.2. The thickness could be controlled within ± 10 μm. Epoxy encapsulants having thickness 410, 305 252 and 180 μm were also cast by spin coater with a thickness tolerance ± 10 μm. The 1 ± 0.1 mm epoxy cast FEF sensor were prepared by spin coater at a spin speed of 500 rpm. The other spin coating parameters were kept same.

Table 2: Spin coating parameters for encapsulant

S. No	Coating thickness (μm)	Spin acceleration time (sec)	Spin speed (rpm)	Spin time (Sec)	Deceleration time (Sec)
1	153	60	2300	45	30
2	182	60	2000	45	30
3	240	60	1500	45	30
4	286	60	1300	45	30
5	406	60	900	45	30

3.5.1.2. Preparation of encapsulant sheet samples

PU and epoxy encapsulant test samples were made in the sheet form for measuring FFIS by the fringing electric field impedance probe. Encapsulant test samples of PU and epoxy materials were prepared by casting in an open mould. PU and epoxy resins after removing air bubbles were poured in an open mould of size 100 x 100 x 3 mm. The resin was allowed to cure for 48 hours at room temperature (27 ± 1º C). The thickness of the coating was 2 ± 0. 2 mm.

The prepared rubber compound as per ASTM D-3182 was compression moulded at 105 kg/cm^2 pressure at 150°C for 20 minutes . The measured thickness of the rubber sample was 2 ± 0. 2 mm.

3.5.2. Preparation of test samples for EISY

3.5.2.1. Substrate preparation

A copper plate was used as the coating substrate for EISY study which acts as the working electrode in the experiment. Copper substrate was selected in EIS study to have the same type of encapsulant-sensor interface as in FFISY technique. Copper sheet (2 mm thickness) was cut into dimension of 7 x 7 cm and was cleaned by acetone.

3.5.2.2. Application of encapsulant

An encapsulant was made over the copper sheet and sensor PCB by two different methods; casting and compression moulding. Polyurethane and epoxy

encapsulant were made by casting the resin over the metal substrate. Rubber encapsulant was made by a conventional compression moulding technique. No adhesives or primers were used in the preparation of samples to avoid an extra layer of coating of a different polymer.

The freshly cleaned substrate is placed on the chunk of the spin coater. PU and epoxy resins were poured over the copper plate and sensor PCB and the required thickness of the encapsulant was achieved by controlling the spinning speed. PU encapsulant test samples were prepared of different thickness (153 μm, 182 μm, 240 μm, 286 μm and 406 μm) by spin coating with a thickness tolerance ± 10 μm. Similarly epoxy encapsulant test samples were also prepared.

CR samples were prepared by compression moulding the rubber compound over the freshly cleaned copper sheet at 105 kg/cm² pressure and 150°C temperature.

3.5.3. Encapsulant thickness measurement

The thickness of the encapsulant over the sensors was measured using the coating thickness gauge with an accuracy ± 5 μm (Surfix Easy E-FN gauge). The spin coater gives a uniform coating all over the PCB and hence coating thickness over the miniature sensors were assumed as the same as that over the copper pad. The thickness of the coating over the metal for EISY study samples were also measured by coating thickness gauge.

3.6. Recording of fringing field impedance spectra

Fringing field impedance spectra of encapsulant material were recorded by FEF sensor using an electrical impedance analyzer (Waynker Model: 3204) (Fig.20).
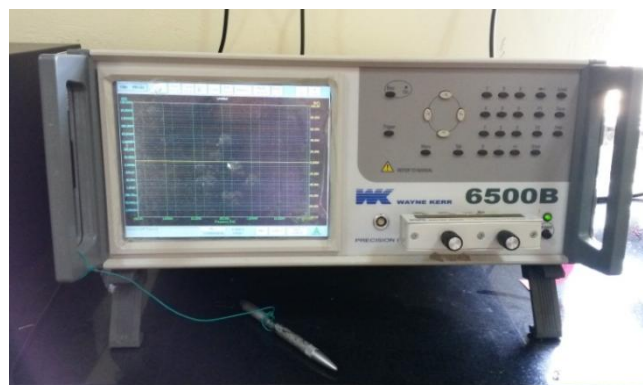
Fig.20. Electrical impedance analyzer

The sensor was connected to the two terminals of the impedance analyzer and a small sinusoidal voltage (20 mV) was applied to the sensor. The impedance and phase were measured at each frequency from 100 Hz to 1 MHz to find out the optimum frequency for the sensor measurements. The experiment was carried out at room temperature (27 ± 1° C) and at controlled humidity (45 ± 1%). The accuracy of impedance measurement was ± 0.05%.

The coated sensors were kept in a petri dish and the sides were sealed before immersing in 3.5 wt% NaCl aqueous solution. This was to ensure that water ingress occurs only through the coating surface and not through the sides (Fig.21). 3.5 wt % NaCl aqueous solution was chosen deliberately due to two reasons; (1) salt water content in sea water is approximately 3.5 wt % NaCl which is the working environment of encapsulated transducers, (2) the results from FFISY could be compared with that of EISY as the same medium is used as the electrolyte in EISY. The electrical leads were taken from each sensor for measurement. FFIS were measured from frequency 100 Hz to 100 kHz by the impedance analyzer periodically for two months. A high precision capacitance measuring circuit with measurement accuracy ± 100 fF was also used for measuring the capacitance changes.
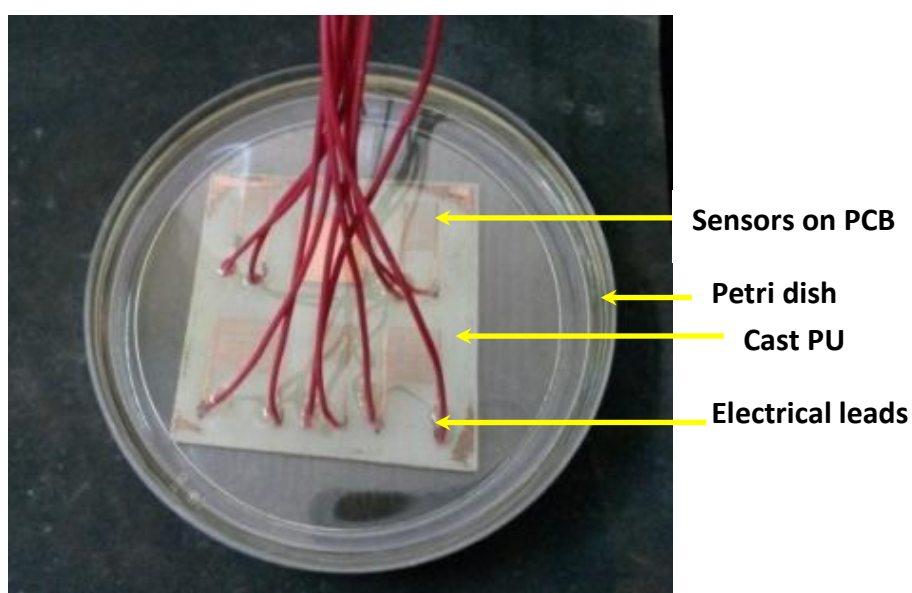
Fig.21. Experimental set up for FFISY: PU coated sensors in 3.5 wt % NaCl aqueous solution.

3.7. Recording of electrochemical impedance spectra

The electrochemical impedance measurements were performed using an Autolab Frequency Response Analyser over a frequency range of 10 mHz to 100 kHz with five points per decade (Fig.22). A sinusoidal voltage 20 mV was applied to generate the electrochemical impedance spectrum (Fig.22). The experimental set up for electrochemical investigation consisted of a hollow glass cylinder (dia. 5cm) glued to the surface of the coated panel in order to create a vessel to hold the 3.5 wt% NaCl aqueous solution (Fig. 23). The exposed coating area was 19.6 cm². The coated panel was the working electrode (WE) of electrolytic cell and a saturated Ag/AgCl electrode was used as the reference electrode (RE). A platinum cylindrical mesh was used as counter electrode (CE) as shown in Fig. 23.

Fig. 22. EIS measurement setup Autolab PGSTAT30   Fig. 23: Electrochemical cell
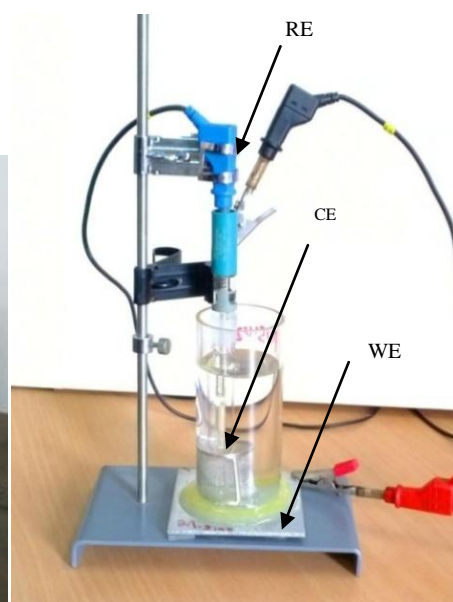
3.8. Estimation of capacitance and electrical resistance from FFIS

Capacitance of the encapsulants were determined from FFIS by fitting the curve to an electrical equivalent circuit. This was done using a software 'ZSimpWin' from Princeton Applied Research [130]. The selection of the equivalent circuit for fitting fringing field impedance spectra was based on the work done by Laureyna et al. on impedimetric biosensing using interdigitated electrode [71]. The equivalent circuit for fitting FFIS of encapsulant is shown in Fig.24. R_{coat} is the resistance and C_{coat} is the capacitance of the coating. Residual χ^2 value of fitting the curve was <

0.001 for all the fitting curves indicating that equivalent circuit model is coinciding with the experimental data very closely.
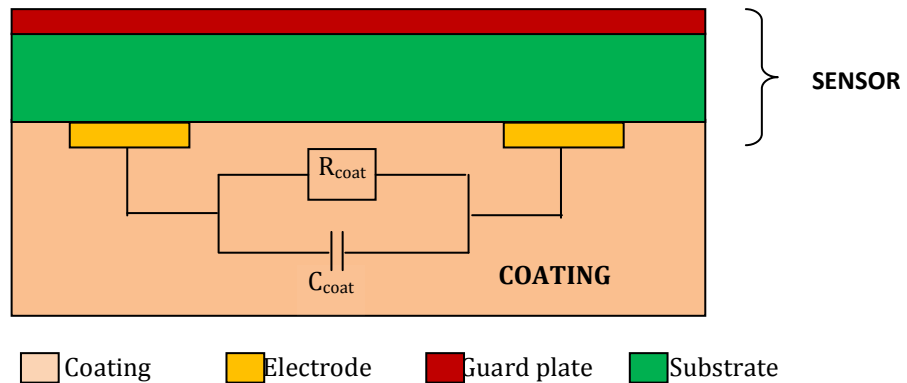
Fig. 24. Schematic lay out & equivalent circuit of FEF sensor.

3.9. Estimation of capacitance and electrical resistance from EIS

Capacitance of the encapsulants were determined from EIS by fitting the curve to that of an equivalent circuit shown in Fig. 7. This is the most widely accepted equivalent circuit by coating technologists to represent coatings during water uptake [49]. In the equivalent circuit, R_S represents solution resistance or uncompensated resistance, or R_C represents pore resistance of the coating and C_C represents coating capacitance of the coating. Residual χ^2 value of fitting the curve was < 0.001. Electrical degradation was calculated from the EIS (100 Hz 100 kHz) for better comparison with FFISY as the minimum measurement frequency in FFISY is 100 Hz.

3.10. Gravimetry

Water uptake in the encapsulant samples was measured by gravimetric technique to compare with that from EISY and FFISY. Two types of gravimetric techniques were used; free encapsulant and attached encapsulant gravimetry.

3.10.1. Gravimetric experiment for free encapsulant

The encapsulant samples of size 5x5 cm were kept for two days in controlled temperature (27 ± 1º) and humidity (45 ±1 RH) for conditioning and then weighed to find out the initial weight or 'dry weight'. The weighing was performed using a microbalance having four decimal accuracy. These samples were immersed in 3.5

wt% NaCl aqueous solution and were weighed at regular intervals. The samples were wiped with lint free water absorbing paper and allowed to dry at room temperature in air for 30 minutes before each weighing. The experiment continued till constant weight was achieved. The volume percentage of water content (X_v) in the sample was calculated from the following equation [10, 18].

$$X_V \ \% = \ \frac{100 \ d \ (W_w - W_D)}{W_D} \qquad (11)$$

where d is the density of dry encapsulant, W_w is wet weight of the encapsulant after immersed in water , W_D is the dry weight of the encapsulant.

3.10.2.   Gravimetric experiment for attached encapsulant

A light weight cylinder of very thin acrylic glass of diameter 5 cm and height 6 cm was placed over an acrylic sheet (6x6 cm) (Fig.25). A pre-weighed quantity of PU resin-hardener mixture was poured into the cylinder to form a thin layer and it was allowed to cure for 48 hours to form PU encapsulant. Thickness of the encapsulant was 1 mm which was measured after detaching the acrylic tube of another sample prepared by similar fashion.
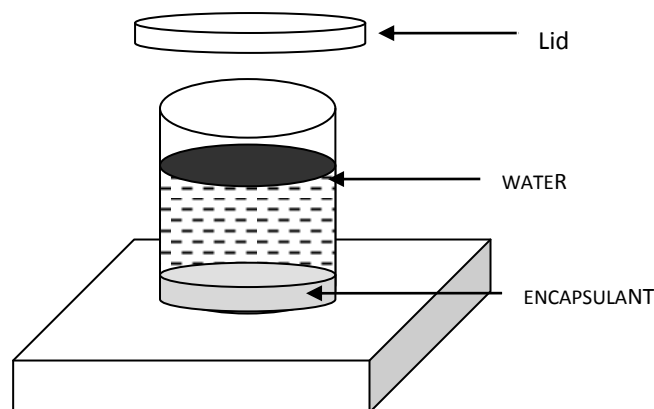
Fig.25. Schematic of gravimetric experiment set up for attached encapsulant

The cylinder was filled with 3.5 wt% NaCl aqueous solution and the experiment was conducted in room temperature (27 ± 1º C). The cylinder was provided with a cap to avoid trapping of any dust particles inside the cylinder. The weight of the encapsulant was calculated by subtracting the weight of total set up

before and after casting resin. The schematic of the experimental set up is shown in Fig. 25. The water was completely removed from the cylinder and traces of water remaining on the surface of the encapsulant is removed by lint free water absorbing paper. The set up is allowed to dry at room temperature in air for 30 minutes before each measurement. The water uptake by the encapsulant was measured at each time by measuring the weight in a digital balance to the accuracy of four decimal points.

CHAPTER – 4

Development of Fringing Electric Field Sensor

4.1. Objective

a) Development of fringing electric field (FEF) sensors to measure fringing field impedance spectra of encapsulants.

4.2. Introduction

FEF sensor should have sufficient sensitivity to measure the changes in the capacitance and electrical resistance of encapsulant during water ingress. In this chapter, an analytical study was done on the effect of electrode configuration on the sensitivity and penetration depth of the sensor. Later, the analytical results were validated with results from experiments conducted in ideal experimental conditions.

4.3. Determination of optimum sensor electrode configuration

FEF sensor should be sensitive to measure the changes in capacitance and electrical resistance during water ingress in the encapsulant. Also, the sensor should be able to measure the capacitance and electrical resistance of the encapsulant across its complete thickness. The latter is related to the penetration depth (PD) of the sensor.
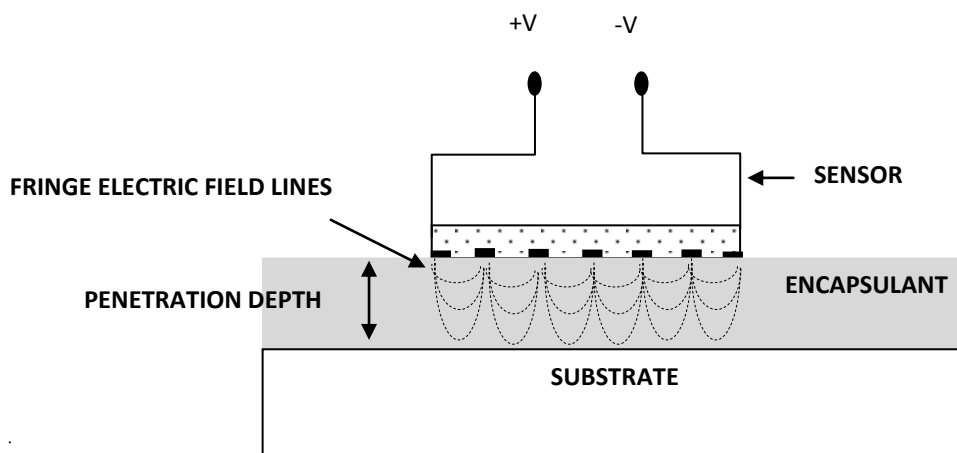
Fig.26. Schematic of measurement method of a fringe electric field sensor

The PD of an FEF sensor is the depth up to which the electric field from the sensor can penetrate into the encapsulant (Fig.26). The sensor does not have any measurement sensitivity beyond the PD of the sensor [65]. Hence, FEF sensor should be designed in such a way that the electric field should penetrate completely through the encapsulant. PD of an FEF sensor is approximately the sum of electrode width and gap between electrodes [115].

4.3.1. Analytical study-Effect of electrode configuration on sensitivity

FEF sensor is basically an interdigitated capacitor and the encapsulant material acts as the dielectric of the capacitor. The dielectric constant of the encapsulant increases due to water ingress as per Eqn.3 proposed by Hartshorn et al. [25]. As a result, the sensor capacitance increases due to increase in dielectric constant of the encapsulant. It is possible to determine the water uptake in the encapsulant from the increase in capacitance using the B-K formula as per Eqn.2 [10].

The sensor sensitivity to detect capacitance increase is dependent on the electrode configuration of the sensor and material used for making the sensor. These parameters are required to be optimized to enhance the sensitivity of the sensor. The important design parameters considered in the analytical study are listed in Table 3.

Table 3. Design parameters of FEF sensors on water uptake study

S.No	Design parameters	Sensor characteristics
1	Electrode width (w)	
2	Gap between electrode (s)	
3	Dielectric constant of the electrode substrate (ε)	Sensitivity Penetration depth
4	Thickness of electrode (T)	
5	Area of sensor Length (L) X No. of electrodes (N)	

Abu-Abed et al. [69] calculated capacitance of a sensor having an interdigitated electrode configuration and an infinite thick liquid crystal film as its

dielectric material. This equation is used in this work to calculate the sensor capacitance, assuming that an infinite thick encapsulant acts as the dielectric material of the sensor. An encapsulant can be considered as infinitely thick if its thickness is more than the PD of the sensor. In other words, the sensor readings will not be affected by the change in encapsulant thickness beyond the PD of the sensor. This assumption is useful to simplify the analytical studies by neglecting the change in encapsulant thickness due to swelling or any other reason. The following theoretical calculations are for an encapsulant with infinite thickness.

The FEF sensor has two electrodes in an interdigitated configuration on a substrate and each electrode consists of N fingers (Fig.27). Each finger has a width W and the space between any two adjacent fingers was S. The spatial distance of the periodic interdigitated cell is called unit cell which could be defined as the distance between the centre lines of the adjacent fingers belonging to the same electrode.
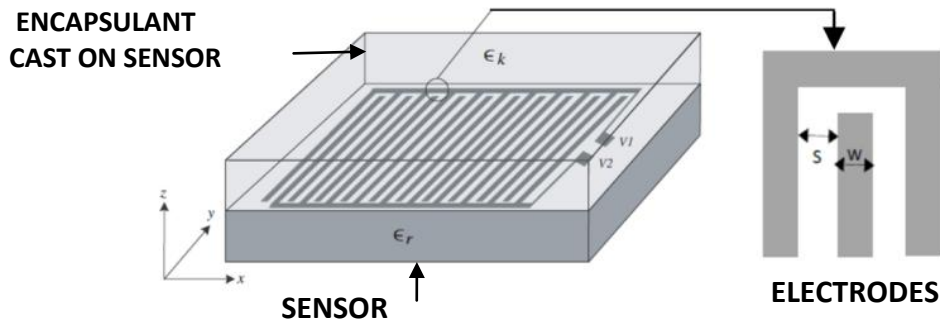
Fig.27. Encapsulant cast on FEF sensor and electrodes of sensor [69]

FEF sensor capacitance depends on width of electrode, W, and spacing between the electrodes, S, where transverse capacitance depends on the electrode's thickness, t and the distance between the adjacent electrodes. When the encapsulant is in contact with the electrode, the unit cell capacitance per length is given by the closed form,

$$C_{uc} = \varepsilon_0(\varepsilon_r + \varepsilon_k) \frac{K\left(\sqrt{1 - \left(\frac{w}{2(w+s)}\right)^2}\right)}{K\left(\frac{w}{2(w+s)}\right)} + 2\varepsilon_0\varepsilon_k \frac{t}{s} \qquad (12)$$

where ε_0 is the dielectric constant in the free space, ε_r and ε_k are the dielectric constants of the substrate and the encapsulant, respectively. The function '$K(.)$' is the complete elliptic integral of the first kind.

When an organic coating absorbs water, its dielectric constant changes. Hartshorn [25] proposed a formula to find out the mixed dielectric constant, ε_m of the coating (Eqn.3). It is assumed that coating and its interface with the sensor is free of voids and hence the term $\varepsilon_{air}^{(v_{air}/V)}$ is neglected in further calculations. The dielectric constant, ε_r of the substrate is taken as 4, which is the dielectric constant value of commercially available copper clad Flame Retardant Printed Circuit Board (FR-4 PCB) [72]. A commercially available organic coating or encapsulant has a dielectric constant (ε_k) value approximately 4 [28] and assumed that it absorbs 10 vol% water in wet environments for the study. The dielectric constant of the coating increases from 4 to 5.4 during 0 to 10 vol% water ingress as per Eqn.3. The changes in sensor unit capacitance during water absorption in the encapsulant are analytically calculated for different electrode configuration. Sensor capacitance will not be affected by the change in encapsulant thickness as it occurs outside the sensing area and hence not accounted in the analytical modelling.
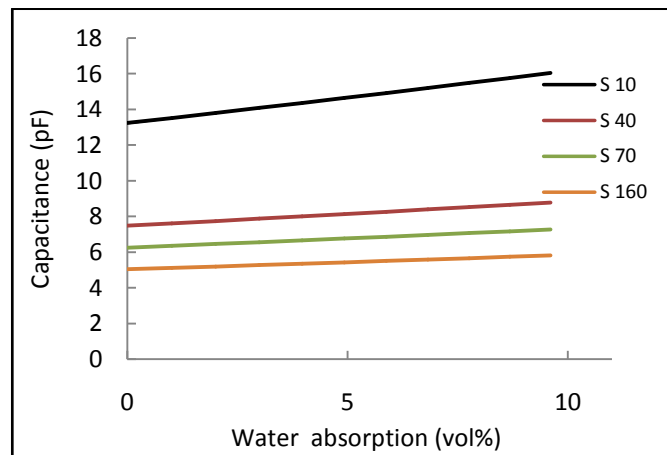
Fig.28. Theoretically calculated sensor unit capacitance changes during water absorption in the encapsulant for variation in electrode spacing (S=10-160 μm). Other parameters were fixed at W=10 μm, t=20 μm, N=10 and L=5000 μm.

The effect of gap between electrodes on sensor capacitance during water absorption, is shown in Fig.28. The gap is varied from 10 to 160 μm in the study. The lower range is limited to fabrication constraints and higher range is limited to

the overall size of the sensor. The sensor is more sensitive (change in capacitance per unit percentage water absorption) to water uptake around 10 μm gap and estimated maximum sensitivity is 0.47 pF/vol%. Similarly, capacitance of sensor increases with electrode width (Fig.29).
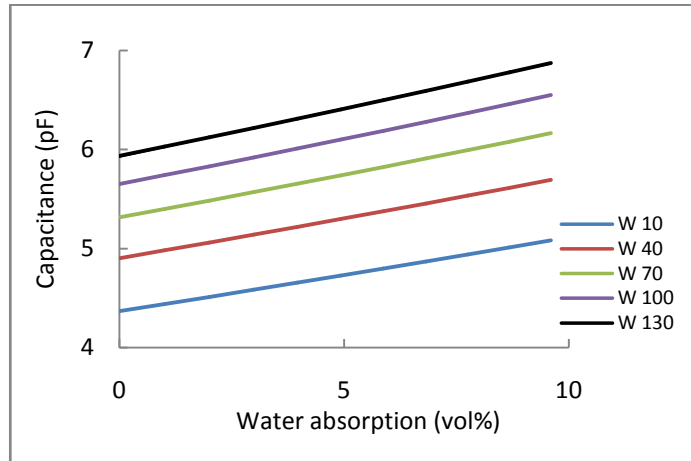
Fig.29. Theoretically calculated sensor unit capacitance changes during water absorption in the encapsulant for variation in electrode width (W=10-130 μm). Other parameters were fixed at S=10 μm, t=20 μm, N=10, L=5000 μm.
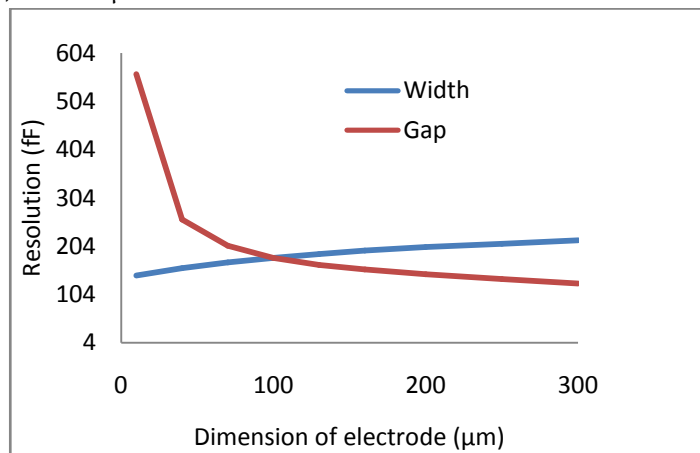
Fig.30. Theoretical results of the effect of electrode width and gap on the resolution of the sensor during water absorption 0- 2vol% by the organic encapsulant and the other parameters are fixed as above.

The effect of change in electrode width and spacing on the resolution of the sensor is compared in Fig.30. Resolution is calculated as the difference in sensor capacitance for 0 % and 2 % water absorption by the encapsulant. As the resolution increases the sensitivity of the sensor enhances. It is observed that sensor with narrow electrode gap and wider electrode width has maximum resolution. Electrode gap has more effect on sensor resolution than electrode width.

The effect of electrode thickness on sensor unit capacitance was studied for the range, 10 to 45 μm based on the commercially available copper clad substrates. Electrode thickness enhances the sensor capacitance as shown in Fig.31.

The effect of change in the dielectric constant of the substrate on sensor unit capacitance is calculated for the range 3 to 6 (Fig.32). Even though, an increase in sensor capacitance is observed with increase in dielectric constant, the change is very small (0.5pF/change in dielectric constant) compared to other sensor parameters. The substrate capacitance being an inbuilt capacitance remains same during water ingress. Hence, inbuilt capacitance due to electrode configuration and substrate dielectric constant will not contribute towards the sensitivity of the sensor [104].
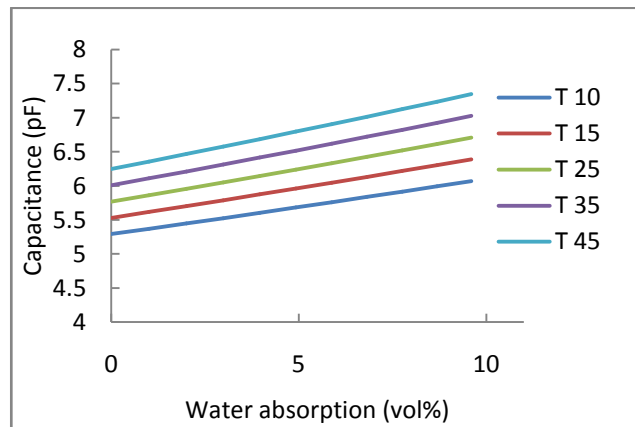
Fig.31. Theoretically calculated capacitance changes during water absorption in the encapsulant for variation in electrode thickness (t=10-45 μm) and S=100 μm, W=100 μm, N=10, L=5000 μm
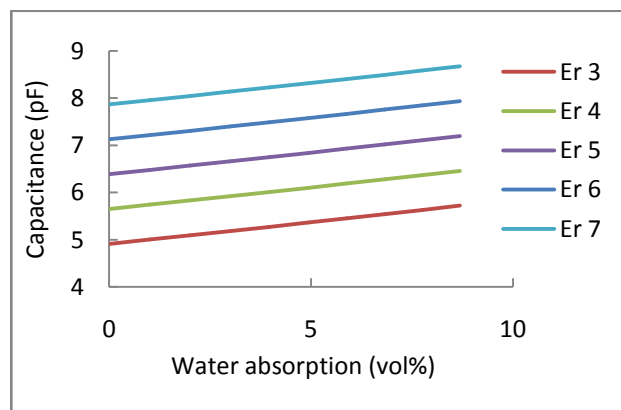
Fig.32. Theoretically calculated capacitance changes during water absorption in the encapsulant for variation in substrate dielectric constant (ε_r) and S=100μm, W=100μm, t=20 μm, N=10, L=5000μm

Electrode width and gap are the most important parameter that determines the sensitivity of the unit cell. By making full use of symmetry and neglecting the

capacitances of the edges, the total capacitance of the FEF sensor can be calculated using the Eqn.13 [69],

$$C_{TOTAL} = C_{uc}\,(N - 1)L \qquad (13)$$

Where N is the number of unit cells in the capacitor and L is the over lapping length of electrode fingers.

The effect of sensor area on capacitance of the sensor was studied (Fig.33). It is observed that sensor capacitance has a linear relation with sensor area for a fixed sensor material and electrode configuration. As the sensor area increases the sensor capacitance increases. The sensitivity of the sensor to detect water uptake could be increased by 4 times by one unit increase in sensor area.
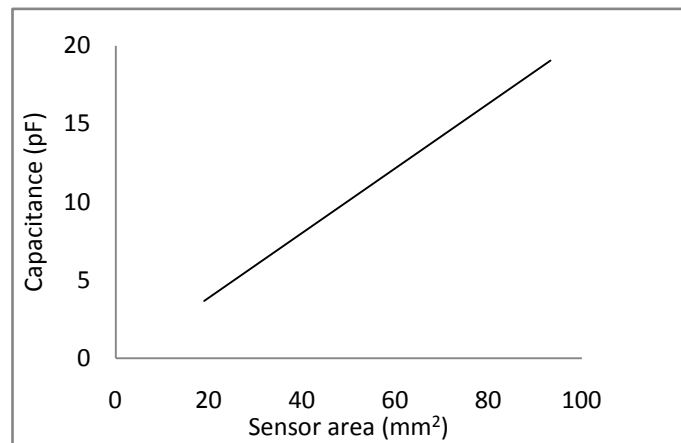
Fig.33. Variation of sensor capacitance with sensor area

4.3.2. Experimental study- Effect of penetration depth on sensitivity

Five FEF sensors of same area (10 cm^2) were fabricated to study the effect of electrode configuration on electrical resistance. The dimensions of the fabricated sensors (Fig.34) are given in the Table 4 .The effect of change of 'S + W' (penetration depth) of sensors of same area on sensor electrical resistance was analysed. The electrical resistance were measured in air at 100 Hz by impedance analyzer.

The capacitance of the sensor decreases as the PD of the sensor increases for a fixed sensor area 10 cm^2 (Fig.35). The capacitance decreases very sharply before 500 μm. Hence PD of the sensor should be below 500 μm for better sensitivity. However, an encapsulant having thickness more than 500 μm cannot be evaluated

in full depth using a sensor with PD 500 µm.

<div align="center">(1)   (2)   (3)</div>

<div align="center">.(4)   (5)</div>
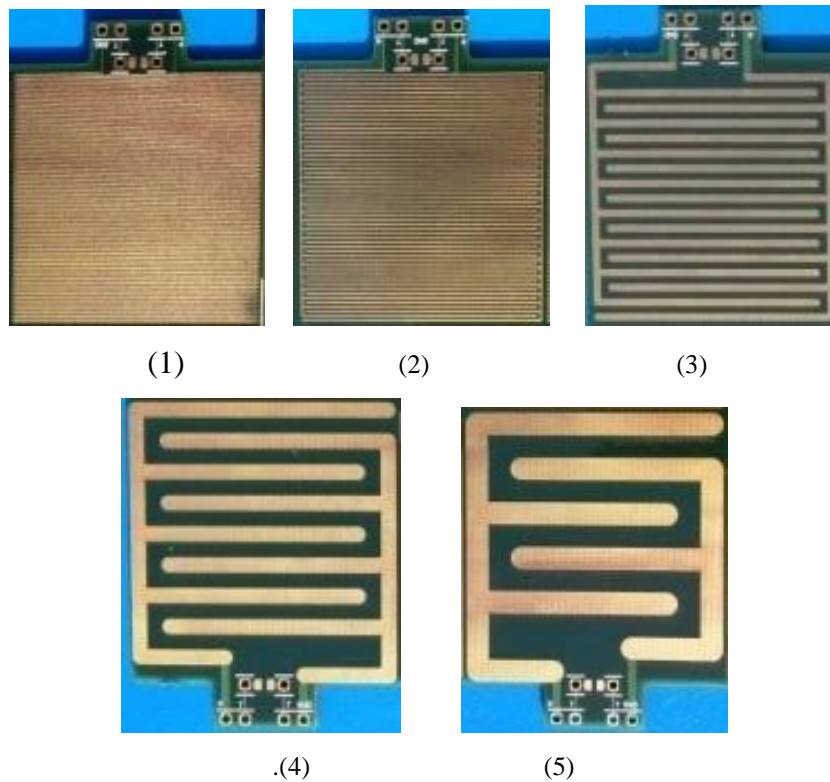
Fig 34: FEF sensors with dimensions as (1) S,W=150 µm, (2) S,W=300 µm,(3) S,W=1 mm, (4) S,W=2 mm and (5) S,W=3 mm

Table 4. Dimensions of sensors of same area with different electrode configuration

Sensor No.	Electrode width (w)	Electrode spacing (S)
1	150 µm	150 µm
2	300 µm	300 µm
3	1 mm	1 mm
4	2 mm	2 mm
5	3 mm	3 mm

It is observed that, the resistance of the sensor increases sharply as the PD increases towards 500 µm (Fig.36). The capacitance of the interdigitated FEF sensor decreases with increase in sensor electrode gap as understood from theoretical study. On the other hand, electrical resistance of the sensor increases as the electrode gap increases from 150 µm to 3 mm.
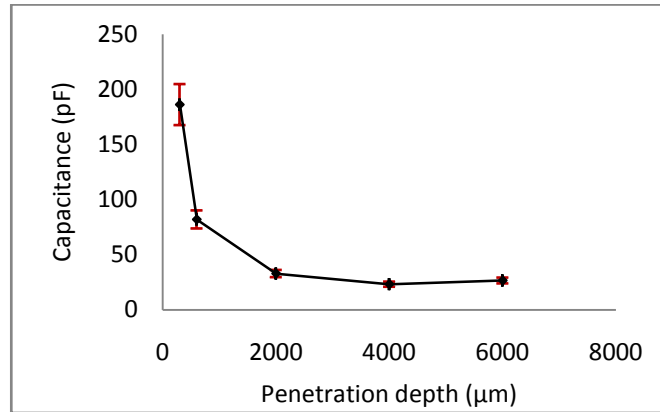
Fig 35: Effect of penetration depth on sensor capacitance for FEF sensors with a fixed area 10 cm^2
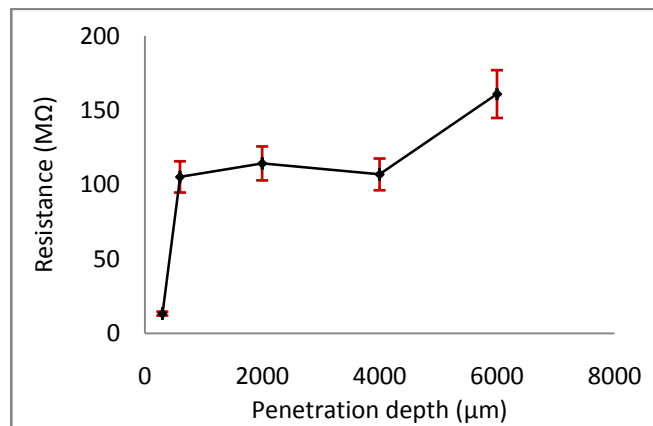
Fig 36: Effect of penetration depth on electrical resistance of the sensor

The FFIS of five sensors described above are shown in Fig. 37. Impedance increases as the electrode spacing increases. Sensor with higher values of capacitance and electrical resistance is required for sensitive measurement of water uptake and electrical degradation respectively. It was observed that below a PD of 500 μm, the measured sensor capacitance decreases exponentially and electrical resistance increases considerably with increase in PD. Hence, as a compromise FEF sensor with PD ~ 500 μm was selected for fabrication for better sensitivity (Type I sensor). The electric field from this sensor can be used only for evaluating encapsulants having thickness less than 500 μm as the field penetration is limited to encapsulant depth of ~ 500 μm only. Hence this sensor was used for evaluating encapsulants having thickness less than 500 μm and termed 'thin encapsulants' in this research work. In order to study encapsulants with thickness higher than 500 μm (termed thick encapsulants), another FEF sensor with PD 2 mm was fabricated
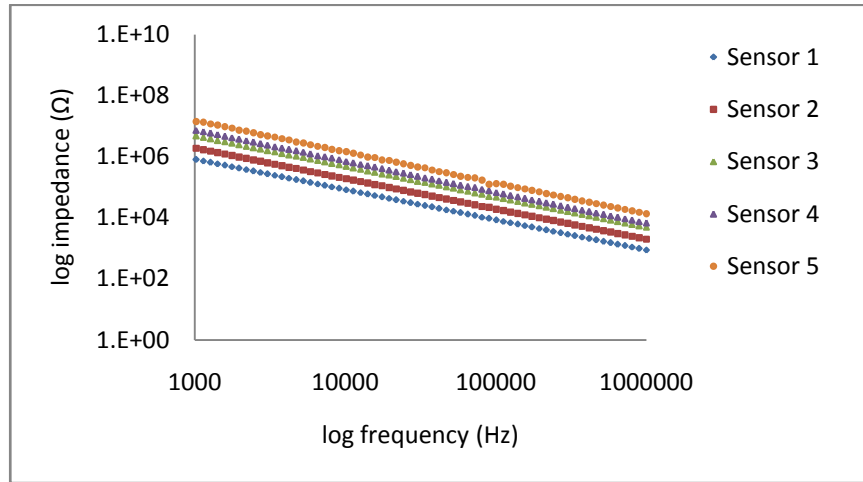
(Type II sensor).

Fig 37: Fringing field impedance spectra of fabricated sensors

Type II sensors have lower sensitivity for capacitance measurement due to its wider electrode gap. Hence, area of Type II sensor should be increased to enhance the sensitivity. As the increase in sensor area has practical constrains, an optimum electrode configuration and sensor area should be selected for the sensitive measurement of water uptake and electrical degradation. In all these electrode configurations, a metallic copper layer was provided below sensor substrate as a shielding to prevent field leakage to the back side of the sensor.

4.4. Fabrication of FEF sensor

Type -1 FEF sensors were fabricated by lithographic process and Type-II FEF sensor was fabricated by PCB fabrication process.

4.4.1. FEF sensor for thin encapsulants

In order to conduct controlled experiments, five numbers of Type -I FEF sensors were fabricated with different area less than 100 mm^2 and they were termed as miniature sensors. All the five sensors were fabricated as 'miniature' for co-locating them on a platform of size 5 x 5 cm, which is suitable to hold on the chuck of a spin coater. There are two advantages for conducting controlled experiments, (i) it is possible to fabricate sensors by lithography process with high dimensional tolerance in ± 5 μm, (ii) Coating of same thickness can be applied on all sensors.

The sensors were fabricated by conventional photolithographic process on

copper clad FR-4 PCB laminates. The mask for the sensor pattern was made by transferring the CAD drawing to a 50 µm Polyethylene naphalate (PEN) sheet by a high resolution laser printer. This flexible patterned sheet was used as mask for 1:1 contact lithography. The sensor pattern was transferred to the photoresist coated on commercially available FR-4 PCB by UV photolithography using mask aligner. The positive photoresist S1813 was used for the lithography process with its developer. The patterned copper clad PCB was exposed to ferric chloride solution to remove the exposed copper and thus the sensor pattern on FR-4 was formed (Fig.38). Five sensors were fabricated by this method. Contact pads were provided for each sensor to take electrical leads for the measurement. A 10x10 mm² copper pad was also patterned in the centre to measure the coating thickness using thickness gauge.

The fabrication cost for the sensor was less due to the use of a low cost PEN mask and FR-4 PCB. All the fabricated sensors had same '**s + w**' and hence same penetration depth ~460 µm. The gap between the electrodes was designed as wider than electrode width so that encapsulant could be cast over the sensor without any voids. The narrow gap may cause entrapment of air when casting on miniature sensors.
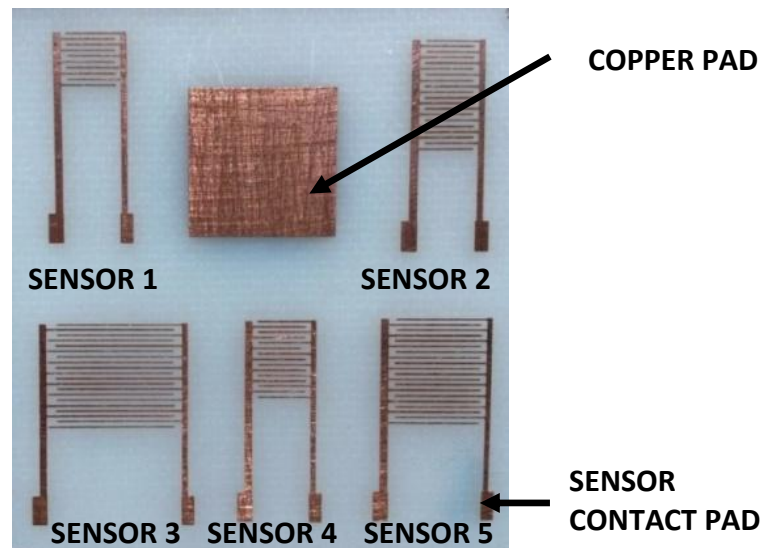
Fig.38. Photograph of the fabricated sensors

Dimensions of the fabricated miniature FEF sensors are given in Table 5. Sensor No. 3 has the highest area among other sensors. Dimensional accuracy of the sensor was ± 5 µm measured through optical microscope.

Table 5: Dimensions of the fabricated miniature Type I FEF sensors

Sensor	Width (W) μm	Gap (S) μm	No.of fingers (N)	Length of fingers (L) μm	Area of the sensor (A) mm^2	Inbuilt capacitance pF @100 kHz
1	160	300	10	4400	19	5.63
2	160	300	20	4400	39	7.28
3	160	300	20	10480	93	8.73
4	160	300	15	4400	29	6.24
5	160	300	20	7500	67	8.30

The sensor has an inbuilt capacitance due to its electrode configuration and substrate. The value of this capacitance was measured by measuring the capacitance of the sensor in air at 100 kHz. The inbuilt capacitance of the five sensors are given in the Table. 5. Inbuilt capacitance will not contribute to the sensor resolution as its value remains constant during experiment [106].

4.4.2. FEF sensor for thick encapsulants

In order to study encapsulants with thickness higher than 500 μm (termed thick encapsulants), another FEF sensor with PD 2 mm was fabricated (Type II sensor) by commercial PCB fabrication process. This sensor has electrode width and electrode spacing 1 mm each (Fig.39). As per analytical study, the sensor has less sensitivity compared to Type I FEF sensors. Hence, larger sensor area (10 cm^2) was used to enhance the sensitivity.
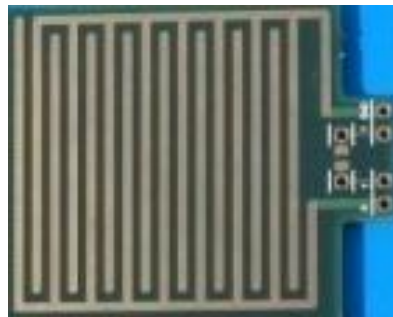
Fig.39. Type II FEF sensor with electrode width and gap 1 mm each.

The layer stack up in the construction of all FEF sensors were as shown in Fig.40 as

available commercially. A copper layer (layer-1) was patterned to form interdigitated electrodes of FEF sensor on a 345 μm thick dielectric layer. The dielectric layer is of FR-4 and has dielectric constant 4. Another copper layer (layer-3) acts as a guard to prevent leakage of field to the backside of the sensor. Leads were taken from two electrodes and the guard plate.

Layer 1 ----> Copper ----> Thickness:				**35 μm**
Layer 2 ----> Dielectric--> Thickness:				**345 μm**
Layer 3 ----> Copper ----> Thickness:				**17 μm**

Fig. 40. PCB layer stack up of fabricated FEF sensor

4.5. Validation of analytical studies

The analytical results were confirmed by experimental measurements in ideal conditions. The ideal condition of void free encapsulant with known dielectric constant, intimate sensor-encapsulant interface and controlled increase in water uptake was created in a novel method. Dielectric liquid layer over the sensor forms as the ideal encapsulant. The capacitance change measured by the sensor due to a known percentage of water ingress in the encapsulant could be computed from the measured capacitance change of the sensor immersed in different dielectric liquids of known dielectric constant. In order to do that, a few different dielectric liquids were selected in such a way that their dielectric constants lies in the range of dielectric variation of encapsulants during water ingress.

Capacitance is a frequency dependent quantity and hence optimum frequency for measuring sensor capacitance need to be known. Hence, the capacitance spectra (Fig.41 to 45) of all the sensors were measured from 100 Hz to 10 MHz using impedance analyzer (model: Wayken) in selected liquids (AR grade) and their dielectric constants are given in the bracket; Hexane (ε_r=1.88), Tetrahydro furan (THF) (ε_r=7.52), Ethanol (ε_r=24.6), water (ε_r=78.3).

For most of the substances, the dielectric constant is constant only for a limited frequency range. The dielectric constant decreases with a frequency rise. These abrupt changes represent a specific polarization mechanism and are called dispersions. Polar molecules show high dispersions at low frequencies. As the

polarity of the molecules increases, the level of dispersion increases [136]. Hence water shows the highest dispersion in low frequency among other dielectric liquids. All sensors show a plateau in the same frequency region independent of its area.
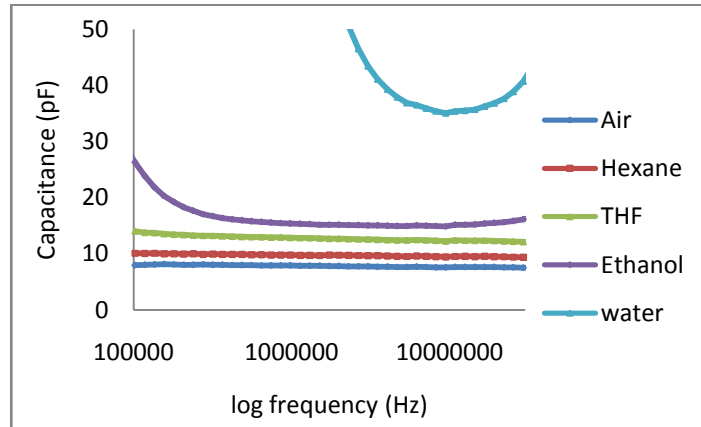
Fig.41. Capacitance spectra of sensor having an area of 19 mm² in different dielectric liquids
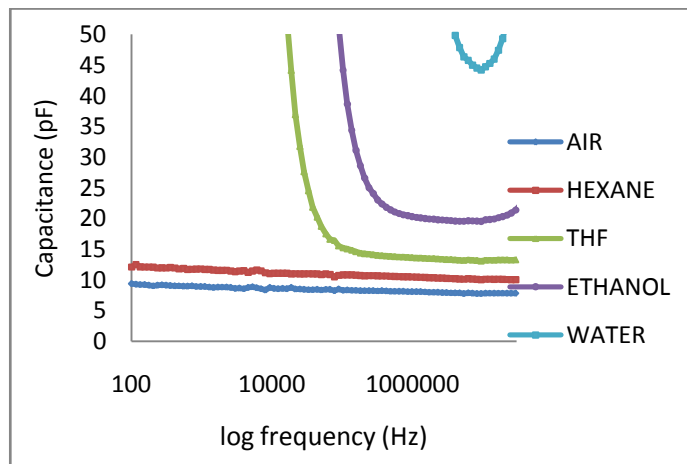
Fig.42. Capacitance spectra of sensor having an area of 39 mm² in different dielectric liquids
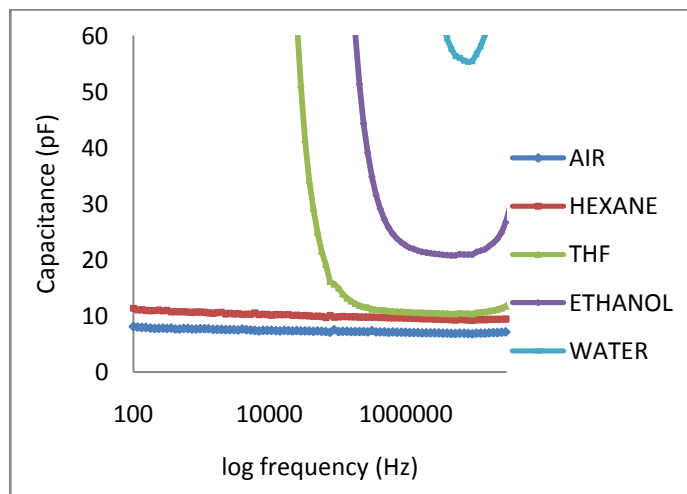
Fig.43. Capacitance spectra of sensor having an area of 93 mm² in different dielectric liquids
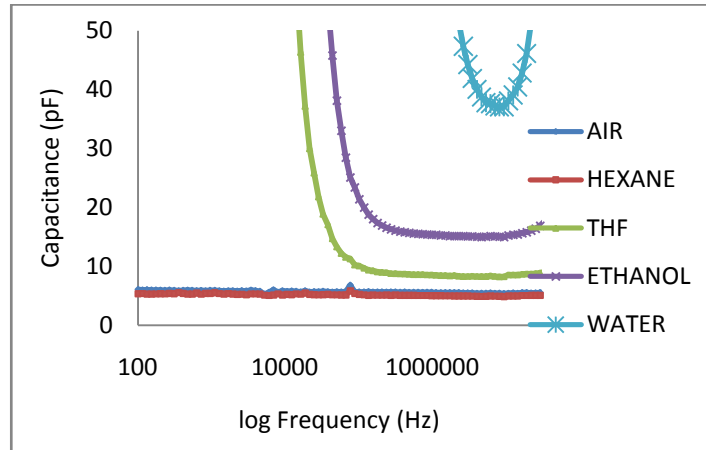
Fig.44. Capacitance spectra of sensor having an area of 29 mm^2 in different dielectric liquids
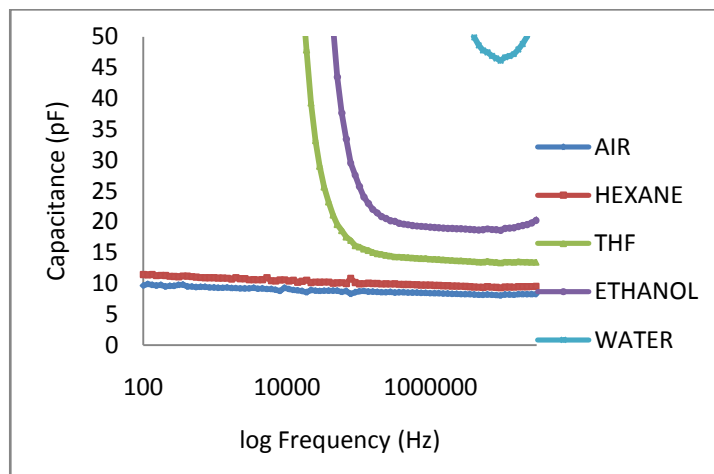
Fig.45. Capacitance spectra of sensor having an area of 67 mm^2 in different dielectric liquids

The relation between sensor capacitance and dielectric constant of liquids is analyzed and found a linear relation in the plateau region. The coefficient of linearity (R^2) is computed and the best linear fit is obtained at a minimum frequency 120 kHz for the dielectric constant range 1-24. However, for the dielectric constant range 1-6 (the dielectric change during water ingress in encapsulant), the best linear fit is obtained at 100 kHz frequency (Fig.46). Hence, subsequent capacitance measurements were done at 100 kHz.

Theoretically calculated sensor capacitance was verified with the experimental values of five miniature sensors. The theoretical and experimental capacitance values are in the ±5 pF range. The deviation from the theoretical value may be attributed to the unknown error in estimating the theoretical value (Fig.47).

Sensor with maximum sensitivity is selected from the slope of linear fit of capacitance-dielectric constant curve (Fig.48). The sensor-3 with largest area (93

mm^2) shows maximum sensitivity of 0.602 pF/unit dielectric constant. In other words the sensor shows a capacitance change of 83.68 fF per vol% of water as per eqn.3. Hence, sensor-3 is used for the evaluation of encapsulant. A high precision capacitance measuring circuit was also used in experiments to find out water uptake in encapsulants.
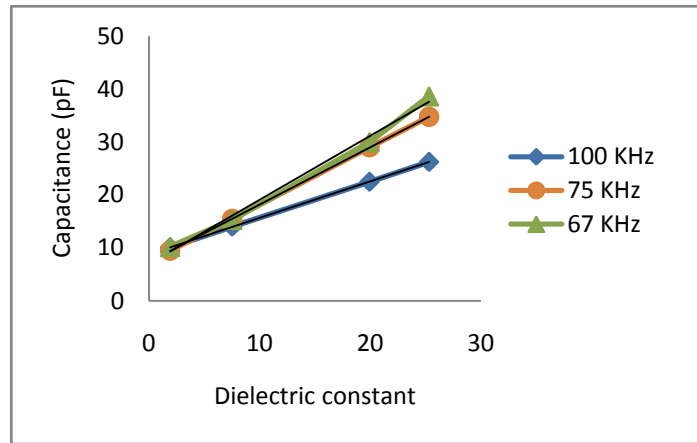
Fig.46. Variation of capacitance with dielectric constant at different measurement frequencies.
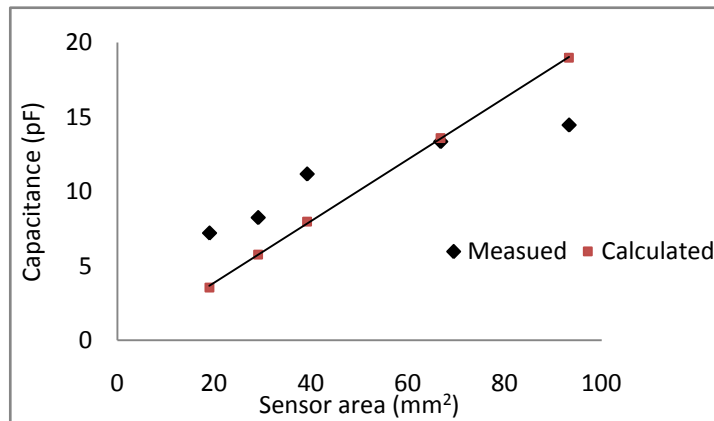
Fig.47. Variation of measured and theoretical capacitance with sensor area.
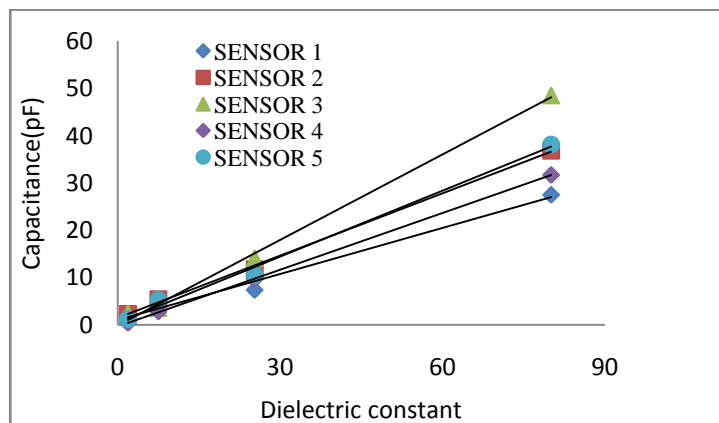
Fig.48. Variation of capacitance with dielectric constant

4.6. Calibration of FEF sensor for electrical resistance measurements

Electrical degradation of the encapsulant is monitored by measuring the decrease in electrical resistance. Electrical degradation is estimated from the decrease in electrical resistance measured by FEF sensor (FFIS electrical resistance) Hence, the measurement of electrical resistivity of the encapsulant is not relevant in this study. However, FEF sensor can measure the electrical resistivity by knowing the parameter called 'cell constant'. Cell constant is a unique number of an FEF sensor and it depends entirely on the geometry of the sensor [70]. The resistance (R_{coat}) of the encapsulant is related to its resistivity (ρ_{coat}) by the cell constant K_{Cell} as described by equations 7,8,9 & 10. Cell constant is usually expressed in cm^{-1}. The theoretical cell constants of the five miniature sensors are given in Table.6.

Table 6. Theoretical cell constant of fabricated sensors

Sensor No.	Area of the sensor (A) mm^2	Cell constant (K) cm^{-1}
1	19	0.613
2	39	0.299
3	93	0.125
4	29	0.406
5	67	0.176
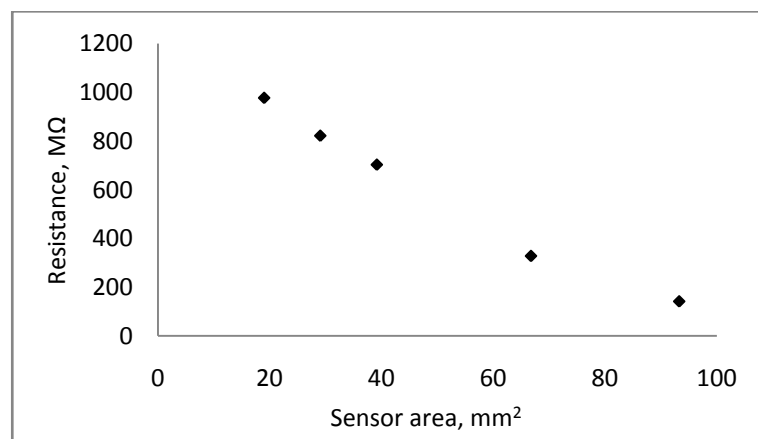
Fig.49. Variation of electrical impedance with sensor area

A correlation exists between sensor area and resistance of the sensor (Fig.48). The FEF sensor resistance measured at 100 Hz decreases linearly with increase in sensor area. The cell constant of the sensor depends on electrode width, spacing between electrodes, length of electrodes and number of electrodes as given in eqn. 8. The resistance of the sensor increases with increase in cell constant (Fig.49).
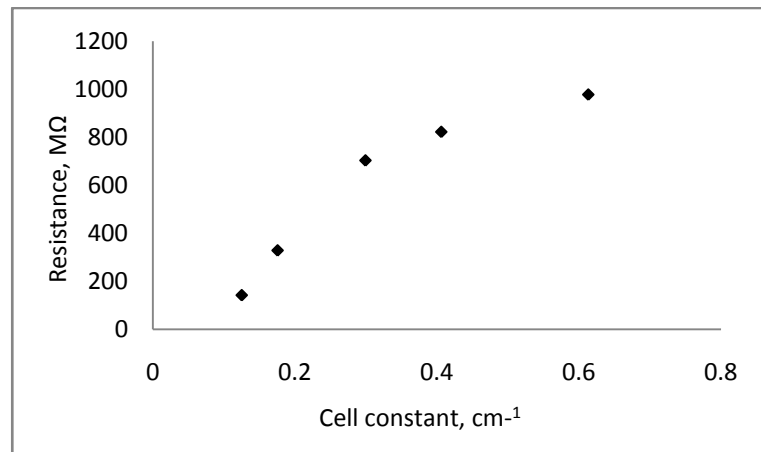
Fig.50. Variation of electrical impedance with cell constant

4.7. Conclusion

The aim of the study is to estimate the change in capacitance and electrical resistance of the encapsulants from measured FFIS. Water uptake will be estimated by the increase in capacitance and electrical degradation will be estimated by the decrease in electrical resistance of the encapsulants.

Analytical studies were done to understand the effect of sensor electrode configuration on water uptake (capacitance changes). Analytical studies revealed that the water uptake by the encapsulant could be measured by an FEF sensor. 1 vol % of water uptake by the encapsulant resulted in the increase of measured sensor unit capacitance by 0.47 pF for the electrode dimensions, **S** =10 μm, **W** = 300 μm and **L** = 5000 μm. The sensitivity of the sensor to detect water uptake could be increased by 4 times by increasing the sensor area by one unit. The other findings of analytical studies are,

a. As the gap between electrodes decreases, the sensor sensitivity to measure water uptake in the encapsulant increases.

b. As the electrode width increases, the sensor sensitivity to measure water uptake in the encapsulant increases.

c. The effect of electrode gap on sensitivity is 6 times more than width for gap below 50 μm.

d. The FEF sensor has an inbuilt capacitance in the absence of an encapsulant and its value is determined by the electrode thickness and dielectric constant of sensor substrate in addition to the electrode width and gap. As the electrode thickness and dielectric constant of sensor substrate increases, the inbuilt capacitance increases.

The analytical results were confirmed by experimental measurements in ideal conditions. The ideal condition of void free encapsulant with known dielectric constant, intimate sensor-encapsulant interface and controlled increase in water uptake was created in a novel method using dielectric liquids. At 100 kHz frequency, all the five fabricated sensors show linearity between sensor capacitance and dielectric constant and also the experimental results were comparable with analytical results at 100 kHz frequency.

The relation between the sensor capacitance and PD of the sensor was found out analytically and experimentally. It was observed that below a PD of 500 μm, the measured sensor capacitance decreases exponentially with increase in PD for a fixed area.

The effect of sensor electrode configuration on change in electrical resistance was determined experimentally. Electrical resistance increases with increase in PD up to 500 μm.

Hence, FEF sensor was fabricated with PD around 500 μm for optimum sensitivity in measurement, termed Type - I sensor. The electric field from this sensor penetrates up to an encapsulant depth of ~ 500 μm. Hence this sensor was used for encapsulants having thickness less than 500 μm and termed 'thin encapsulants' in this research work.

FEF sensor with penetration depth ~500 μm cannot measure the properties of encapsulants thickness more than ~500 μm (termed thick encapsulants). Hence, a FEF sensor with penetration depth 2 mm was selected for fabrication (Type II sensor). This can measure the properties of encapsulants up to 2 mm thick.

A factor called cell constant was theoretically calculated for the FEF sensors. The cell constant can be used for finding the electrical resistivity of the encapsulant from the measured FFIS electrical resistance.

CHAPTER – 5

Fringing Field Impedance Spectroscopy

5.1. Objective

i) Study the effect of sensor area and encapsulant thickness on fringing field impedance spectra of encapsulants.

ii) Measure fringing field impedance spectra of encapsulant materials immersed in 3.5 wt % NaCl aqueous solution continuously for two months and analyze the change in pattern of the spectra.

5.2. Introduction

In this chapter, the developed FEF sensors were used to measure the fringing field impedance spectra (FFIS) of encapsulants. The effect of sensor area and thickness of encapsulant on fringing field impedance spectra were studied in the first stage. Later, the fringing field impedance spectra of encapsulants immersed in 3.5 wt% NaCl aqueous solution, were frequently measured. As discussed in earlier chapters, increase in capacitance and decrease in electrical resistance of the encapsulant due to water ingress can be estimated from the frequently measured fringing field impedance spectra (FFIS).

5.3. Effect of sensor area

The fringing field impedance spectra of encapsulant will change according to the sensor area for a fixed electrode configuration [106, 107]. Five miniature FEF sensors of different area having same electrode width and gap were used to study the effect of sensor area on FFIS. A controlled experiment was possible as all the five sensors were in a single PCB and because of that an encapsulant with same thickness could be coated on all the sensors in one step spin coating process. A 410 µm thick PU encapsulant was cast over the FEF sensors and FFIS were measured in air (Fig.51).

The FFIS of each sensor was different. FFIS was a straight line with a negative slop which is a typical impedance spectroscopy plot of a dielectric material

[41]. The sensor having the highest area has the least impedance. The spectra line placed parallel one below another according to the increase in sensor area.
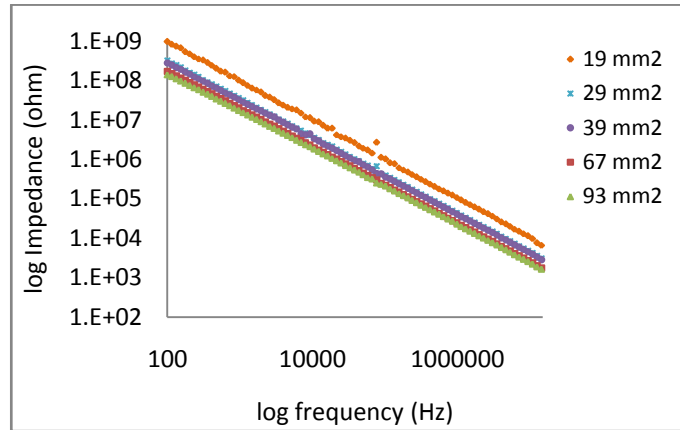
Fig.51.Fringing feild impedance spectra measured by five types of FEF sensors with different area
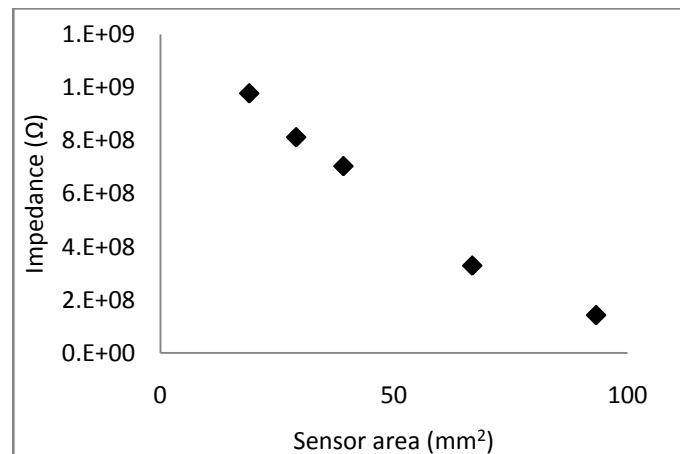
Fig.52.Variation of impedance at 100 Hz with sensor area

Relation between sensor impedance and sensor area derived from the measured FFIS of five sensors. Fig.52 is a graph showing the relation between sensor impedance (at 100 Hz) and corresponding sensor area. The relation between sensor impedance and sensor area was inversly proportional (Fig.52). The impedance of the sensor coated with 410 μm PU encapsulant, decreased from 1 GΩ to 142 MΩ as the sensor area increased from 19 mm² to 93 mm².

The capacitance of all the five sensors were measured for the frequency range 100   Hz to 10 MHz (Fig.53). All sensors have high capacitance value (hundreds of microfarad) in the lower frequency range and show large change in capacitance with frequency in the range 100 Hz to 10 kHz. Dielectric polymers

shows large change in capacitance with frequency in the lower frequncy range. This due to the polarisation effects in the polymer [136].
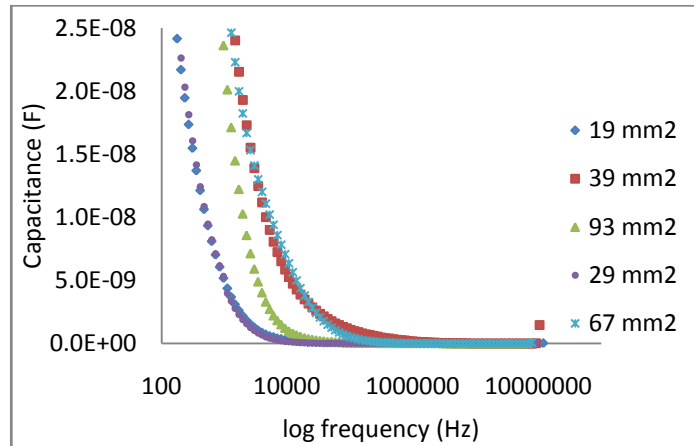
Fig.53. Capacitance-frequency spectrum for sensors with specified area in mm as shown.
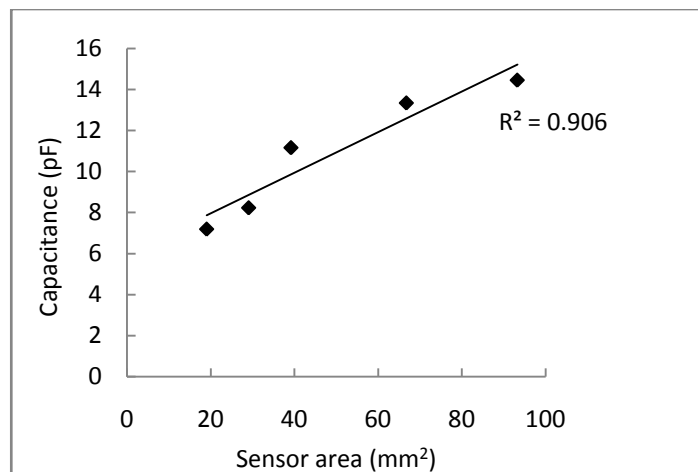
Fig.54. Variation of capacitance with sensor area for 1 mm thick PU encapsulant @100 kHz

A linear correlation between capacitance and sensor area exists at 100 kHz and above (Fig.54).   The value of capacitance of all the sensors coated with encapsulant was below 20 pF in this region. The sensor having area 93 mm^2 has highest value of capacitance. showed   Also, it was found that measurements were repeatable around this frequency. This was similar to the capacitance spectra of dielectric liquids described in last chapter.

5.4. Effect of encapsulant thickness

The sensor having highest capacitance value (sensor having area 93 mm^2) was chosen to study the effect of encapsulant thickness on sensor capacitance. Encapsulants of different thickness were coated over six different sensors. The capacitance of the encapsulated sensor increases with increase in encapsulant thickness below thickness ~500 μm (Fig.55). The sensor capacitance increased to 13.5 pF as encapsulant thickness reaches ~500 μm and thereafter remained same with increase in thickness.

FEF sensor is an interdigitated electrode capacitor. Here, the encapsulant is the dielectric material for the interdigitated capacitor. The capacitance of an interdigitated electrode capacitor increases with increase in thickness of the dielectric material as reported in literature [97]. The same relation was experimentally quantified for encapsulant cast FEF sensor. In the case of FEF sensor having sensor area 93 mm^2 , capacitance increases and reaches a constant value after attaining an encapsulant thickness of 460-500 μm.
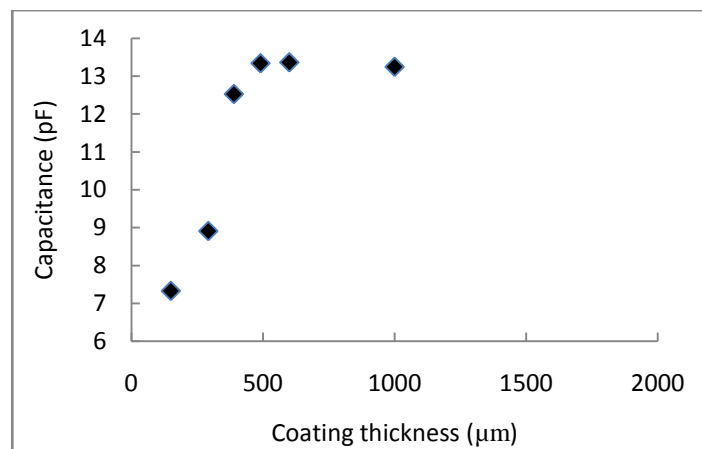
Fig. 55. Variation of capacitance of a 93 mm^2 area sensor with different PU encapsulant thickness

The capacitance of the encapsulant cast FEF sensor was not affected by further increase in encapsulant thickness after ~480 ± 20 μm. In other words, the sensor did not sense any change in encapsulant after this thickness. It means that the sensor has a penetration depth ~480 ± 20 μm and this agree with the theoretically computed penetration depth (460 μm).

The impedance of the encapsulant cast sensor decreases with increase in encapsulant thickness within the penetration depth of the sensor (Fig.56). It can be

explained by the following way; the encapsulant replaces the air above the sensor as the encapsulant thickness increases. As the air has more electrical impedance than polymeric material, the sensor impedance decreases with the replacement of air within the penetration depth of sensor and this inference is supported by literature [137]. The decrease in impedance was less after the theoretically determined penetration depth.
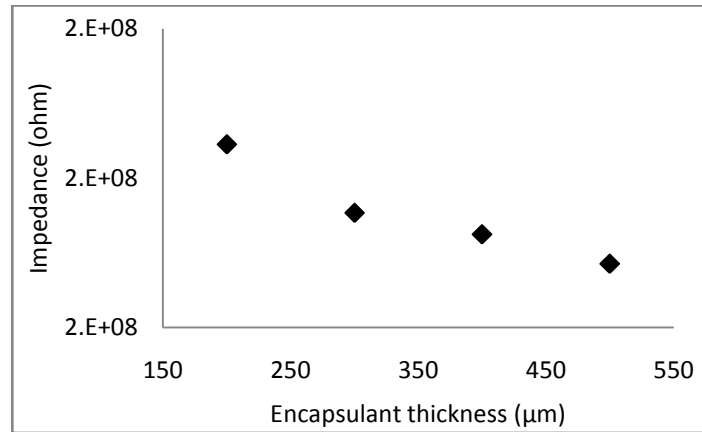
Fig. 56. Variation of impedance of a 93 mm² area sensor with different PU encapsulant thickness

5.5. Effect of metal substrate

There are cases in which the thickness of the cast encapsulant is below the theoretical penetration depth of sensor. In this case, the fringing electric field from the sensor will go beyond the encapsulant thickness. In this case, how far the field go beyond the encapsulant boundary is dependent on the outer boundary of the encapsulant. In the case of encapsulant applied on metal and sensor measures the FFIS from the other side, the metal acts as the boundary. Air can be considered as the boundary in other cases where encapsulant is free on one surface.

A study was done to understand the effect of two different boundaries of encapsulant on the measured impedance and capacitance. Encapsulants having thickness 182 ± 5 µm , 240± 5 µm , 394± 5 µm, 540± 5 µm were chosen for the study and they were cast on FEF sensor with PD 460 µm. The fringing field impedance and capacitance of the encapsulant were measured with and without metal (air) over it. The values of measured fringing field impedance and capacitance are given in Table.7.

The capacitance increased and impedance decreased when metal placed over the encapsulant of thickness less than penetration depth of the sensor. In this case metal acted as a fringe electric field guider and confined the field within the encapsulant [65]. As the encapsulant has higher dielectric constant than air, the sensor capacitance increases. Due to the increased capacitance, the impedance contributed by the capacitance decreases as per relation given in eqn.4. There was no change in capacitance and impedance in 540± 5 μm thick encapsulant due to higher thickness than the penetration depth of the sensor.

Table 7. The measured fringing field impedance and capacitance of encapsulant with air and metal as boundaries.

S.No.	Encapsulant thickness (μm)	Air		Metal	
		Impedance (MΩ)	Capacitance (pF)	Impedance (MΩ)	Capacitance (pF)
1	182	203	7.86	110	14
2	240	170	9.12	107	13.68
3	286	151	11.02	113	14.3
4	394	136	13.12	115	14.43
5	540	138	13.51	137	13.51

5.6. Measurement of FFIS of encapsulants exposed to 3.5 wt % NaCl aqueous solution

FFIS of PU, CR and epoxy immersed in 3.5 wt % NaCl aqueous solution, were measured by FEF sensors at regular intervals of time. . The measurement frequency range was 100 Hz to 100 kHz. The electrical and dielectric properties of the material were estimated by fitting the impedance spectrum in the above mentioned frequency range [41]. FFIS of thin PU and epoxy encapsulants were measured by Type I FEF sensor. FFIS of thick PU, epoxy and CR encapsulants were measured by Type II FEF sensor. The water uptake and electrical degradation of encapsulants due to water ingress is estimated from the measured FFIS in coming chapters. Phase

angle spectra of encapsulant is a supporting information and hence measured only in some cases.

5.6.1. Thin encapsulants

Fringing field impedance spectra of PU and epoxy thin encapsulants were measured by Type I FEF sensor periodically for two months.

5.6.1.1. Polyurethane encapsulants

Fringing field impedance spectra of 410 μm thick PU encapsulant material exposed to 3.5 wt % NaCl aqueous solution, were measured by FEF sensor. The measured FFIS was a straight line and the corresponding phase angle was 90⁰ throughout the measured frequency range (Fig.57 & Fig.58). The spectrum is similar to the electrochemical impedance spectrum indicates that the current flow through the material was by capacitive coupling [41,117].

Fig.57. Fringing field impdenace spectra of 410 μm thick PU encapsulant immersed in 3.5 wt % NaCl aquoues solution for 60 days.

The FFIS shifts down with time as clear from the graph. The electrical impedance of the encapsulant decreased with time in all the frequencies. The decrease is observed more in the low frequency range of the spectrum. The electrical impedance at 100 Hz of the encapsulant decreased from 270 MΩ to 150 MΩ during the 60 days of immersion in NaCl solution.

The decrease in electrical impedance is due to the water ingress in the encapsulant as per literature. It is reported that even a good encapsulant contains inherent microscopic regions that are prone to attack by water and ions [120-123].

These microscopic regions are 'hydrophilic' in nature and these are regions of low molecular weight or low cross linked polymers. They take up water, have a low resistance to ion transport and are susceptible to water attack, e.g hydrolysis and dissolution. Hence the water uptake by the encapsulant results in decrease in electrical impedance. Phase angle of the impedance is in the capacitive region (near to 90°) throughout the evaluation period, indicates that the encapsulant act as a perfect dielectric material.
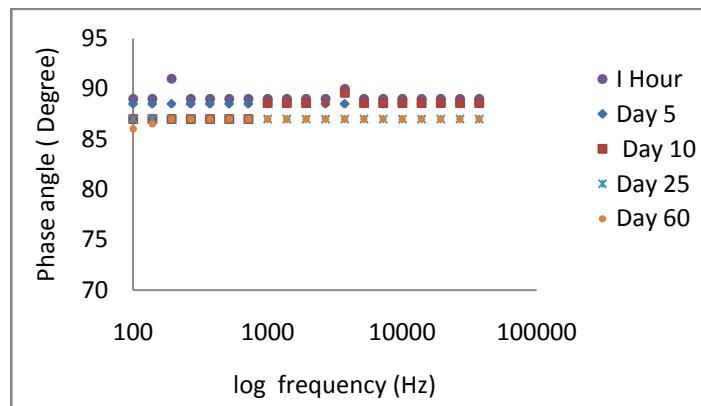
Fig.58. Variation of phase angle with time for 410 µm thick PU encapsulant exposed to 3.5 wt % NaCl aquoues solution for 60 days.

FFIS of 290 µm thick encapsulant immersed in 3.5 wt % NaCl aqueous solution is shown in Fig.59. Simialr to 410 µm thick encapsulant, 290 µm thick encapsulant also behaves as a dielectric material during the evaluation period.
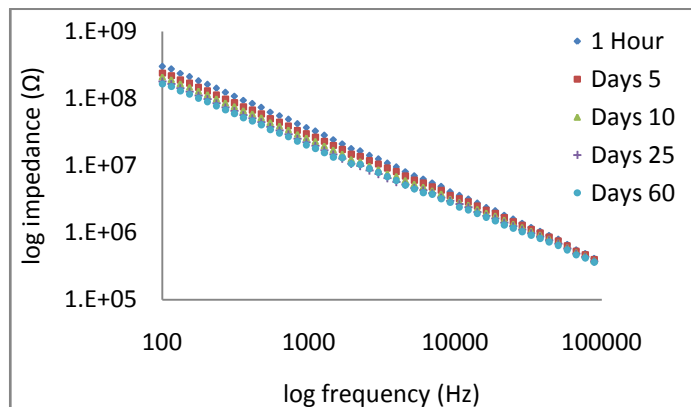
Fig.59. Fringing field impdenace spectra of 290 µm thick PU encapsulant immersed in 3.5 wt % NaCl in different days.

The phase angle remains in the capacitive region through out the evaluation period, indicates that the encapsulant is a dielectric material (Fig.60). The straight

lines in the FFIS shifted down as the immersion time increased. The impedance measured at 100 Hz, decreased from 300 to 155 MΩ.
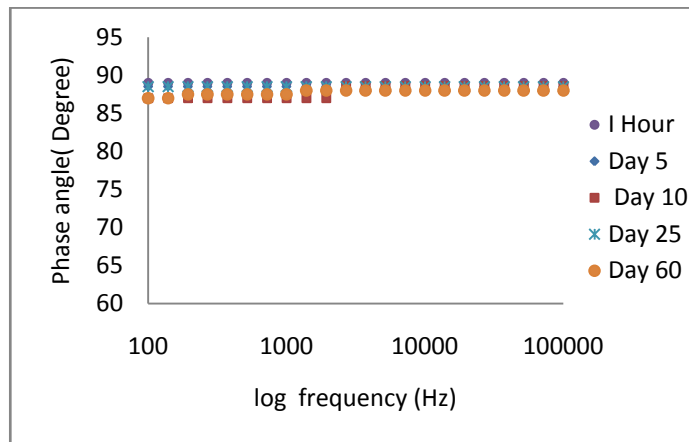
Fig.60. Variation of phase angle with time for 290 µm thick PU encapsulant exposed to 3.5 wt % NaCl aquoues solution for 60 days.

FFIS of 245 µm thick encapsulant immersed in 3.5 wt % NaCl aqueous solution is shown in Fig.61. The spectra is a straight line and shifted down during the evaluation period.
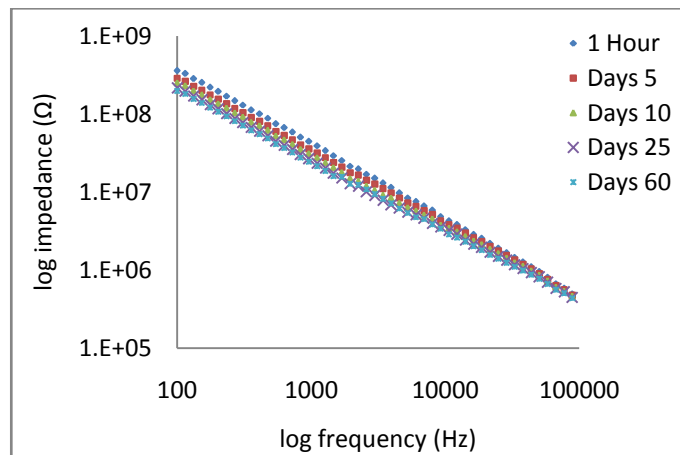
Fig.61. Fringing field impdenace spectra of 245 µm thick PU encapsulant immersed in 3.5 wt % NaCl in different days.

The straight line indicates that encapsulant acts as a dielectric coating through out the 60 days of evaluation period. The impedance (at 100 Hz) of the encapsulant decreased from 360 MΩ to 180 MΩ with time. It is clear from the the phase angle spectra that the angle remains in the capacitive region through out the evaluation period for all frequencies (Fig.62).
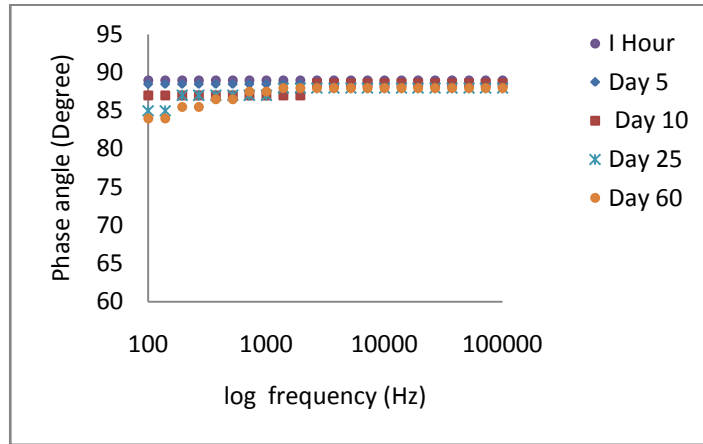
Fig.62. Variation of phase angle with time for 245 μm thick PU encapsulant exposed to 3.5 wt % NaCl aquoues solution for 60 days.

The measured FFIS of 183 μm thick encapsulant were straight lines during the evaluation period (Fig.63). The spectra shifted down as the immersion time progressed and   the impedance decreases from 400 MΩ to 190 MΩ during water ingress.
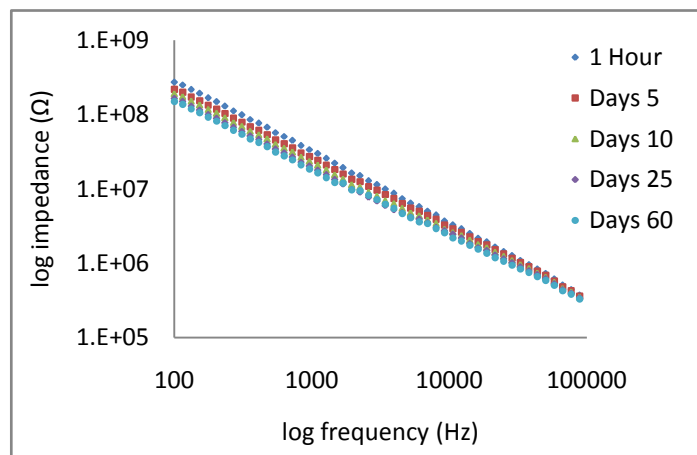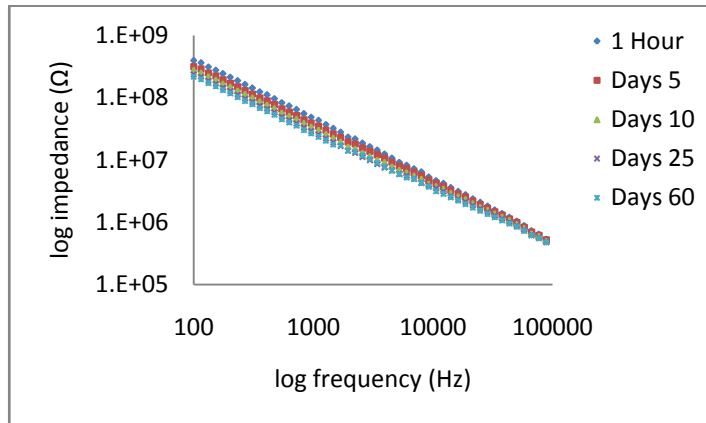

Fig.63. Fringing field impedance spectra of 183 μm thick PU encapsulant in 3.5 wt % NaCl aquoues solution for 60 days.
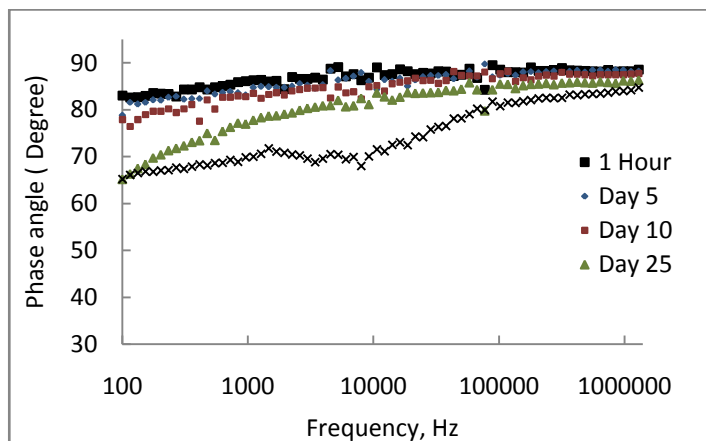
Fig.64. Variation of phase angle with time for 183 μm thick PU encapsulant exposed to 3.5 wt % NaCl aquoues solution for 60 days.

The encapsulant behaved as a dielectric material as indicated by the straight line in the spectra. This is supported by the phase angle value in the capacitive region(Fig.64). However, there was a small decrease in the phase angle from 90^0 to 65^0 towards the end of the end of the evaluation period.

Fringing field impedance spectroscopy could measure the decrease in the impedance of the encapsulant during water ingress for all the studied encapsulants. Also, there was a increase in impedance due to increase in encapsulant thickness as discussed in section 5.4. All the evaluated thin encapsulants (thickness varies from 183 to 410 μm) behaves as a perfect dielectric material and all shows phase angle in the capacitive region. However, water ingress has happened in all the encapsulants indicated by the decrease in electrical impedance.

As explained earlier, water attacks the micro hydrophilic regions in the encapsulant when it is immersed in saline water. First water uptake will be on the hydrophilic regions of top layers. Other regions in the bottom layer will be attacked during the course of time by the osmosis of water molecules [120]. The impedance of the encapsulant slowly decreases with increased amount of water and ions in the material. The next stage is the formation of a conductive path by joining of all these hydrophilic regions. This stage will be indicated by the phase angle 0° in the low frequency region of impedance spectra. It is obvious that the time taken for this second stage will be dependent on the thickness of the encapsulant. This stage did not observe even for the thinner encapsulant 183 μm during 60 days of evaluation. The stage at which phase angle reaches near to 0° was observed in aged epoxy encapsulant which is discussed below.

5.6.1.2. Epoxy encapsulants

Two types of epoxies were selected for the study; fresh epoxy (Araldite AY 103 and Aradur HY 951) and aged epoxy as mentioned in the chapter 3.

5.6.1.2.1. Aged epoxy encapsulants

FFIS of a 410 μm thick aged epoxy encapsulant was measured regularly in 3.5 wt % NaCl aqueous solution. The spectra was a straight line in the beginning and then a bend was observed in the measured spectra of 60th day (Fig.65). A significant reduction in electrical impedance of the aged encapsulant was observed

in the material .The initial impedance of the sample was ~124 MΩ and decreased to ~9 MΩ within 60 days.

In the initial periods of exposure, encapsulant showed a purely capacitive nature. At this stage the current transmission across the encapsulant is by capacitive coupling. This is indicated by the ~90^0 phase angle in the FFIS (Fig.66). During prolonged salt water exposure, electrical impedance decreased and a flat region was observed in the bode plot in the low frequency spectrum. It indicates that encapsulant lost its dielectric nature due to water ingress and this statement was supported by reduction in the phase angle to 20°.

Fig.65. Fringing field impedance spectra of 410 μm thick aged epoxy encapsulant exposed to 3.5 wt % NaCl aquoues solution for 60 days.
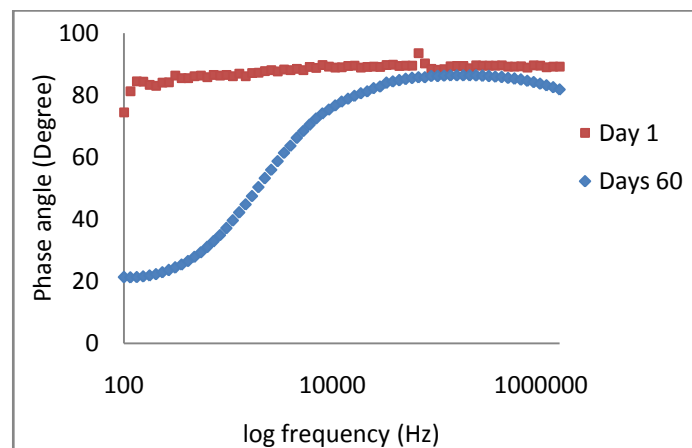
Fig.66. Phase angle variation of 410 μm thick aged epoxy encapsulant exposed to 3.5 wt % NaCl

It is reported that thermal oxidation of Bisphenol-A diglycidyl ether based epoxy leads to carbonyl and amide formation with subsequent chain scission[133]. Glass transition temperatures (Tg) of the polymer decreases and sol fraction

increases due the thermal oxidation [134]. After thermal oxidation, the polymer is expected to absorb more water due to the formation of hydrophilic degradation products in the polymer. Due to the more number of hydrophilic regions, the water and ions will ingress easily and results in a drastic reduction of electrical impedance.

5.6.1.2.2. Fresh epoxy encapsulants

The measured FFIS of a fresh epoxy encapsulant of thickness 410 ± 10 μm exposed to 3.5wt % NaCl aqueous solution, is shown in Fig. 67.   The FFIS of fresh epoxy encapsulant has higher impedance than aged encapsulant. The initial impedance of the sample was 360 MΩ and decreased to 198 MΩ during 60 days of exposure in saline water. The phase angle spectra showed that the dielectric nature of the encapsulant retained during 60 days of exposure (Fig.68).

Fig.67. Fringing field impedance spectra variation of 410 μm thick epoxy encapsulant exposed to 3.5 wt % NaCl aqueous solution.

Fig.68. Phase angle variation of fresh 410 μm thick epoxy encapsulant exposed to 3.5 wt % NaCl aqueous solution

FFIS of a 305 µm thick encapsulant immersed in 3.5 wt % NaCl aqueous solution, is shown in Fig.69. Impedance spectra is a perfect straight line indicates that it is a perfect dielectric material. The impedance of the encapsulant decreases with time due to the water ingress as explained earlier. Also, the impedance of the encapsulant increases due to the reduction in encapsulant thickness. The effect of encapsulant thickness on the impedance of the sensor was explained in section 5.4 of this chapter.
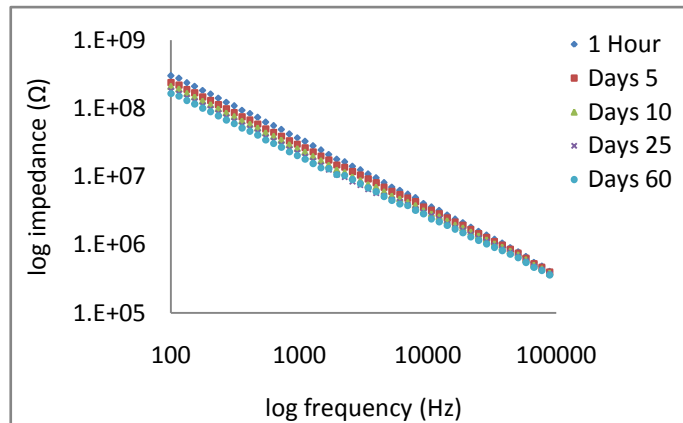
Fig.69. FFIS variation of 305 µm thick epoxy encapsulant in 3.5 wt % NaCl for 60 days

Fringing field impedance spectrum of 252 µm thick epoxy encapsulant is shown in Fig.70. The impedance increased from 300 MΩ to 360 MΩ due to decreased encapsulant thickness. This encapsulant behaves as a dielectric material indicated by the perfect straight line. Encapsulant retained its dielectric nature during 60 days of evaluation.
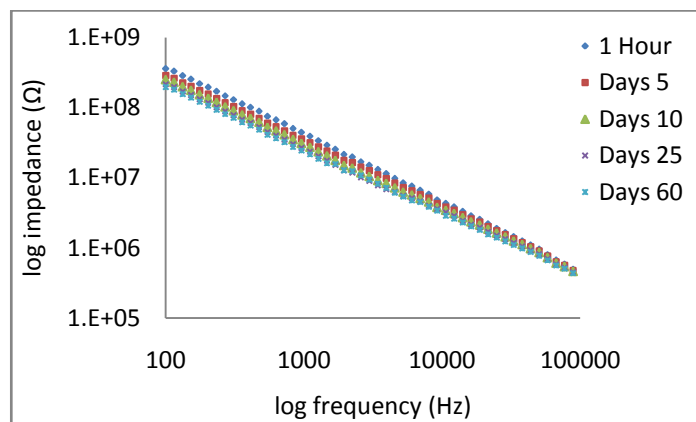
Fig.70. Fringing field impedance spectra variation of 252 µm thick epoxy encapsulant in 3.5 wt % NaCl for 60 days

Fringing field impedance spectrum of 180 μm thick epoxy encapsulant is shown in Fig.71. Similar to higher thick encapsulants, 180 μm thick encapsulant also retains its dielectric nature during the evaluation period. The impedance of the encapsulant is high compared to higher thick encapsulants. Impedance spectra is a perfect straight line indicates the dielectric nature of the encapsulant.
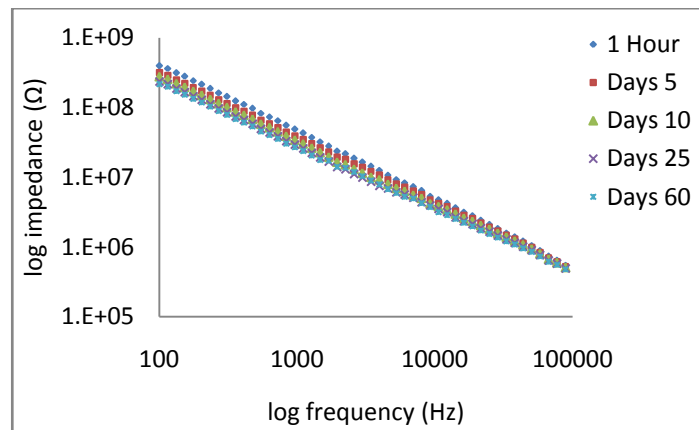
Fig.71. Fringing field impedance spectra variation of 180 μm thick epoxy encapsulant in 3.5 wt % NaCl aqueous solution for 60 days

5.6.2. Thick encapsulants

The fringing field impedance spectra of thick encapsulants were measured by Type II FEF sensor. Three thick encapsulant samples were selected for study; 2 ± 0.2 mm thick PU, CR and epoxy encapsulant. The low frequency phase angle spectra were highly noisy for all the thick encapsulants and hence could not be recorded due to instrument limitations

5.6.2.1. Polyurethane encapsulants

The fringing field impedance spectra of 2 ± 0.2 mm thick PU encapsulant in saline water is shown in Fig. 72. The measured impedance spectrum of all the days were straight line. The spectrum line shifted down with time of immersion as in the case of thin encapsulants. The value of impedance at 100 Hz decreased from 60 MΩ to 45 MΩ. The phase angle spectra was 90 $^\circ$ throughout the evaluation period (Fig.73). The phase angle spectra in the low frequency region were highly noisy and hence could not be recorded due to the hardware limitation of the measuring instrument.

FFISY could measure these changes and these changes were taken for the estimation of water uptake and electrical degradation in the encapsulant in chapter 7 & 8
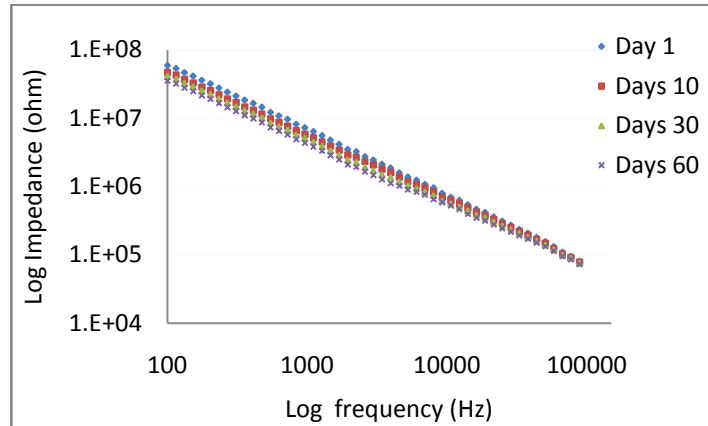
Fig.72. Fringing field impedance spectra of 2 mm thick PU encapsulant in 3.5 wt % NaCl aqueous solution for 60 days
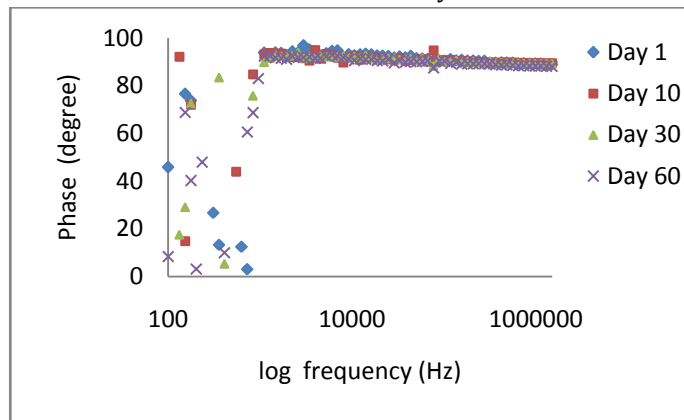
Fig.73. Phase angle spectrum of 2 mm thick PU encapsulant in 3.5 wt % NaCl aqueous solution for 60 days

5.6.2.2. Polychloroprene encapsulants

The measured fringing field impedance spectra of 2 ± 0.2 mm thick polychloroprene (CR) encapsulant immersed in saline water is shown in Fig.74. The impedance of the CR encapsulant has higher value than PU encapsulant of same thickness, 72 MΩ and 60 MΩ respectively. The measured spectrum of all days were straight line and phase angle was 90⁰ though out the evaluation period (Fig.75). The low frequency phase angle spectra were highly noisy and hence could not be recorded due to instrument limitations.
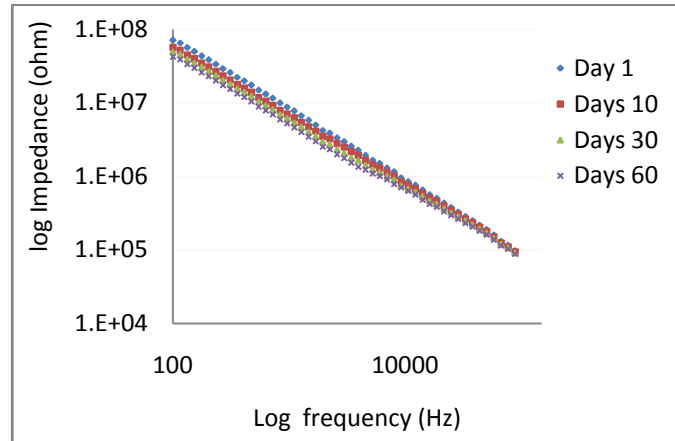
Fig.74. Fringing field impedance spectra of 2 mm thick CR encapsulant in 3.5 wt % NaCl aqueous solution for 60 days
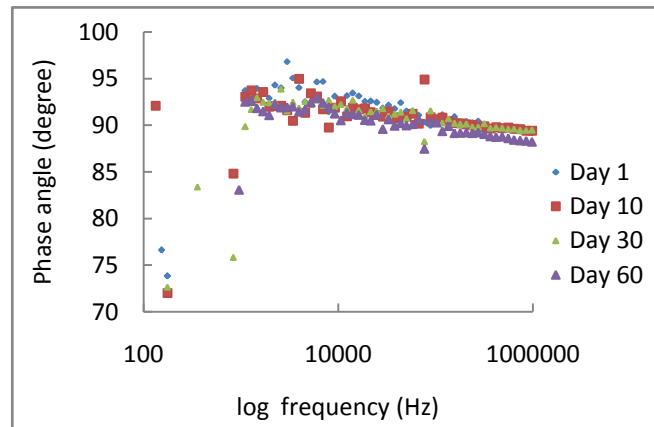
Fig.75. Phase angle spectra of 2 mm thick CR encapsulant exposed to 3.5 wt % NaCl aqueous solution for 60 days

5.6.2.3. Epoxy encapsulants

The measured FFIS of 2 ± 0.2 mm thick epoxy encapsulant immersed in saline water is shown in Fig. 76. Impedance spectra were a straight line and the phase angle was 90^0 throughout the evaluation period (Fig.77). The spectrum shifted down as the encapsulant immersion time increased.

Thick encapsulants were all evaluated using Type-II FEF sensor. Type-II FEF sensors have larger area than Type-I sensors which was used for the evaluation of thin encapsulants. Hence, the measured impedance of thick encapsulants was one order less than thin encapsulants due to the difference in inbuilt impedance. PU and CR show higher impedance value than epoxy for the same encapsulant thickness. This may be due to the inherent material properties. And in addition, due to the increase in encapsulant thickness the impedance of the encapsulant coated sensor decreases, which were discussed in section 5.4 of this chapter.
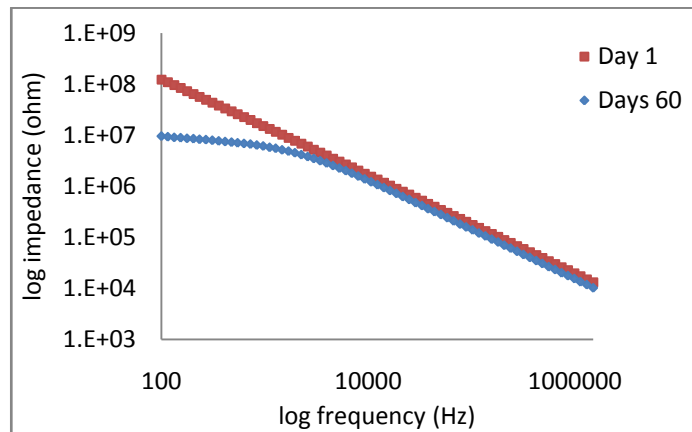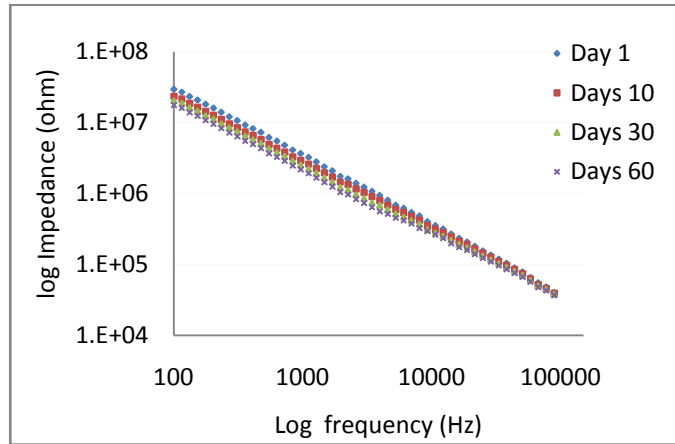
Fig.76. Fringing field impedance spectra of 2 mm thick epoxy encapsulant exposed to 3.5 wt % NaCl aqueous solution for 60 days
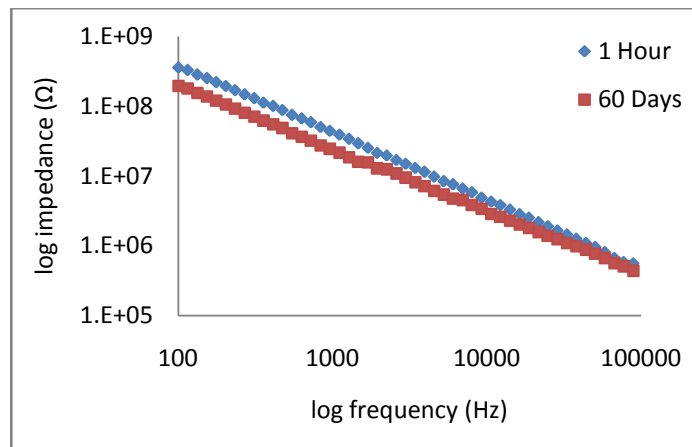

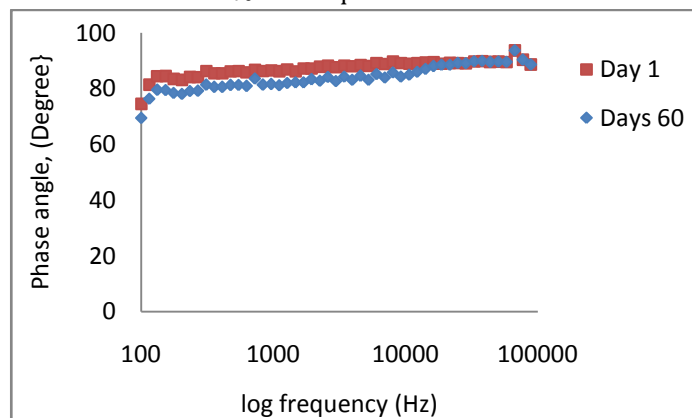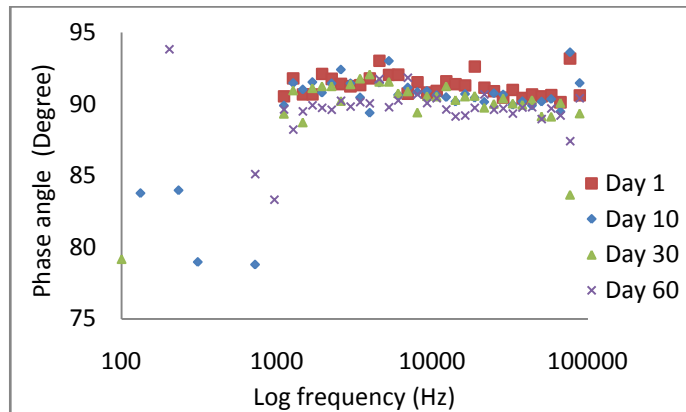Fig.77. Phase angle spectra of 2 mm thick epoxy encapsulant exposed to 3.5 wt % NaCl aqueous solution for 60 days

5.7. Fringing field impedance spectra of filler loaded encapsulants

Different types of filler loaded PU encapsulants having 1± 0.05 mm thickness were selected to study the effect of fillers on FFIS. Also changes in FFIS during its exposure to 3.5 wt % NaCl aqueous solution were studied for 60 days. FFIS was recorded using type-II FEF sensor. The phase angle spectra were highly noisy and hence not reported in this thesis. .

5.7.1. Carbon black loaded polyurethane encapsulants

CB was added in 2 wt%, 4 wt% and 6 wt% in the PU matrix to study the effect of CB loading on fringing field impedance spectra. The fringing field impedance spectra shifts downwards on addition of CB (Fig.78). The impedance decreases from 126 MΩ to 68 MΩ on addition of 6 wt % CB. FEF carbon black powder reduces the electrical resistivity of the compound when used as filler [80].

As the CB % increased in the PU matrix, the impedance of the loaded encapsulant decreased.

FEF senor could measure the decrease in impedance on the addition of carbon black. The order of impedance is: 2 wt% > 4 wt%> 6 wt%. The reason for the rank may be explained as follows: the organic binder of the coating is non-conducting, and the number of the charge carriers such as active electrons are very less so the electrical resistance is high. When a conductive additive is added to the binder, there will be more charge carriers, so the conductivity of the coating will be increased and the electrical resistance of the coating will be decreased with increasing carbon black powder.

A small bend was observed in the low frequency region. This is similar to the appearance of flat region in electrochemical impedance spectra in the low frequency region. The flat region indicated that a conductive path was formed through the encapsulant. A flat region was observed even before the water ingress in the coating in the case of coatings with metallic fillers or conductive fillers. This is characteristic of conductive coating [128,129]. The flat region is more prominent upon addition of more and more carbon black fillers.
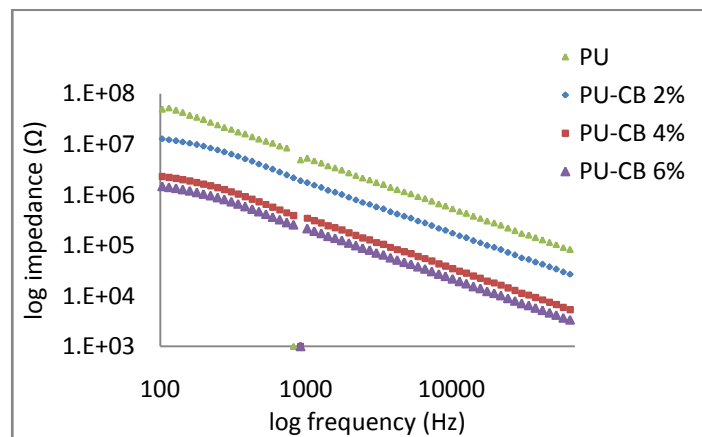
Fig.78. Fringing field impedance spectra of 1 mm thick PU-CB encapsulant with different % loading exposed to 3.5 wt % NaCl aqueous solution for 60 days

The measured fringing field impedance spectra of 1 mm thick 2 % CB loaded PU encapsulant exposed to 3.5 wt % NaCl aqueous solutions, is given in Fig. 79. The electrical impedance value at 100 Hz, decreased from 25 MΩ to 14 MΩ during the evaluation period.
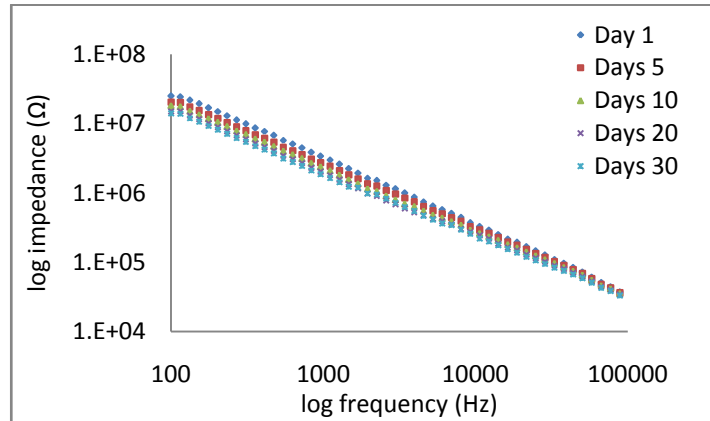
Fig.79. Fringing field impedance spectra of 1 mm thick PU-CB 2% encapsulant exposed to 3.5 wt % NaCl aqueous solution for 30 days.

5.7.2. Nano silica loaded polyurethane encapsulants

There was no appreciable changes between the fringing field impedance spectra of 2 wt%, 3 wt% and 4 wt% loaded nano silica fillers (Fig. 80). The addition of 4 wt% nano silica fillers in PU may not be sufficient to impart any change in the impedance spectra. More addition of nano silica was avoided as the nano effect will be lost on higher addition of nano fillers.
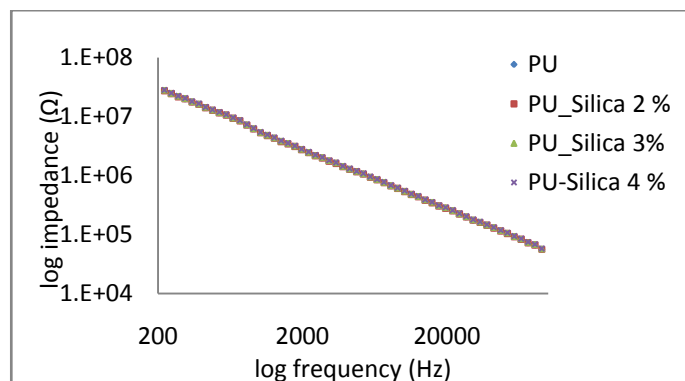
Fig.80. Fringing field Impedance spectra of 1 mm thick PU encapsulant loaded with different percentage of silica

The changes in the FFIS   of   PU encapsulant loaded with 4 % nano silica, immersed in 3.5 wt % NaCl aqueous solution for a period of 60 days, is given in Fig.81. The impedance of the encapsulant decreases with time during the evaluation period. The initial low frequency impedance was 30 MΩ and then decreases gradually to 17.1 MΩ during the evaluation period.
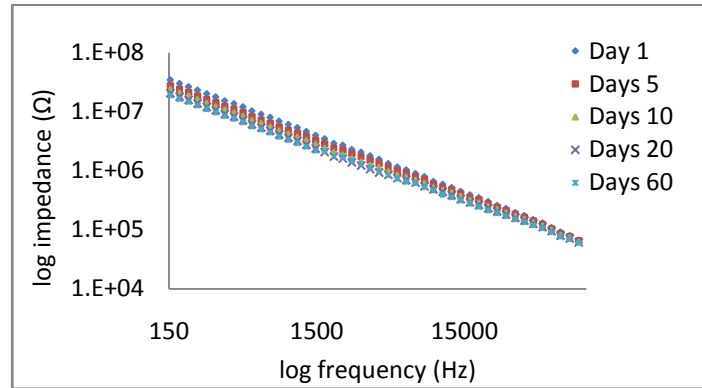
Fig.81. Fringing field impedance spectra of 1 mm thick PU-silica 4 % encapsulant in 3.5 wt % NaCl solution for 60 days

However, the percentage of decrease of electrical resistance was low for nano silica loaded PU compared to neat PU. The changes in the capacitance and electrical resistance are estimated from the measured FFIS in chapters 7 & 8 to determine the water uptake electrical degradation in the encapsulant.

5.7.3. PANi loaded polyurethane encapsulants

PANi is used in the range of 10 to 40 wt % in the polymer coating to get antifouling properties during its use in sea water [82, 83]. At this percentage, sufficient PANi may be available on the surface of the coating to exhibit any antifouling characteristics. The higher percentage is always limited by the processability of the system to form a smooth coating. In the study, three PANi-PU systems are selected; 10, 15, 20% for the reason mentioned above.
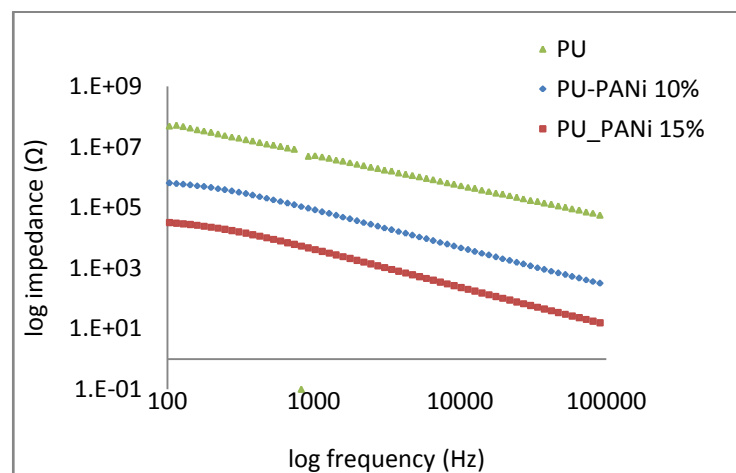
Fig.82. Fringing field impedance spectra of 1 mm thick PU encapsulant loaded with different percentage of PANi

Fig.82 shows the fringing field impedance spectra of PU-PANi system with different loading percentage as mentioned in the figure. Addition of PANi decrease the electrical impedance of the encapsulant. It is obvious that, the total impedance of the encapsulant reduces, when conductive PANi is added to the system.The changes in fringing field impedance spectra of of 20% PANi in 3.5 wt % NaCl, was not able to measure by the impedance analyser due to hardware limitations. The readings were out of range of the impedance analyser.

In brief, a clear change in the fringing filed impedance spectra of the encapsulant during the water ingress was observed and from these changes, the performance of the encapsulant could be inferred. These measured fringing field impedance spectra will be used to estimate the changes in capacitance and electrical resistance to find out the percentage of water uptake and electrical resistance degradation respectively in chapter 7 & 8.

5.8. Determination of curing profile of thermoset resins by FEF sensor

Over the past decades, different techniques have been experimented for cure monitoring of thermosetting resins, including differential scanning calorimetry (DSC) [84, 85], dynamic mechanical thermal analysis (DMTA) [86, 87], dielectric analysis (DEA) [88–90], Fourier Transform FT-IR spectroscopy [91], near infrared spectroscopy (NIR) [92,93], and Raman spectroscopy [94]. However, many of these cure monitoring methods are laboratory based and hence not suitable for industrial application, require expensive equipment, are destructive, and typically suited to working with small samples of restricted dimensions [95].

As an extension of present research work, the developed FEF sensor was used to measure the curing profile of thermoset resins. In the present approach, a simple low cost miniature cure monitoring system using FEF sensor with first order filter measuring circuit is developed. This simple measuring circuit records the cure profile in terms of voltage-time curve.

5.8.1. Theory

 FEF sensor is an interdigitated capacitor as discussed in previous sections. By applying different potentials on the interdigitated electrodes, $V1$ and $V2$, the generated electric field travels from one electrode, penetrating the dielectric film to

the other electrode. The capacitance measured between the electrodes depends on the dielectric constants of the dielectric film. In this application, the thermoset resin acts as the dielectric film.

The main characteristic of thermosets is that during their processing, they undergo a molecular crosslinking process, called "curing", during which they change irreversibly from being viscous liquids to rigid and highly cross-linked polymer solids. The dielectric properties of the material change during the curing process [124] and accordingly capacitance changes which can be monitored by the sensor.

5.8.2. First order high pass filter circuit

A low cost measuring circuit (first order high pass filter circuit) has been chosen for this application. The circuit consists of an AC source (V_{ac}), a resistor (R), and a capacitor (C) as shown in Fig.83. The transfer function of the filter circuit (H (f)) is calculated as follows [75]:
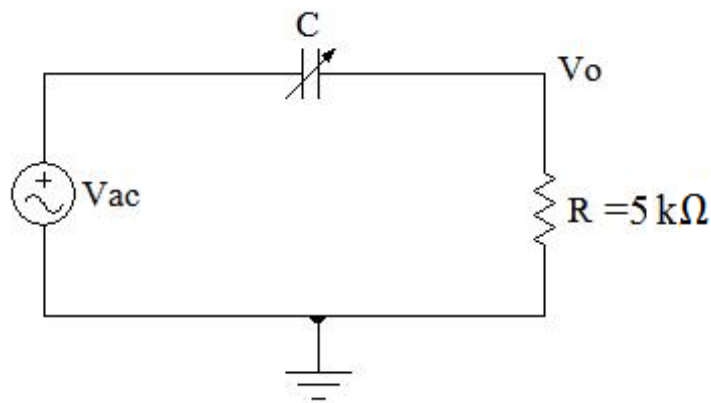
Fig.83. A first order high pass filter circuit [75]

$$H(f) = \frac{V_0}{V_{ac}} = \frac{R}{R + \frac{1}{j\,2\pi f C}} \qquad (14)$$

$$|H(f)| = \frac{R}{\sqrt{R^2 + \frac{1}{(2\pi f C)^2}}} \qquad (15)$$

$$f_c = \frac{1}{2\pi RC} \qquad (16)$$

Where V_o is the output voltage, V_{ac} is the driving signal voltage, f is the operating frequency, and f_c is the cutoff frequency.

The transfer function of the circuit for the fabricated sensor is illustrated in Fig.84 when R=5 kΩ and sensor capacitance, C=12 pF, then the cut off frequency is 3.6 MHz. In Fig.84, the transfer function characteristic illustrates that the slope is linear in the transition zone, while other frequencies, which are higher than f_c, get saturated.
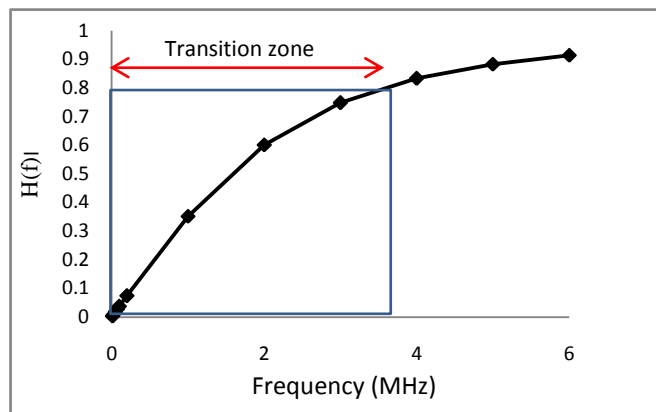
Fig 84. The transfer function of the first order high pass filter with R=5 kΩ and C=12 pF

5.8.3. Materials for cure profile determination

Two types of epoxy were selected with a different cure time. Type-1 was Araldite AY 103 resin and Aradur HY 951 hardener with a ratio of 1:1.3. Araldite AY 103 is Bis-Phenol A-Epichlorohydrin based epoxy resin system and Aradur is an amine based hardener. This epoxy system is of low viscosity with a 24hour curing time at room temperature(∼27°C).

Epoxy Type-2 epoxy is an embedding resin (Fluka) for electron microscopy applications. This is a three component system that comprises of the following;

Resin   :Triglycidyl ether of glycerol

Hardner-1   :Dodecenyl succinic anhydride

Hardner-2   :Methyl nadic anhydride

The resin- hardener ratio is 0.5:0.23:0.27 and the epoxy system was mixed as per the direction of the manufacturer.2 ml of accelerator DMP30 (Tris

(dimethylaminomethyl) phenol) was added to this mixture to accelerate the reaction. This system had a 48 hour cure time at room temperature ($27 \pm 1°C$).

5.8.4. Calibration of sensor

Output voltage for the five different FEF sensors with PD 460 μm was measured in liquids with known dielectric constants; hexane, ethyl acetate, 2-propanol and ethyl alcohol [Fig.85].
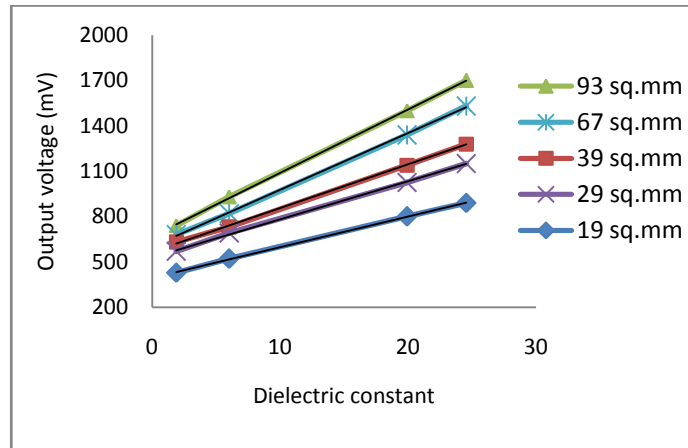
Figure 85.Effect of sensor area on the sensor output voltage for the dielectric constant variation 1-25
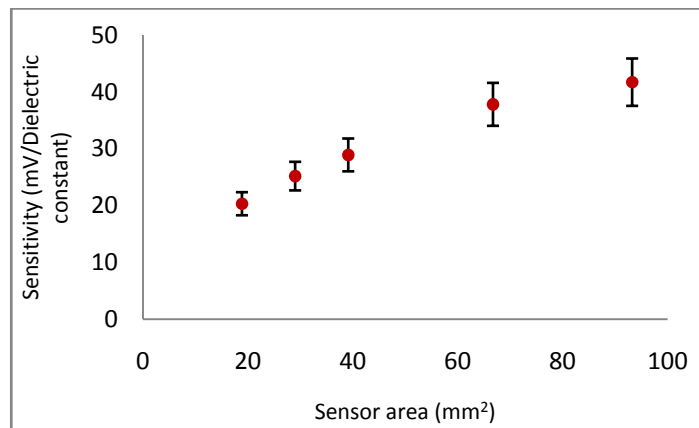
Fig.86. Effect of sensor area on sensitivity of the sensor

A linear relation exists between dielectric constant and sensor output for all the sensors at 1 MHz. The relation between sensitivity and sensor area is linear which is evident from the graph (Fig.86). 40 mV per change in dielectric constant of the material was obtained for sensor having area 93 mm^2.

The sensor output is measured by FEF sensor having area 93 mm^2 at different frequencies over the study range of dielectric constant. This was   to

analyse the effect of frequency on linearity and repeatability [Fig.87]. The linearity of the sensor at different measuring frequency is plotted for the dielectric range. The value of the measured output decreases at lower driving signal frequency.
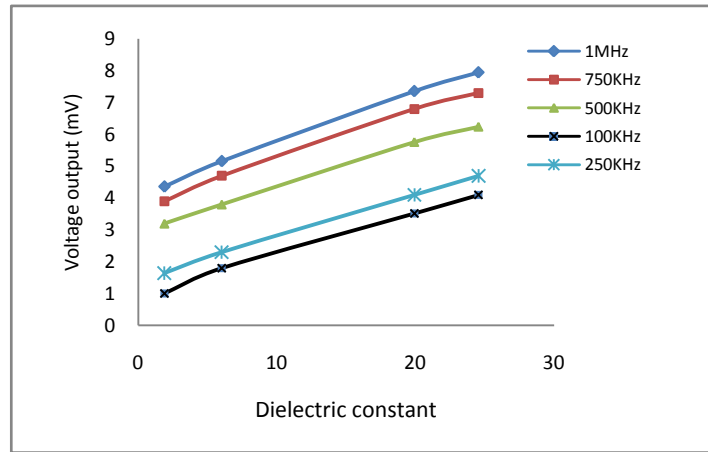
Fig.87. Variation of measured capacitance of the fabricated sensors with sensor area.

5.8.5. Cure profile monitoring

The epoxy resin system is applied over the FEF sensors and a sinusoidal signal of 10 volt at 1MHz, was applied to the sensor by a function generator. The voltage was measured from the output. The thickness of the resin layer over the sensor was 2 mm above the penetration depth of the sensor and hence the change in thickness of the resin layer due to shrinkage will not affect the output voltage.
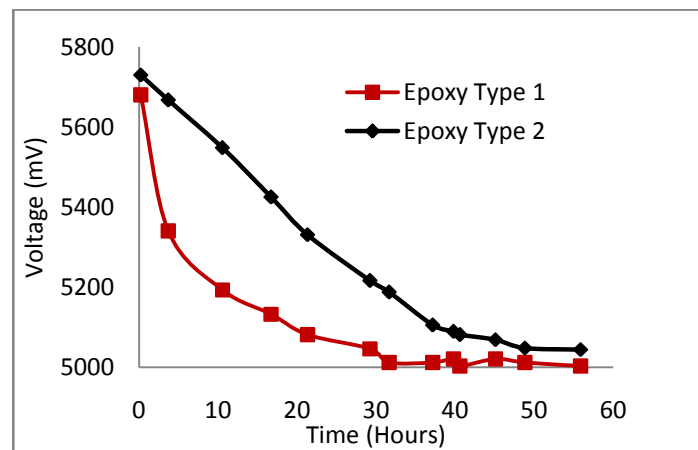
Fig.88. Cure profile of two different epoxy systems measured by FEF sensor.

Two epoxy systems with known and different cure time were studied using the calibrated FEF sensor. The resin immediately after mixing with hardener is poured on the sensor which was kept on petridish. The voltage output is measured

at regular time intervals and the variation of voltage with time is plotted as shown in Fig.88. Epoxy Type 1 immediately started to cure as indicated by a steep decrease in voltage and 50% of the curing occurs in the initial five hours itself. In the initial stages, the resin changes from a free flowing low viscosity liquid to a highly viscous paste. Curing is completed in 30 hours indicated by the flat voltage response.

During the curing process, the quantity of free polarisable molecules decrease which is attributed to the lowering of dielectric constant. As a result, voltage decreases and finally reaches saturation towards the complete curing. The cure profile of Epoxy Type 2 indicates that around 48 hours are required for the complete curing at 27 °C. The cure time given by the manufacturers supports this data [138].

5.9. Conclusion

A measurable change was observed in the fringing filed impedance spectra of all the studied encapsulants, during the water ingress. These measured fringing field impedance spectra will be used to estimate the changes in capacitance and electrical resistance to find out the percentage of water uptake and electrical resistance degradation respectively in chapter 7 & 8.

FEF sensor can be used for monitoring the curing process of thermoset resin. The sensor is sensitive to measure the change in dielectric constant during the curing reaction of a thermoset resin. 40 mV per unit change in dielectric constant of the material was obtained for Type I sensor. The low cost material and the fabrication process employed in developing the sensor provide a cost effective method to monitor the curing process of thermosetting resins.

CHAPTER – 6

Electrochemical Impedance Spectroscopy

6.1. Objective

To measure and analyze the electrochemical impedance spectrum (EIS) of underwater encapsulants immersed in 3.5 wt % NaCl aqueous solution continuously for two months in order to compare with the results of FFISY study.

6.2. Introduction

Electrochemical impedance spectroscopy (EISY) is used extensively for the characterization of commercial coatings like paints, varnishes etc. These are thin coatings of less than 100 μm thickness, applied usually on metal substrates. In a typical EISY study, the coating is exposed to an electrolyte (usually NaCl) and the electrochemical impedance spectra is measured at regular intervals of time until a substantial damage occurs to the coating. The electrochemical impedance spectra is fitted to an appropriate equivalent circuit and the values of circuit components are estimated using non linear least square method with the help of a software [5].

This is a well established technique to monitor the degradation of coating in wet conditions. The coating degradation is assessed by monitoring the change in different parameters such as coating capacitance, electrical resistance (usually described as pore resistance), double layer capacitance and polarization resistance etc. [3, 5,116]. In case of very thick organic coatings like encapsulants, it takes a long time to detect any significant sign of corrosion [119], as a result a significant portion of the previous studies was devoted to the evaluation of thin coatings [109-113].

The aim of the study was to compare the water uptake and electrical degradation estimated by FFISY with that of EISY. Water uptake and electrical degradation was measured for same encapsulant materials and thickness taken for FFISY studies in the last chapter. Similar to FFISY study, monitoring of changes in the encapsulant capacitance and electrical resistance were done for two months. A higher percentage of water uptake occurs in coating in the initial few hours to days of

immersion. After the initial water ingress, the water uptake slows down and reaches almost a saturation stage. Water uptake percentage from the initial period of immersion give quantitative information about the water barrier properties of encapsulants [109]. Substantial percentage of electrical degradation also occurs due to water ingress in the encapsulants during these initial periods. Hence 60 days data was sufficient to compare the results of FFISY and EISY.

In this chapter, electrochemical impedance spectra of polyurethane, polychloroprene and epoxy encapsulants immersed in 3.5 wt % NaCl aqueous solutions, were measured periodically. Also, electrochemical impedance spectra of polyurethane loaded with different type and percentage of fillers were also measured. The estimation of values water uptake and electrical degradation of encapsulants were done by equivalent circuit fitting of electrochemical impedance spectra. Hence , phase angle spectra of all encapsulants were not measured except a few cases for supporting information. Also, phase angle spectra were very noisy in many measurements especially in thicker encapsulants due to hardware limitations of measuring instrument.

The measured electrochemical impedance spectra was used for the estimation water uptake and electrical degradation in chapter 7 & 8 respectively. These values of water uptake and electrical degradation was used to compare with the results of FFISY technique. Evaluation of encapsulants was done under two categories; (1) Thin encapsulants and (2) Thick encapsulants.

6.3. EIS studies of thin encapsulants

PU encapsulant of different thickness below ~500 μm, was selected for measuring electrochemical impedance spectra. The effect of thickness on the electrochemical impedance spectra was studied by measuring the electrochemical impedance spectra of polyurethane of different thickness.

6.3.1. Polyurethane encapsulants

EIS of 153 μm thick PU encapsulant exposed to 3.5 wt% NaCl solution is shown in Fig. 89. The EIS were measured periodically at regular intervals for two months. The impedance spectra of encapsulant shifts down with time and he spectra of the 40th and 60th day showed a plateau in the low frequency region. A plateau

region in the EIS indicates that in this region, the measured impedance is frequency independent [3]. In other words, the impedance is purely resistive. The charge transfer across the encapsulant is similar to that in a resistor.
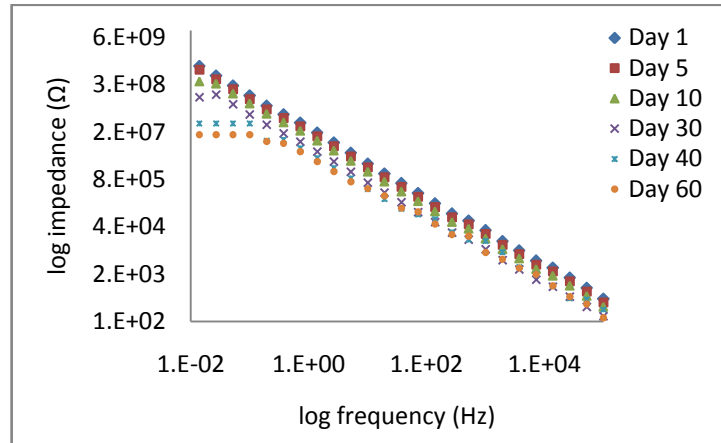
Fig. 89: Electrochemical impedance spectra of a 153 μm thick PU encapsulant

The phase angle between applied voltage and resultant current give indication about the mode of charge transfer across the encapsulant. If the phase angle between voltage and current is 90° or near to that, charge transfer across the encapsulant is similar to that through a capacitor. In other words, encapsulant acts as a dielectric material. If the phase angle between voltage and current is 0° or near to that, charge transfer across the encapsulant is similar to that through a resistor. In other words, encapsulant acts as a resistor and a resistor (conductor) path is formed through the encapsulant [24]. In EISY, this resistance is called pore resistance. Pore resistance is the electrical resistance of the coating when electrical current pass through the pores filled with water and ions. The impedance value in the plateau region in the low frequency range of spectra is approximately equal to the sum of pore resistance and solution resistance [5].

Hence, the presence of flat region in the electrochemical impedance spectra is the indication of water and ions ingress in the coating through micro pores [3]. In the case of 153 μm PU encapsulant, phase angle was around 90° in the initial days, indicates that encapsulant was a perfect dielectric material (Fig.90). However, phase angle decreased to 0° after 40 days which indicate the water ingress in the encapsulant and resultant pore resistance development. However, there is no indication of formation of double layer formation (presence of two bends in the

curve) and hence 153 μm encapsulant acts as a barrier to water during the evaluation period [3,4].
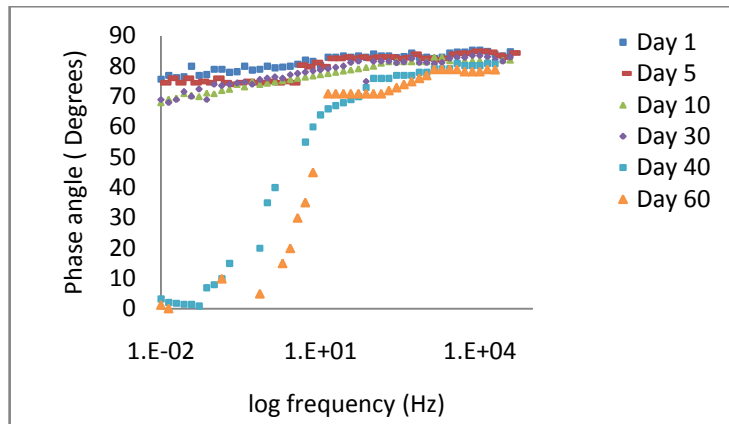
Fig. 90. Electrochemical phase spectra of a 153 μm thick PU encapsulant

Electrochemical impedance spectra of 182 μm thick encapsulant is shown in Fig. 91. A plateau was observed in the low frequency region of 60th day spectra. The spectra of encapsulant measured before 60th day, was a perfect straight line. The corresponding phase angle spectra of different days (Fig.92) indicate the encapsulant was a perfect dielectric material just before 60th day. The phase angle spectrum of 60th day is 0 º in the low frequency regions confirms the formation of a conductive path in the encapsulant.
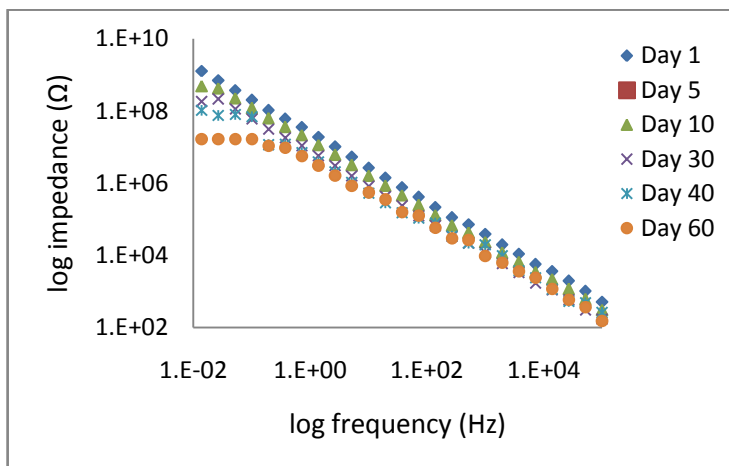
Fig. 91: Electrochemical impedance spectra of a 182 μm thick PU encapsulant

However, water ingress started from the initial hours as understood from the decrease in impedance. The pore resistance appeared in the impedance spectrum towards the end of 60 days whereas it was the end of 40th day in 152 μm thick

encapsulant. The formation of conductive path was delayed in 182 μm thick encapsulant due to increase thickness. Also, it is to be noted that, the low frequency impedance value increased from ~ 1.1 GΩ to ~1.3 GΩ due to increased thickness.
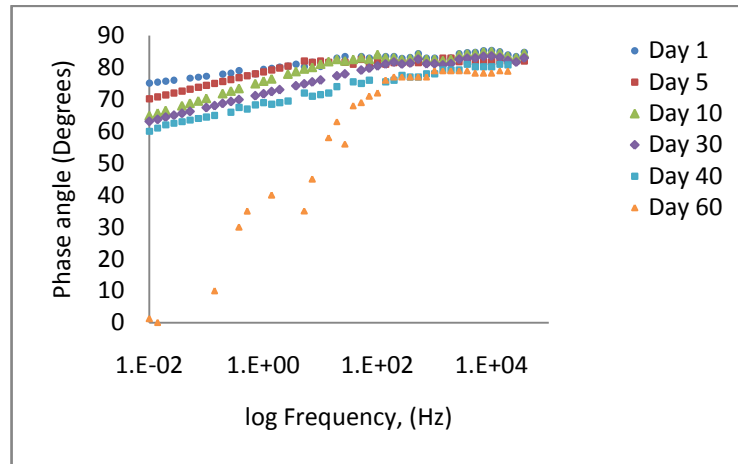
Fig. 92: Electrochemical phase spectra of a 182 μm thick PU encapsulant

Electrochemical impedance spectra of 240 μm thick encapsulant immersed in 3.5 wt% NaCl for two months are shown in Fig. 93. Impedance at lower frequency has increased from 1.3 GΩ to 1.5 GΩ due to increased thickness. The encapsulant performed as an excellent dielectric material with a straight impedance plot in all the days of evaluation. However, the impedance of the encapsulant decreased with time. It indicates that water ingress started in the encapsulant material and as a result electrical resistance decreased [117]. A conductive path across the encapsulant was yet to form at this stage.

Fig. 93: Electrochemical impedance spectra of a 240 μm thick polyurethane encapsulant

Fig. 94 shows the electrochemical impedance spectra of a 286 μm thick encapsulant measured in different days for two months period. The measured spectra was a straight line in all the days. In other words, dielectric nature of the encapsulant remained same during the evaluation period. But, the low frequency impedance of the encapsulant decreased with time during the evaluation period.
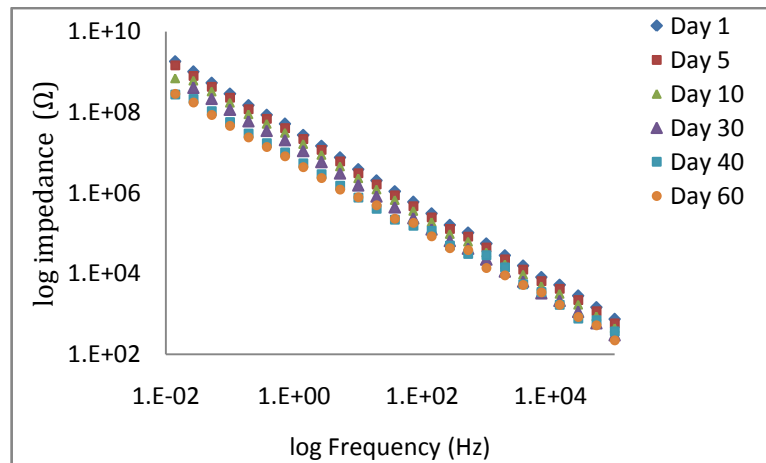
Fig. 94: Electrochemical impedance spectra of a 286 μm thick polyurethane encapsulant

The measured electrochemical impedance spectra of 406 μm thick encapsulant in different days is shown in Fig.95. The spectra measured in the all days were a straight line indicates that encapsulant performed as a dielectric material during the 60 days evaluation[117]. This encapsulant has impedance (100 mHz) of 2.2 GΩ in the beginning which was higher than other thinner encapsulants previously studied. A conductive path did not form in this encapsulant similar to 286 μm during the measurement period.

Fig. 95: Electrochemical impedance spectra of a 406 μm thick polyurethane encapsulant

6.3.2. Epoxy encapsulants

The measured electrochemical impedance spectra of 180 ± 10 μm thick epoxy encapsulant exposed to 3.5 wt% NaCl solution is shown in Fig.96. The spectra were measured at regular intervals for two months. A plateau region was observed on the 60th day of spectra. This was similar behaviour as that of 180 μm thick polyurethane encapsulant.
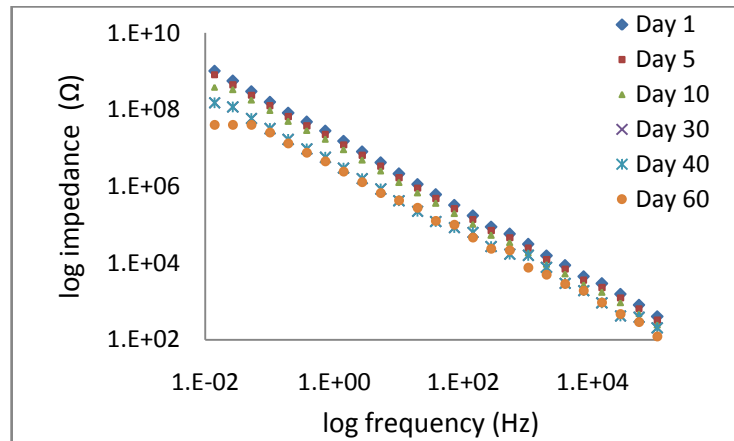
Fig. 96: Electrochemical impedance spectra of a 180 μm thick epoxy encapsulant
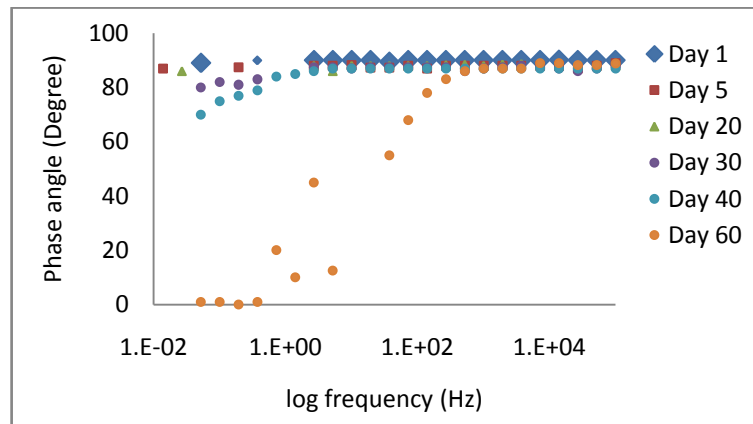
Fig. 97: Phase spectra of a 180 μm thick epoxy encapsulant

The phase spectra of the encapsulant reached 0^0 on 60th day (Fig.97). Water ingress occurred in the encapsulant at this stage and resulted in electrical degradation. It is known that, a complete failure of encapsulant. i.e. a stage at which water molecules permeated to the other side of the encapsulant (interface between encapsulant and metal substrate) is indicated by two bends in the impedance spectra [117]. It is due to the double layer capacitance formation at the encapsulant metal interface. This stage was not observed in the measured spectra during this evaluation.

This indicates that encapsulant still performs as a barrier to water.
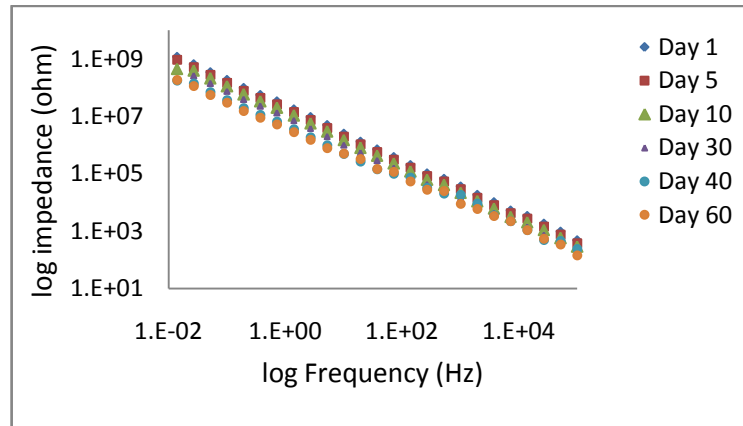
Fig. 98: Electrochemical impedance spectra of a 252 μm thick epoxy encapsulant

Electrochemical impedance spectra of 252 ± 10 μm thick epoxy encapsulant are shown in Fig. 98. The spectra are a straight line without any plateau in the curve. Encapsulant performed as a good dielectric material during the evaluation period. As observed in all other cases, the electrical impedance decreased as the time progressed.
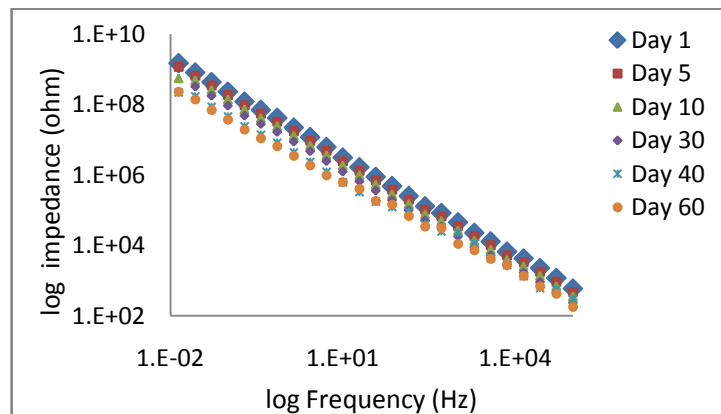
Fig. 99: Electrochemical impedance spectra of a 305 μm thick epoxy encapsulant

Electrochemical impedance spectra of 305 ± 10 μm thick epoxy encapsulant are shown in Fig. 99. The impedance of the encapsulant increased from 1.2 GΩ to 1.5 GΩ (at 10 mHz) due to the increased thickness. Measured impedance spectra of encapsulant were a straight line. As in other cases of encapsulants, the electrical impedance decreased with time of immersion.

The impedance spectra of 410 ± 10 μm thick encapsulant is also a straight line without any plateau indicates a dielectric behaviour The increase in thickness

enhances the impedance of 410 ± 10 μm thick encapsulant. The impedance has increased from 1.5 GΩ to 1.2.5 GΩ (Fig.100). As in all cases, the impedance value decreased gradually with immersion time.
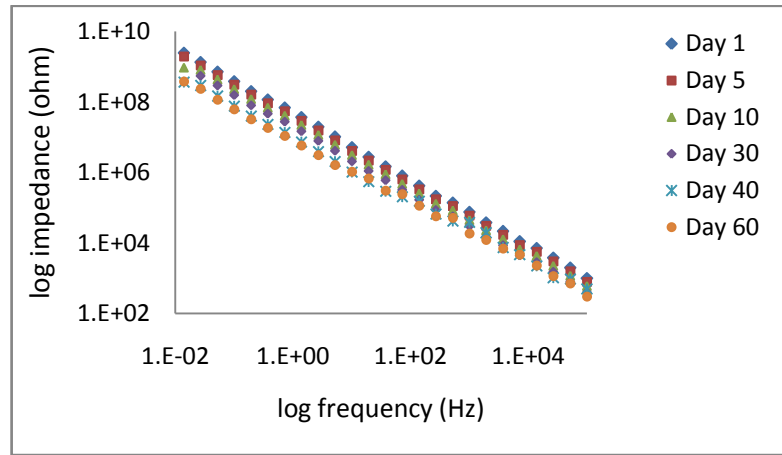
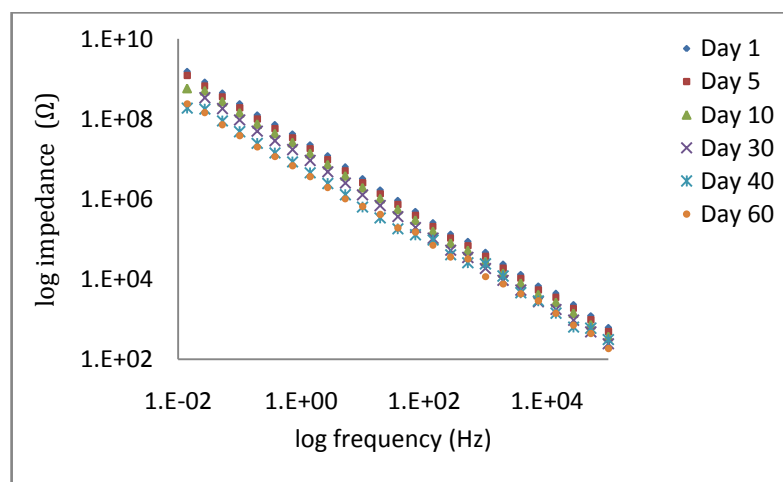Fig. 100: Electrochemical impedance spectra of a 410 μm thick epoxy encapsulant

The electrochemical impedance spectra of all the studied epoxy encapsulants were straight line except 180 μm thick encapsulant. A plateau was observed in the 180 μm thick encapsulant towards the end of 60 days.

6.3.3. Effect of thickness

Encapsulant is a dielectric material and does not allow a direct current (DC) to pass through in normal circumstances. However, an alternating current (AC) passes through the encapsulant below certain thickness for certain voltage and frequency [43]. Once, the current flows across the encapsulant, the impedance offered by the encapsulant increases with increase in thickness. This is due to the increase in the current path similar to the Ohmic conduction in metals. In the study, as the thickness increases the impedance of the PU encapsulant increases from 1.06 GΩ to 2.2 GΩ for the thickness increase from 153 μm to 394 μm. The impedance of the epoxy encapsulant increased from 0.8 GΩ to 2.2 GΩ for the thickness increase from 180 μm to 410 μm.

Even a perfect coating or encapsulant has inherent micro 'hydrophilic regions' of low molecular weight and low cross link density [120]. Water preferentially attacks these micro regions near to the surface and forms water pockets. During prolonged immersion, the water pockets or nuclei join together by osmosis and diffusion and

forms a conductive path across the encapsulant. The time taken for the formation of conductive path increase with increase in thickness. In thicker encapsulants, more time will be taken for forming water pockets and then joining each other to form a conductive pathway across the thickness. Hence, plateau region resulted by the conductive path formation in the encapsulant appeared late for 183 μm thick encapsulant compared to 153 μm thick encapsulant.

The pore resistance was not visible (the presence of plateau) for encapsulants having higher thickness during 60 days study period. However, the electrical impedance has decreased for all encapsulant thickness. Even the encapsulants showing pore resistance retains its barrier property indicated by the absence of any capacitive double layer region in the impedance spectra [49].

6.4. EIS studies of thick encapsulants

Encapsulants thicker than 500 μm is considered as thick encapsulants in this thesis work. Electrochemical impedance spectra of thick PU, CR and epoxy encapsulants immersed in 3.5 wt % NaCl aqueous solution were measured periodically for two months.

6.4.1. Polyurethane encapsulants

Two thick encapsulants of 1± 0.1 mm and 2 ± 0.2 mm were prepared for study. The impedance spectra of the encapsulants immersed in 3.5 wt % NaCl aqueous solution, were measured continuously for two months. The electrochemical impedance spectra of 1 mm thick PU encapsulant is shown in Fig.101. The spectra is a perfect straight line in all days of measurement. 1 mm thick encapsulant has ~ 13 GΩ impedance at 10 mHz in the beginning. As in the cases of all other encapsulants, electrical impedance decreased with time.

EIS analysis of PU encapsulant having 2 ± 0.2 mm thicknesses is shown in Fig. 102. The measured spectra are a straight line throughout the 60 days of evaluation. The initial low frequency impedance of the encapsulant was ~63 GΩ. The encapsulant is a perfect dielectric material with high electrical impedance and it retained its dielectric nature throughout the evaluation period.

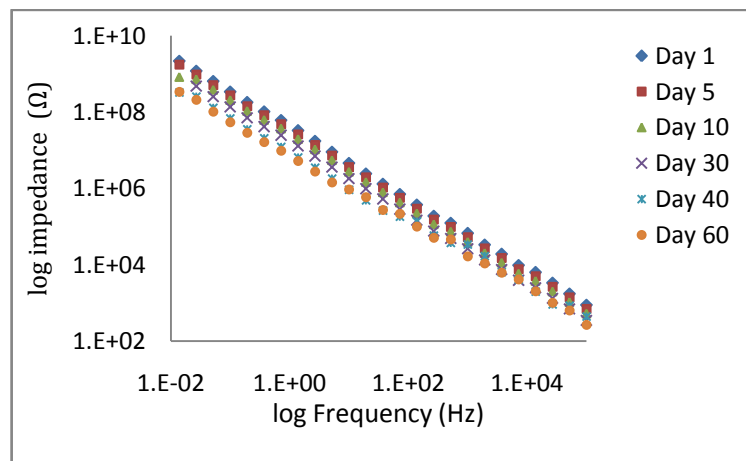Fig. 101: Electrochemical impedance spectra of a 1 mm thick polyurethane encapsulant
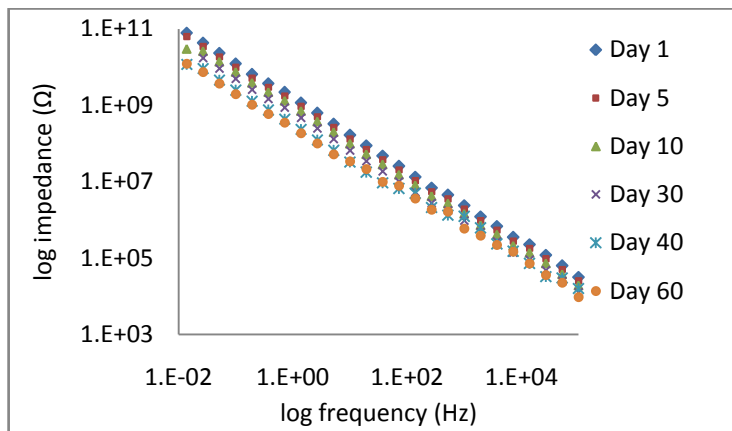
Fig. 102: Electrochemical impedance spectra of a 2 mm thick polyurethane encapsulant

6.4.2. Polychloroprene encapsulants

The electrochemical impedance spectra of a 2 ± 0.2 mm thick CR encapsulant immersed in 3.5 wt % NaCl aqueous solution, were continuously monitored for two months.
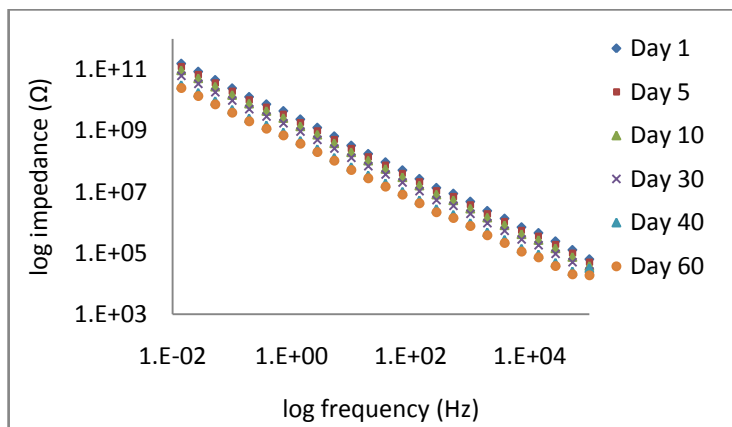
Fig.103. Electrochemical impedance spectra of 2 mm thick CR encapsulant

The electrochemical impedance spectra is a straight line with outstanding electrical impedance. (~158 GΩ at 10 mHz). The electrical impedance of the encapsulant decreased with time during the evaluation as in the case of other encapsulants (Fig.103).

6.4.3. Aged epoxy encapsulants

Fig.104 is the electrochemical impedance spectra of a 2 ± 0.1 mm thick aged epoxy encapsulant measured in different days. As already discussed in chapter 3, the aged encapsulant were prepared by subjecting the epoxy encapsulant to thermal oxidation by exposing the sample at 70º C in an air oven for two months.
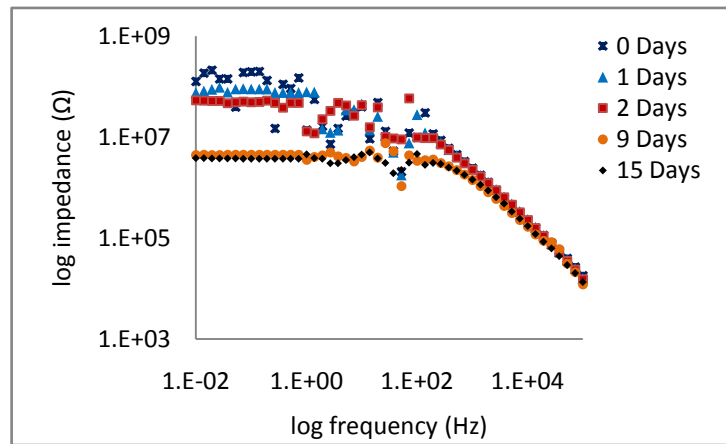
Fig.104. Electrochemical impedance spectra of aged epoxy encapsulant

The electrical impedance of the encapsulant was ~127 MΩ (measured at 10 mHz) in initial hours. On exposure to saline water, the impedance of the coating decreases and reaches 4.5 MΩ within 9 days. The flat region in the low frequency area of the spectrum in the first day itself, shows that a conductive path was formed immediately on immersion [4]. This normally occurs due to the water and ions ingress in the encapsulant. The electrical impedance of the encapsulant rapidly decreased with time and a very significant decrease was observed within two weeks. The measurement discontinued after two weeks after getting sufficient changes in electrical impedance.

Thick encapsulants of PU and CR behave as a perfect dielectric material during the study period. It is inferred that, by enhancing the thickness of the encapsulant, it is possible to enhance electrical impedance of the encapsulant and also possible to

delay the formation of conductive path across the encapsulant. Higher electrical impedance is desirable for an underwater electro-acoustic transducer which operates in kilowatts power [9]. However, higher thickness may hamper the acoustic transparency of the encapsulant. Hence an optimum thickness of encapsulant needs to be selected for the best overall performance of the underwater transducer. The effect of thickness on water uptake and electrical degradation of encapsulant were discussed in chapter 7 & 8 in detail.

It is expected that thick encapsulants do not show any plateau region in the electrochemical impedance spectra within 60 days of evaluation period. In order to generate the spectra of thick encapsulants showing plateau in a short period and compare with FFIS, an epoxy encapsulant which has undergone thermal oxidation, was selected. After thermal oxidation, the polymer is expected to absorb more water due to the formation of hydrophilic degradation products in the polymer. A polymer with low cross link density offer less resistance to water diffusion and osmosis compared to polymer with high cross link density [123].

6.5. Electrochemical impedance spectra of filler loaded encapsulants

Electrochemical impedance spectra of encapsulants loaded with different types and quantity of fillers were measured. The selected fillers were carbon black , polyaniline, and nano silica. Thickness of the all encapsulant samples were 1 ± 0.1 mm.

6.5.1. Carbon black loaded polyurethane encapsulants

Different amounts of carbon black (2 wt%, 4 wt%, 6 wt%) were incorporated in the encapsulant and electrochemical impedance spectra of the encapsulants exposed to 3.5 wt% sodium chloride solution were measured at regular intervals. The measured electrochemical impedance spectra of polyurethane encapsulant with 2 wt% CB, is shown in Fig. 105. A plateau region was observed in the low frequency region in the initial days itself. Also, the impedance value of the encapsulant was ~518 MΩ (10 mHz) in the initial hours which was much lower than neat PU. Since, the flat region of the impedance spectra was observed in the beginning itself, it may not be due to water ingress. It is reported that, coatings loaded with metallic fillers or

conductive fillers, a flat region was observed even before the water ingress in the coating [128] and is characteristic of a conductive coating. The presence of plateau region in the initial days may be due to the resistive path created by the conductive fillers [129]. Since the impedance of the encapsulant was decreased by the addition of CB, it may be assumed that CB fillers created a conductive channel in the encapsulant. It was also observed that, impedance of the encapsulant decreased with time during exposure to saline water and the value reduced from 518 MΩ to 82 MΩ.
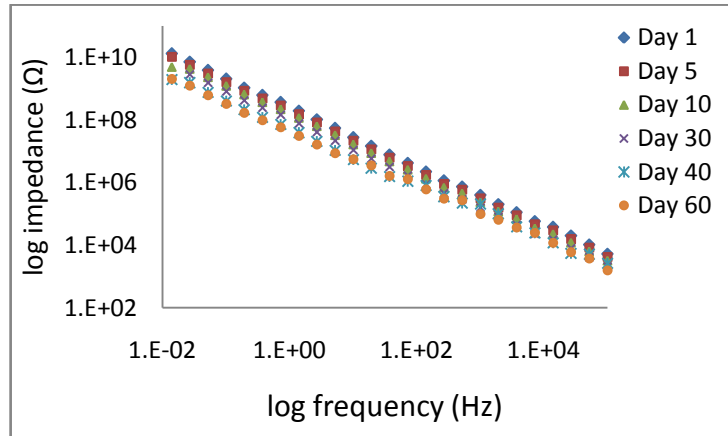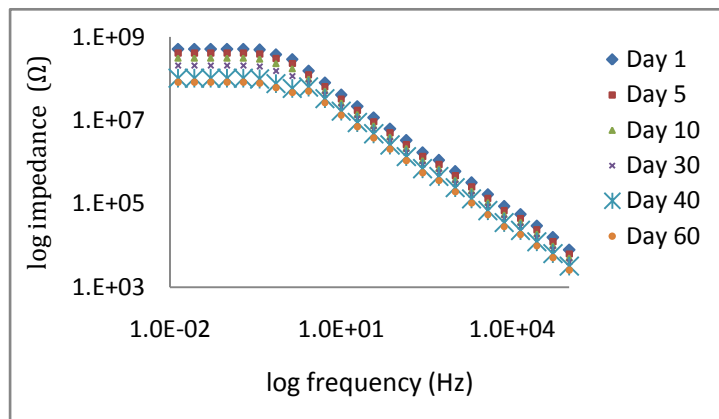

Fig. 105: Electrochemical impedance spectra of 1 mm thick PU encapsulant with 2% CB
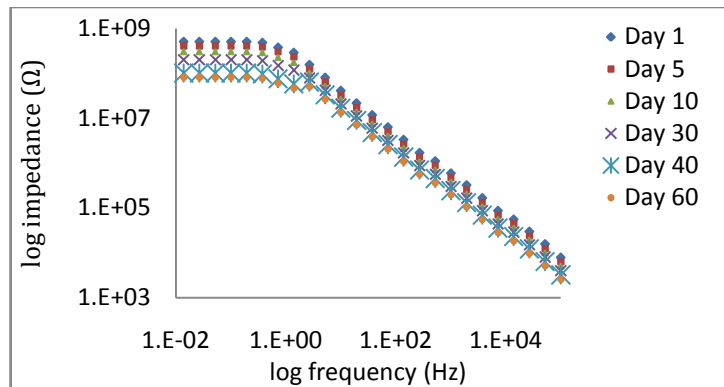
Fig. 106: Electrochemical impedance spectra of 1 mm thick PU encapsulant with 4% CB

Fig. 106 shows the electrochemical impedance spectra of 1 ± 0.1 mm thick encapsulant with 4 wt% carbon black as filler, for a period of 60 days. Similar to 2 wt % CB loaded PU encapsulant, electrical impedance decreased with time on exposure to saline water. The impedance spectra of 6% carbon black filled PU encapsulant is shown in Fig.107. Encapsulant has 495 MΩ impedance during initial period of exposure and reduced to 79 MΩ after 60 days.
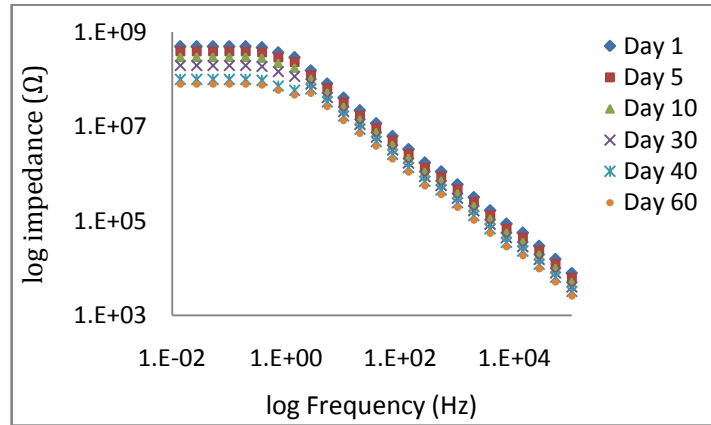
Fig.107: Electrochemical impedance spectra of 1 mm thick PU encapsulant with 6 % CB

The impedance magnitudes decrease with increasing additive content in the order, 2 wt% > 4 wt% > 6 wt%. These changes measured by electrochemical impedance spectroscopy will be used for estimating electrical degradation and comparing the results with that of FFISY. The reason behind the above mentioned order in impedance decrease is explained in section 5.7.1.

6.5.2. Nano silica loaded polyurethane encapsulants

The electrochemical impedance spectra of the nano silica loaded PU encapsulant were measured at regular intervals for two months (Fig.108). The electrical impedance of the encapsulant in the initial period of immersion was 11.6 GΩ (at 10 mHz). The measured spectra is a straight line without any plateau region during the 60 days of measurement. The encapsulant performed as dielectric material during this period. There was a decrease in impedance of the encapsulant with time of immersion. However, encapsulant retained its dielectric nature during this evaluation period.
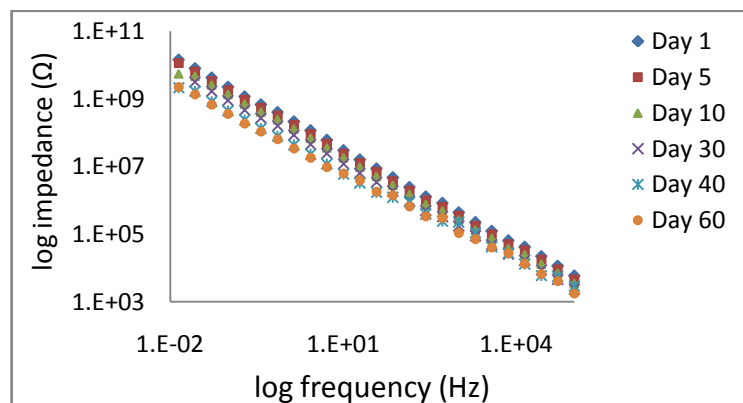
Fig 108: Electrochemical impedance spectra of 2% nano silica filled PU encapsulant.

Fig. 109 shows the electrochemical impedance spectra of 3 wt% nano silica filled encapsulant for a period of 60 days. There was no appreciable change in the impedance of the encapsulant after addition of fillers. The impedance of the encapsulant decreases on continuous exposure to saline water similar to 2 % silica loaded PU. PU encapsulant loaded with 4 wt% nano silica also behaves similar to 2 wt% and 3 wt % nano silica loaded PU in 3.5 wt % NaCl aqueous solution (Fig.110). The percentage decrease of electrical impedance was less for 4 wt% nano silica loaded PU. This may be due to the better barrier property of 4 wt% nano silica than others which is discussed in chapter 7.
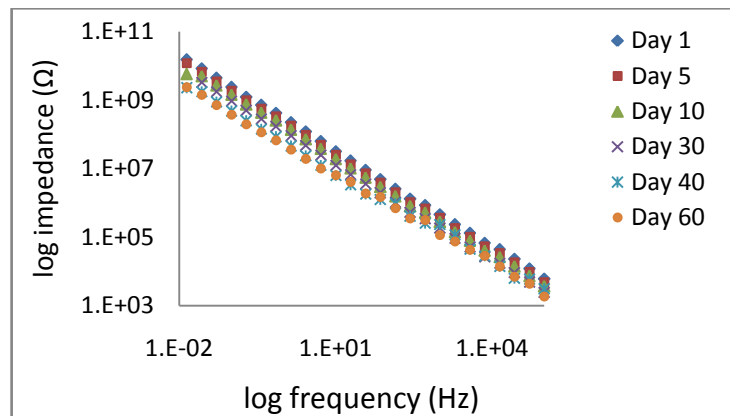
Fig.109: Electrochemical impedance spectra of 3% nano silica filled PU encapsulant.
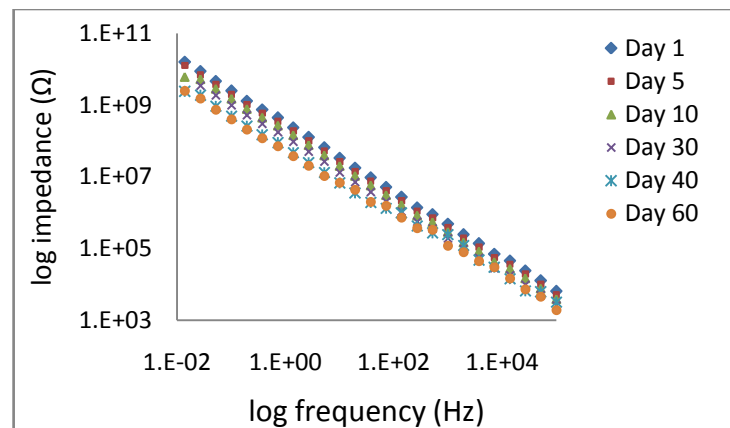
Fig.110: Electrochemical impedance spectra of 4% nano silica filled PU encapsulant.

6.5.3. PANi loaded polyurethane encapsulants

Figs.111 & 112 shows the Bode impedance and phase plots of PU loaded with 10 wt%, 15 wt% and 20 wt% PANi. EISY could measure the decrease in the impedance of the encapsulant on the addition of conductive PANi. A small decrease (~10 kΩ) in impedance is observed on addition of 5 wt% PANi and a large reduction

(900 kΩ) is observed at 20 wt% loading. This observation indicates that the CPVC (Critical Pigment Volume Concentration) of this PU-PANi system lies in 15-20 wt% range. The PU matrix is no longer able to bind the filler above the CPVC and cracks may form in the encapsulant on curing. A conductive path is generated by the interaction of PANi particles which are no longer isolated each other by the PU binder. The EIS of the encapsulant is measured in contact with salt water and these cracks may act as a path for water and ion penetration.
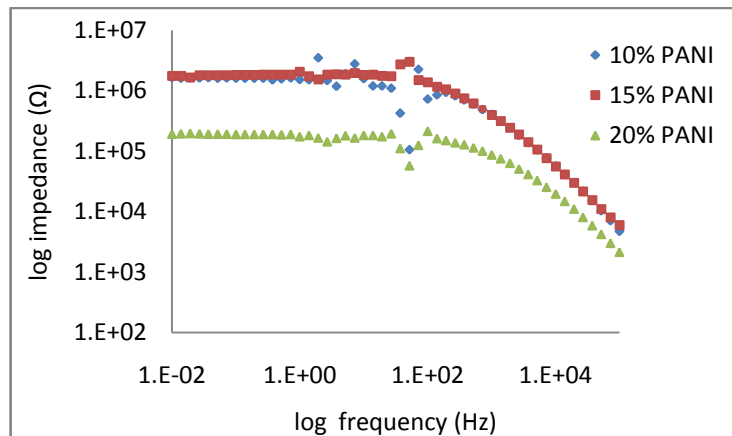
Fig.111. Electrochemical impedance spectra for PU, PANI-PU10%, 15% and 20%
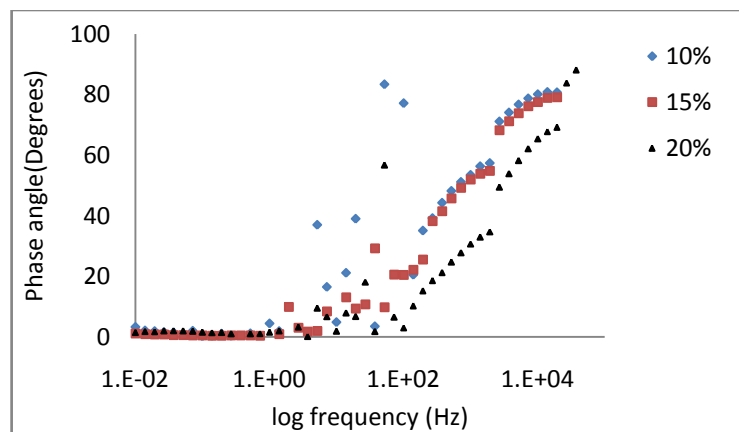
Fig.112. Variation of phase angle with time for PU, PANI-PU10%, 15% and 20%

It was observed in earlier experiments that the phase angle was 90^0 over wide frequencies indicates the capacitive nature of the encapsulant.. The encapsulant became resistive in nature on addition of 10 wt% PANi. It is observed that, there was no significant reduction in the capacitive region in the phase spectra on further addition of PANi (Fig. 112).

The encapsulant material performance in salt water was analysed for the three compositions. A selection of the measured impedance spectra during the exposure to 3.5 wt% NaCl solutions of the coated specimens as recorded at different exposure times is shown in Figs.113-115 for the three different PANi content tested in this work. i.e., 10, 15 and 20 wt% respectively.
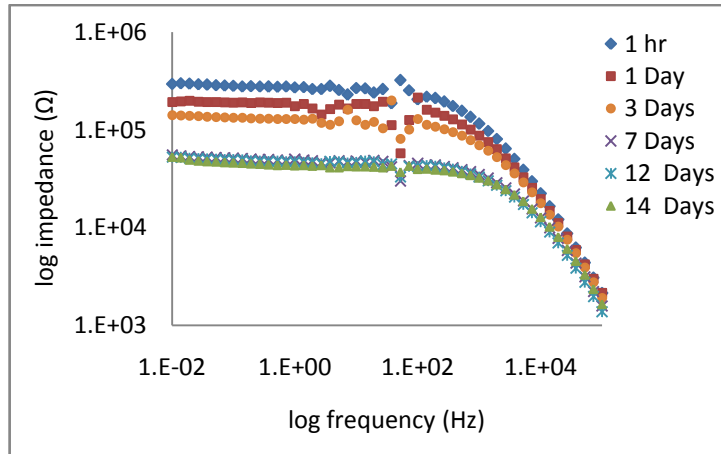
Fig.113. Electrochemical impedance spectra with time for PANi-PU 20%
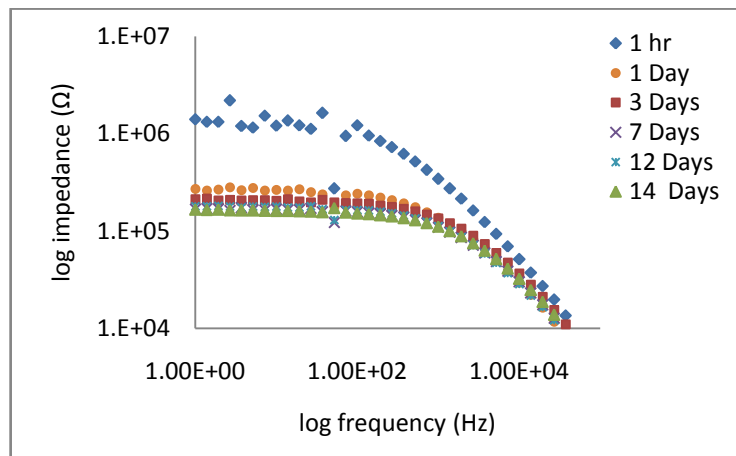
Fig.114 Electrochemical impedance spectra with time for PANiI-PU 15%
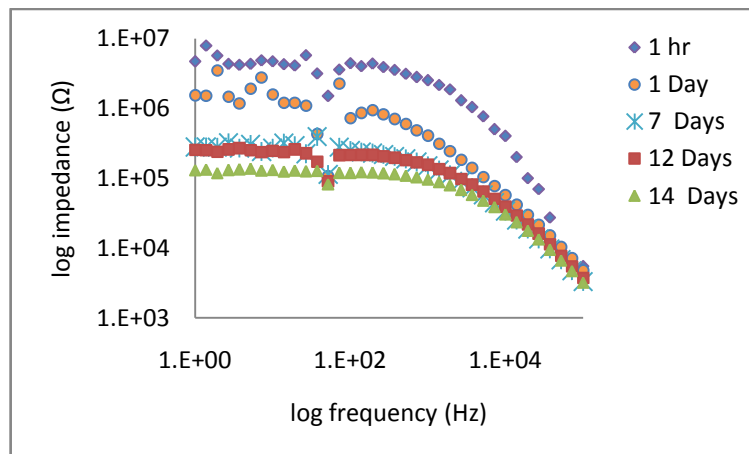
Fig.115. Electrochemical impedance spectra with time for PANi-PU 10%

The evolution of the electrochemical behaviour of the PU-PANi encapsulants is clearly indicated by EIS, and greatly depends on the content of PANi in the encapsulant. In the early hours of immersion, the impedance spectra exhibit a decrease in the impedance values for all the tested specimens. The initial decay in the impedance of the system is fast and slows down after a few hours for all the three systems, indicating that water has entered through the surface pores in the initial hours. The water ingress reduced the electrical resistance of the encapsulant as reflected by the reduction in impedance. There was no particular trend in electrical impedance decrease according to the PANi content. This may be due to the non uniformity in the encapsulant due to poor dispersion of PANi.

6.6. Conclusion

Electrochemical impedance spectra of encapsulants were measured by EISY to estimate the degradation of electrical resistance and water uptake of the encapsulants. This values are for comparing with that of FFISY.   The main observations are,

- Electrical impedance of the encapsulant decreases with time on exposure to saline water. This was due to the water and ion ingress in the encapsulant
- A minimum 200 μm thick encapsulant is required to make a perfect dielectric coating that last for 60 days.
- The performance of the encapsulant could be understood well from the shape and value of the electrochemical impedance spectra.
- The incorporation of fillers like CB and PANi in PU reduced the impedance of the coating.
- Thick encapsulants have high electrical impedance and retain its dielectric nature during 60 days of evaluation period.
- Water uptake and electrical degradation of the encapsulant will be calculated from the measured electrochemical impedance spectra in chapters 7 & 8 by fitting the spectra in the equivalent circuit shown in Fig. 7.

CHAPTER – 7

Estimation of Water Uptake

7.1. Objective

a. Estimation of water uptake by the encapsulant from fringing field impedance spectra and compare the results with that of electrochemical impedance spectra.

b. Compare the water uptake estimated by FFISY with gravimetry.

7.2. Introduction

Water uptake by the coatings during the initial stages of water ingress gives indication about the efficacy of that material as a water barrier [20-26]. The water uptake starts within few minutes after immersion in water and reaches a steady state within hours or days [12-15]. In the case of encapsulants, the time may extend to a few weeks [119]. Hence the FFIS of encapsulants immersed in 3.5 wt % NaCl was measured for two months to estimate the water uptake.

In order to validate the water uptake measured by FFISY, the values were compared with that of EISY technique. The change in capacitance obtained from the measured FFIS (from chapter 5) and EIS (from chapter 6) were used to estimate the water uptake of the encapsulants. The widely used Brasher-Kingsbury equation was used to estimate the water uptake from the change in capacitance of encapsulants [10].

The water uptake estimated by FFISY and EISY are based on change in capacitance of encapsulants during water ingress. The estimated water uptake from these capacitance based techniques is compared with conventional gravimetric technique. The gravimetric technique is commonly used for the water content estimation in the laboratory [18].

7.3. Comparison of water uptake estimated by FFISY and EISY techniques

The water uptake estimated by Brasher-Kingsbury method from capacitance obtained from EIS, is widely accepted for the qualitative and quantitative evaluation of coatings [20-26]. Hence, it is decided to compare the water uptake estimated by FFISY with that of EISY.

FFIS measured by miniature FEF sensor (Type I) and Type II FEF sensor in chapter 5 were used to estimate the water uptake of encapsulants. A case of 1 mm thick epoxy cast over miniature FEF sensor was illustrated here. Water uptake by 1 mm thick epoxy encapsulant estimated from EIS in chapter 6 was used to compare the results.
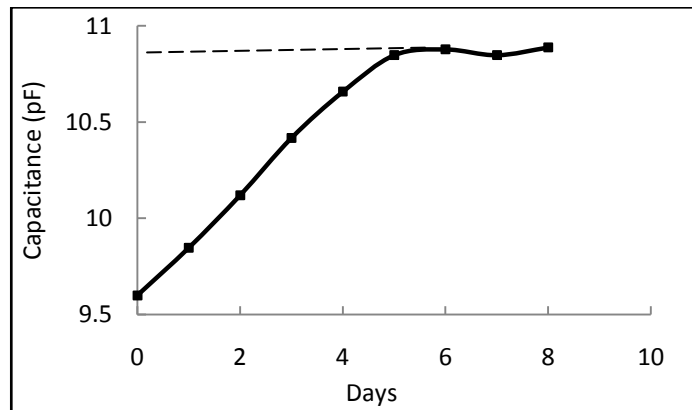
Fig.116. Variation of capacitance in 1 mm thick epoxy encapsulant during water uptake measured by FEF sensor

The saturation capacitance measured by miniature FEF sensor and EISY was 10.8 pF and ~300 pF respectively. The total change in capacitance measured by miniature FEF sensor was around 1.5 pF during the water ingress (Fig.116) and the total change in capacitance in EISY study for the same coating was ~40 pF (Fig.117). This difference is attributed to the difference in the measuring area of FEF sensor and EISY, 93 mm^2 and 19.6 cm^2 respectively.
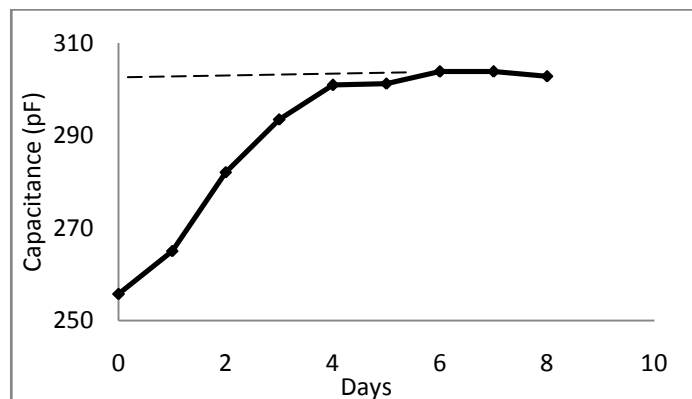
Fig.117. Variation of capacitance in 1 mm thick epoxy encapsulant during water uptake measured by EISY

Water uptake profiles of 1 mm thick epoxy encapsulant, measured by FEF sensor and EISY technique were compared (Fig.118). Water uptake follows Fickian

profile where water uptake is linear in the initial stages and then reaches a steady state. It is clear from the figure that water uptake profile measured by EISY and FFISY are comparable (5.6 and 5.8 vol%).
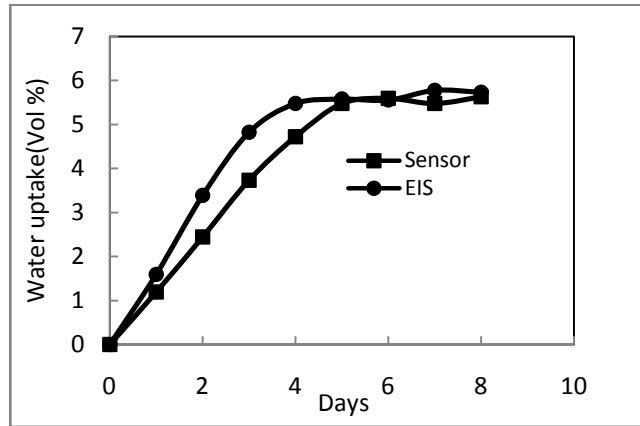
Fig.118. Water uptake profile of 1 mm thick epoxy encapsulant measured by FEF sensor and EISY method.

The water content was estimated from the ratio of saturated capacitance to dry capacitance as per B-K equation. Even though, the capacitance value from these techniques differs significantly, the estimated water uptake was same due to the proportional change in capacitance. More elaborate studies on water uptake in PU and epoxy encapsulants of different thickness are given below.

7.3.1. Comparison for different encapsulant thickness

Water uptake estimated by FFISY and EISY were compared by calculating percentage of difference between them as per the formula,

$$\text{Difference (\%)} = 100 \times (W_{EISY} - W_{FFISY}) / W_{FFISY} \quad (21)$$

Where W_{EIS} and W_{FFIS} are the estimated water uptake by EISY and FFISY respectively.

7.3.1.1. Thin encapsulants

Water uptake of PU encapsulants of thickness 153, 182, 240, 286, 394 and 805 μm (± 10 μm) were estimated by miniature FEF sensor and the results were compared with EIS (Fig.119). The % difference was calculated based on the Eqn. 21 and plotted against encapsulant thickness. The difference between the water uptake estimated by EISY and FFISY is less than 2% for encapsulant thickness 153, 182,

240, 286 and 394 μm. The difference was above 5 % for thickness higher than the penetration depth of the sensor. The water content estimated by FEF sensor and EISY technique were more comparable within the penetration depth of the sensor.
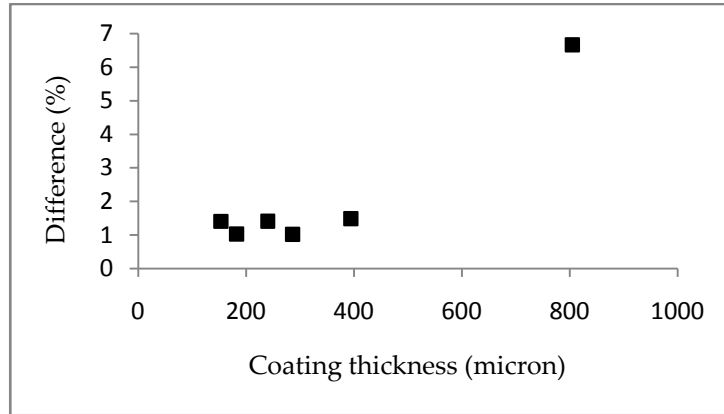
Fig.119. Difference in percentage in the estimated water content from EISY and FFISY for different PU encapsulant thickness
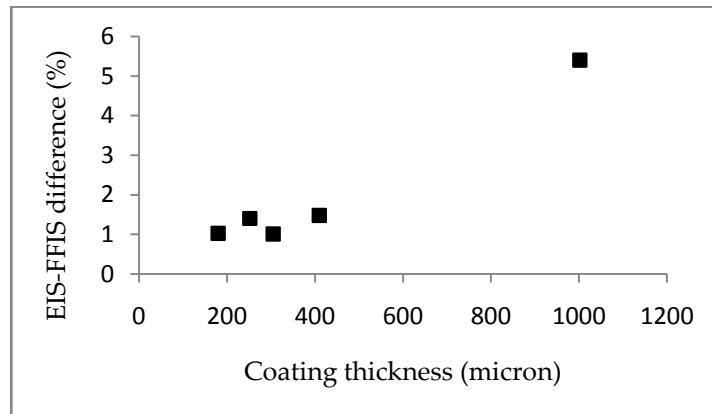
Fig.120. Difference in percentage in the estimated water content from EISY and FFISY for different epoxy encapsulant thickness

Water uptake of epoxy encapsulants of thickness 180, 252, 305 and 410 μm (± 10 μm) was estimated by FFISY. The results were compared with that of EIS in a similar fashion. Similar results as that of PU encapsulants were observed. The difference between the estimated water content between EISY and FFISY was less than 2% for encapsulants of lower thickness than the penetration depth of the sensor (Fig. 120).

The results show that EISY and FFISY techniques have comparable water uptake values for encapsulants of thickness less than penetration depth of the sensor. EISY and FFISY show similar results when experiments conducted in PU

and epoxy encapsulants of different thickness. In subsequent studies, it was observed that the water content estimated by capacitance method increases with increase in thickness for both the techniques. However, if thickness increased beyond the PD of the sensor, the estimated water content value remained same. The sensor could not sense the enhanced thickness beyond the field penetration depth of the sensor [115]. On the other hand, EISY do not have the limitation of penetration depth as it measures across the encapsulant [43]. Hence, water content estimated by EIS increases with increase in thickness whereas that of FFISY stagnates after encapsulant thickness reaches the penetration depth of the sensor. So, the difference between the water content estimated by these two techniques will be higher beyond the penetration depth of the FEF sensor. FEF sensor having penetration depth 460 μm was used in the study. It is clear in the Fig. 119 and Fig.120 that the water uptake estimated for encapsulant having thickness higher than 460 μm of the sensor shows higher difference with that of EISY.

7.3.1.2. Thick encapsulants

Type-II FEF sensor having 2 mm penetration depth was used to estimate the water content and the results were compared with that of EIS. The capacitance–time profiles of a 2 mm thick PU encapsulant estimated by FEF sensor and EISY are shown in the Fig. 121 & 122 respectively.
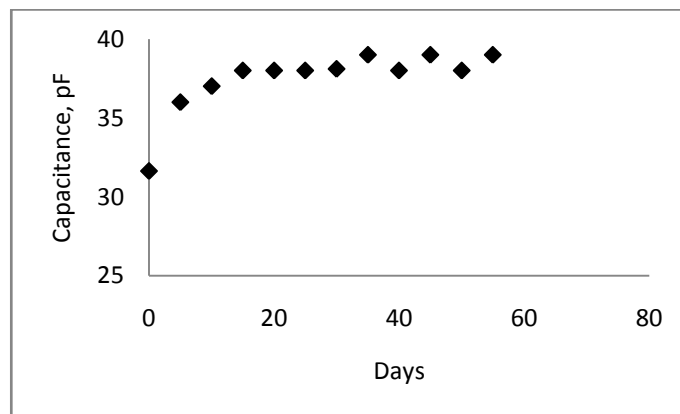
Fig. 121. Capacitance-time profile of 2 mm thick PU encapsulant exposed to 3.5 wt % NaCl aqueous solution, estimated by FEF sensor.

The capacitance variation during water uptake was 7 pF higher than miniature FEF sensor. This is due to the increased area of the sensor even though the unit capacitance of the Type-II sensor is lower than the Type I sensor (miniature FEF

sensor). The capacitance profile of thick encapsulant of same thickness (± 0.05 mm) was also determined by EISY.
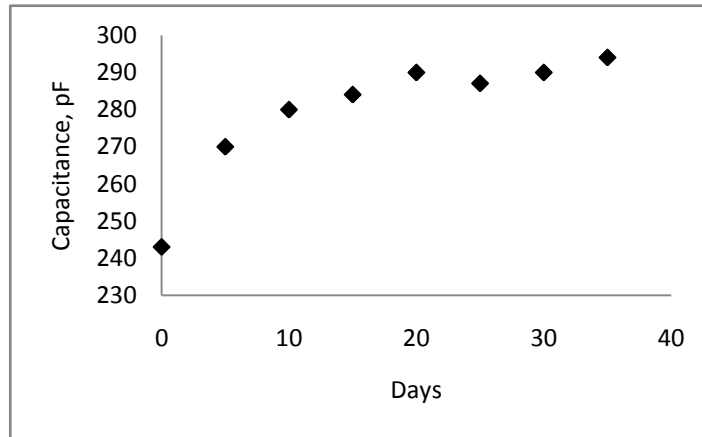
Fig. 122. Capacitance-time profile of 2 mm thick PU encapsulant exposed to 3.5 wt % NaCl aqueous solution estimated by EISY.
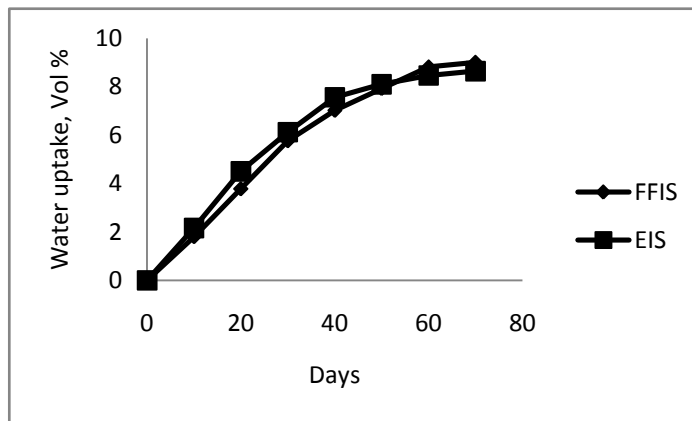
Fig. 123. Water uptake -time profile of 2 mm thick PU encapsulant exposed to 3.5 wt % NaCl aqueous solution estimated by EISY and FIS.

The capacitance measured by EISY technique during the water uptake increased from 255 to 300 pF. The water content estimated by the techniques were compared and observed that the difference in the estimated value is within 2% (Fig.123).

The water uptake-time profile of CR encapsulant was determined by EISY and FFISY technique (Fig.124). Water uptake values determined by both techniques are comparable values and show similar pattern. Another observation is that, the water uptake in rubber does not follow a Fickian behaviour. Fickian behaviours is observed in polymers whose Tg is below room temperature and when water molecules permeates between the polymer chains by chain relaxation process [53-56]. Even though, Tg of rubber is below room temperature, the presence of fillers in

rubber, hinders the natural movement of water molecules through the polymer chains [80].
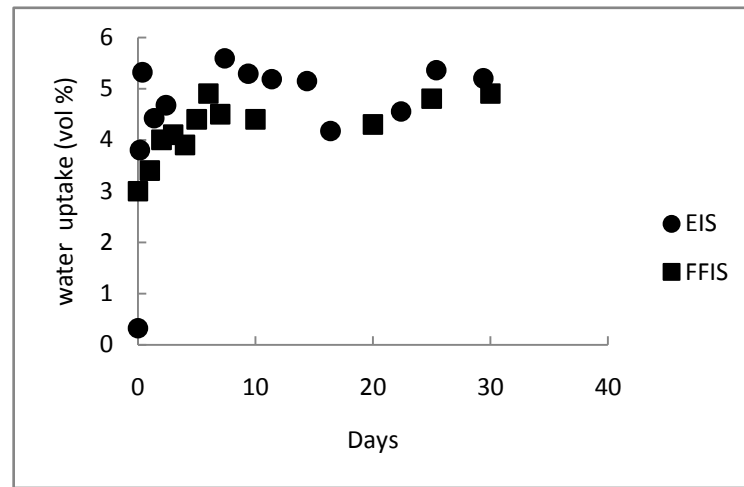
Fig 124: Water uptake profiles of polychloroprene encapsulant

7.4. Comparison of estimated water uptake obtained from capacitance method and gravimetry

The values of water uptake estimated from EISY and FFISY are not absolute values. It is indirectly measured from the capacitance changes of the encapsulant during water ingress. It is reported in the literature that capacitance based estimation of water uptake in coatings always shows higher value than gravimetry, if water distribution is not uniform in the material [53]. However, capacitance based water uptake estimation is widely accepted by coating technologists for comparison studies as it is a convenient and simple technique [24]. A study was done in encapsulants to find out the difference between the water uptake determined by capacitance and gravimetric techniques. Also study was done to analyse the effect of encapsulant thickness on the difference between the water uptake obtained from these two techniques.

7.4.1. Thin encapsulants

Water uptake profile of PU encapsulants with thickness 153, 182, 240, 286 and 394 μm (± 5 μm) are shown in Fig.125. As the thickness increases, the estimated water uptake deviates more from gravimetric values.
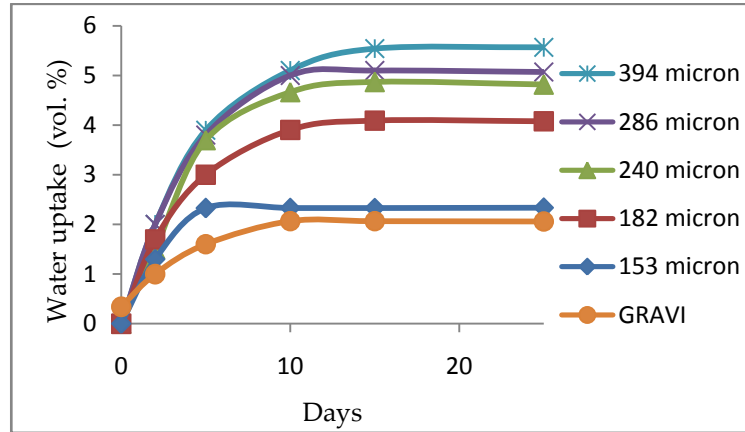
Fig 125: Water uptake profiles of thin PU encapsulants

Water uptake profile of epoxy encapsulants with thickness 180, 252, 305 and 410 µm (± 5 µm) are shown in Fig.126. As the thickness increases, the estimated water uptake deviates more from gravimetric values as in the case of PU.
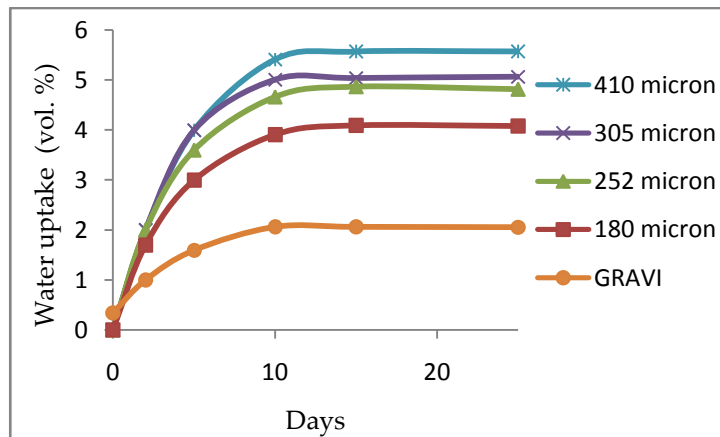
Fig. 126: Water uptake profiles of thin epoxy encapsulants

Deviation percentage is calculated by the following formula to compare the estimated water uptake from capacitance and gravimetry.

$$\% \ Deviation = \frac{(W_c - W_g)}{W_g} \ x \ 100 \qquad (16)$$

Where W_c and W_g are the estimated water uptake from capacitance measurement and gravimetric measurement respectively. W_C deviates from gravimetric estimate as the coating thickness increases (Fig.127),
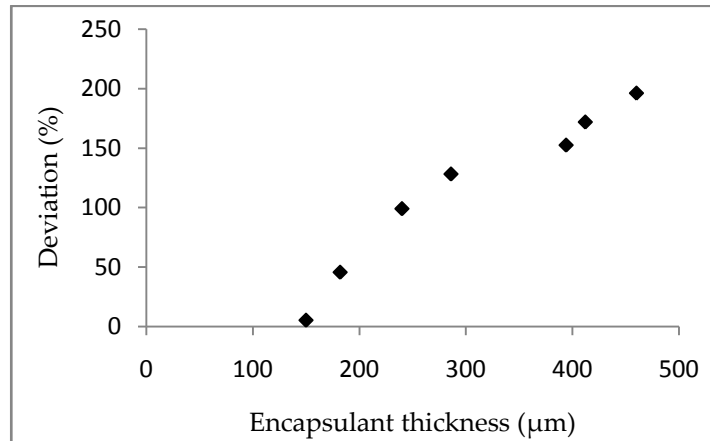
Fig.127.Deviation of water content from gravimetric estimation in neat PU

7.4.2. Thick encapsulants

Similar to the study on thin encapsulants, water uptake of thick encapsulants was also estimated from FFIS and compared with that of EISY. The water uptake profile of 1 mm thick PU encapsulant is shown in Fig.128. It is observed that thick encapsulants show more deviation than thin encapsulants. However, water uptake profile from all the techniques shows similar profile.
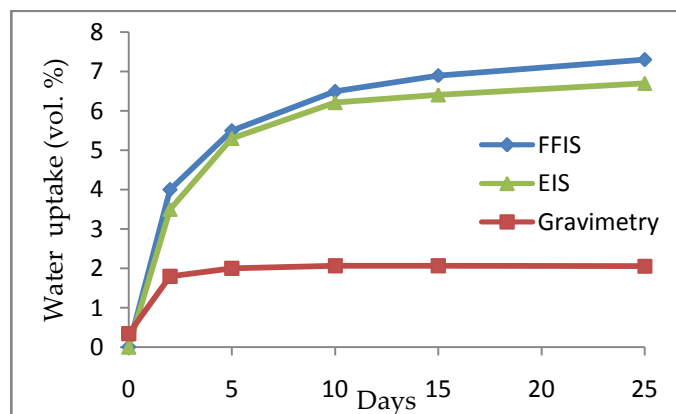
Fig 128: Water uptake profile of 1 mm thick PU encapsulant

Water uptake profile of 1.98 ± 0.05 mm thick PU encapsulant was compared with gravimetry (Fig.129). The estimated water content has higher values than that of gravimetric technique.

It is observed from the above studies that water ingress occurs in all the encapsulants when immersed in water. Water uptake observed even in coatings without any defects or pin holes which was later confirmed by SEM images. In this context, it is relevant to cite literatures that explain about the inherent 'hydrophilic'

microscopic regions present in all coatings that cannot be seen in micrographs [120-124]. These microscopic regions take up more amounts of water compared to other regions as they are low molecular weight or low cross linked regions.
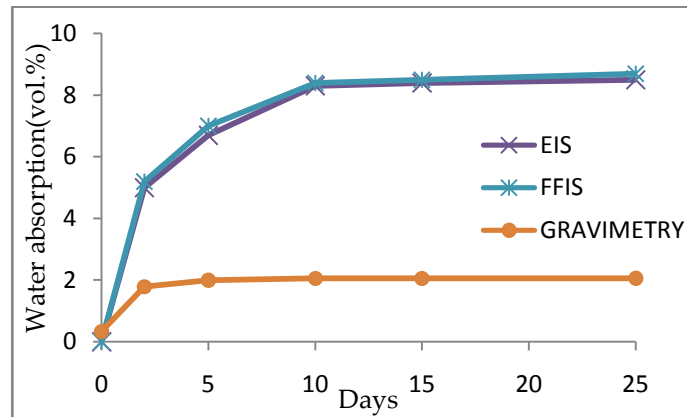
Fig 129: Water uptake profiles of 1.98 mm thick PU encapsulant

It is to be noticed that, in the first few hours, the capacitance values show a much sharper rise than the gravimetric values. This can be interpreted by assuming that the pores or capillaries (or pinholes) normal to the surface are the first to be filled with water, which then spreads out laterally to give a uniform, random distribution [10]. In gravimetric technique, the measured water uptake is very low in the initial stages, because water that has only penetrated the easily accessible pores and capillaries might easily be squeezed out during the drying process.

Water content value from gravimetry technique and capacitance measurement matches when the distribution of water in the coating is random and uniform. The higher water content value than that of gravimetry indicates that, water is distributed normal to the surface as pores and columns [10]. Capacitance measurements show a close agreement with gravimetric results for thinner encapsulants. As the thickness increases, the deviation also increases due to the uneven distribution of water.

Another reason for uneven distribution of water can be the presence of voids in the encapsulant. The presence of voids inside the coating/encapsulant may cause water clogging in and around the voids and this would result in uneven water distribution in the encapsulant. This may results in larger deviation as the percentage of deviation is related to homogeneity of the material as per literature [53]. However, the neat encapsulant or the encapsulant without any filler is

expected to have least number of voids compared to filled encapsulant [53]. In order to verify the presence of micro voids, SEM of sectioned encapsulant were taken.
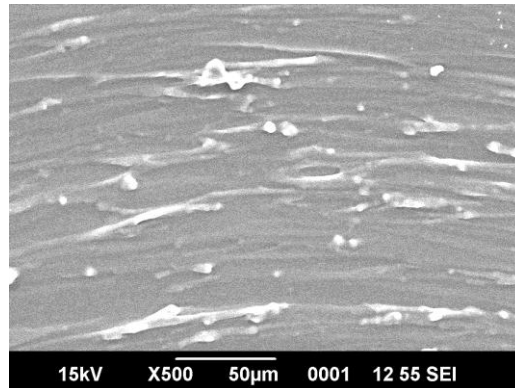
Fig.130. Micro structure of PU (a) X 500 magnification

Micrograph of PU shows the surface of the sectioned PU encapsulant (Fig.130) at 1500 times magnification. Micro voids were not present in the encapsulant verified by SEM. Similarly, presence of micro voids could not be found in SEM cross-section of epoxy encapsulant (Fig.131). Hence, it can be assumed that higher water content value than that of gravimetry is due to the distribution of water in coating normal to the surface as pores and columns [10].
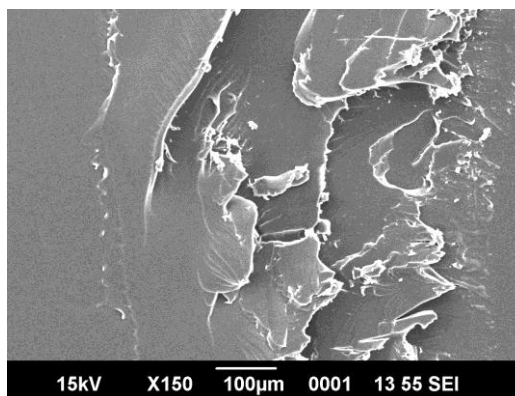
Fig.131. Micro structure of epoxy X 150 magnification

7.4.3. Attached and free encapsulant gravimetry

Water uptake estimated by capacitance measurement is normally compared with free film or encapsulant gravimetry (Fig.132) [10-12]. A comparative study was conducted between capacitance techniques and attached gravimetric technique in addition to free film gravimetric technique. Free film and attached film

gravimetry has different mode of water ingress in the encapsulant; one sided and all sided water ingress. Capacitance technique and attached film gravimetry have similar mode of water ingress and hence compared.
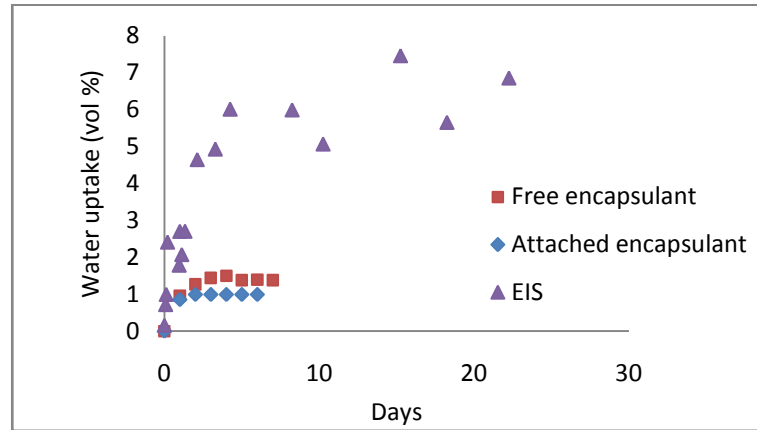
Fig.132. Comparison of water uptake profile from attached encapsulant gravimetry, free encapsulant gravimetry and EISY.

A slightly higher value of water uptake was observed for free encapsulant gravimetry compared to attached encapsulant gravimetric technique. However, estimated water uptake from capacitance measurement using the Brasher equation were higher than gravimetric values as reported by many authors in literature.

Hence it can be assumed that, the uneven distribution of water in PU and epoxy encapsulant is not due to the presence of voids in the encapsulant. According to Brasher-Kingsbury postulation, higher value of water content than that of gravimetric technique was observed due to the distribution of water perpendicular to the surface [10]. Also, Yinghua et al, in his study on PVC plastisol, states that, the deviation of the water content estimated by capacitance technique from gravimetric technique is an indication of the non-homogeneity of the material. A homogenous material shows closer water content values between capacitance technique and gravimetric technique [53]. Thinner encapsulants are expected to have a more homogenous microstructure compared to that of a thick coating. It may be the reason that, the thicker coatings show a larger deviation from gravimetric technique than thinner encapsulants.

It is observed that the water uptake in rubber does not follow Fickian behaviour. Also the water content estimated by the capacitance technique is higher than gravimetric technique. It is to be noted that the recipe of rubber compound

used for underwater encapsulants contains many particulate fillers having different microstructure [80].   The compounding ingredients may present in the form of agglomerates in the matrix. The more the number of fillers, more the number of interfaces with polymer matrix.
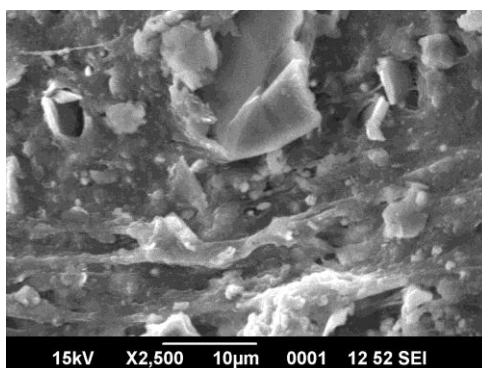
Fig.133. Micro structure of rubber at X 2500 magnification

The interfaces may create microvoids in the encapsulant due to improper wetting. Addition of fillers and curing agents in the highly viscous raw rubber may create voids. The scanning electron micrograph of a cross-section of rubber is shown in Fig. 133 which revealed the presence of particulate fillers and voids.

7.5. Effect of fillers on water uptake of encapsulant studied by FFISY

Addition of fillers introduces heterogeneity in the encapsulant. If the filler is compatible with the polymer matrix, the polymer completely wet the filler and creates an intact polymer–filler interface [3]. A non compatible filler introduces voids in the encapsulant due to improper wetting. A lot of studies have been conducted using EISY technique to study the effect of fillers on the water barrier property of encapsulant [125-129]. In this work FFISY is used to estimate the water uptake in filler loaded encapsulants.

7.5.1. Carbon black loaded polyurethane encapsulants

Water uptake of PU encapsulant filled with carbon black at different loadings was estimated by FFISY and EISY techniques (Fig.134 & 135). All the coatings have thickness 1± 0.1 mm and have different carbon black loading percentage; 2, 4, 6 wt%.
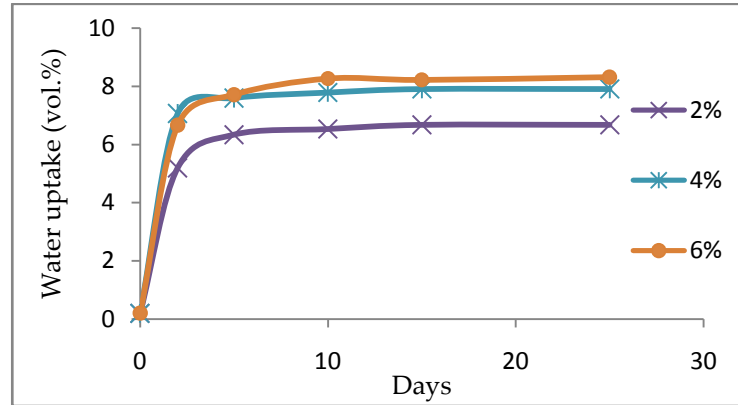
Fig 134: Water uptake profiles of CB loaded PU estimated by FFISY
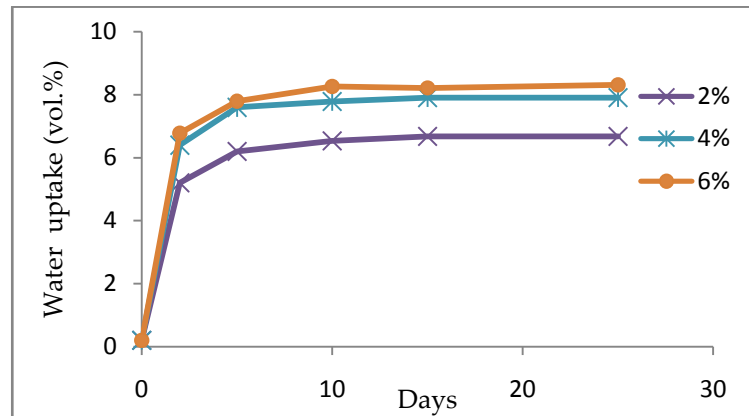
Fig 135: Water uptake profiles of CB loaded PU estimated by EISY

The addition of CB modifies the water uptake characteristics as evident from the graph. The water uptake estimated by EISY also show a similar behaviour and the difference in estimated values between two techniques were within ± 3 % (Fig.135). The saturated water content value increases with the addition of CB. This indicates that water distribution became more non uniform on the addition of CB. CB may create more voids in the encapsulant due to poor wetting and results in the non uniform distribution of water. The reason for the deviation is not relevant in the studies as the aim of the work was to compare the results with that of EISY so that FFISY can be used for estimation of water content in the filler loaded encapsulants.

7.5.2. Nano silica loaded polyurethane encapsulants

PU encapsulant filled with nano silica at different loadings was evaluated to study water uptake characteristics (Fig.136). All the coating has thickness 1 ± 0.1 mm and have silica loading of 2, 3, 4%. The addition of nano silica slightly

decreases the water uptake of the encapsulant. The water uptake estimated by EISY also showed similar behaviour and the difference in the estimated water content was within ± 2%.
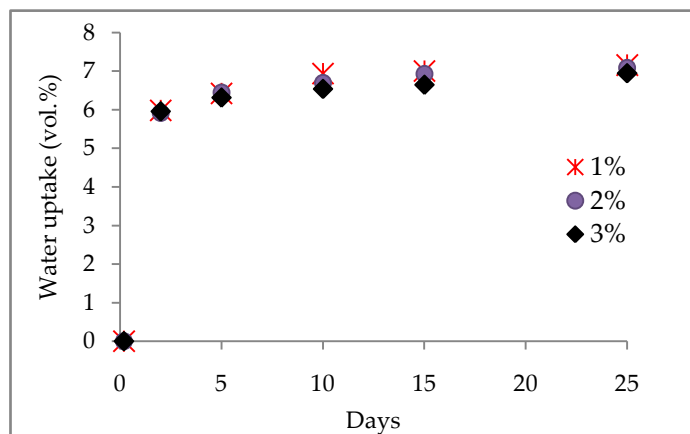
Fig 136: Water uptake profiles of nano silica filled PU

The slight decrease (0.2 %) in the water uptake of PU-silica encapsulant on addition of silica nano particles was observed. Many studies have reported that, addition of nano silica has improved the water barrier properties [125-127]. Nano fillers have a high surface energy due to its increased surface area per unit volume. A well dispersed nano particles interact with the polymer matrix and improves the water barrier properties of the encapsulant by creating a tortuous path for the water molecules.

7.5.3. PANi loaded polyurethane encapsulants

Water uptake profile of PANi loaded PU was estimated by FFISY technique (Fig.137). The addition of PANi enhances the water uptake of encapsulant. Water uptake profile of 20 % PANi could not be estimated by FFISY due to electrical short circuiting. The water uptake estimated by FFISY technique was compared with that of EISY technique (Fig. 138). The difference between the values from the two techniques was ~15 % for 15 % PANi and 8 % for 10 % PANi. It was also observed that, the water uptake is the maximum for 20% loading and the least for 10 %. If the PANi is well dispersed and uniformly distributed through the resin, and there are no agglomerates within the coating, water can only permeate by circumnavigation of the pigment particles, increasing the effective path length for diffusion and therefore lowering the permeability [3].
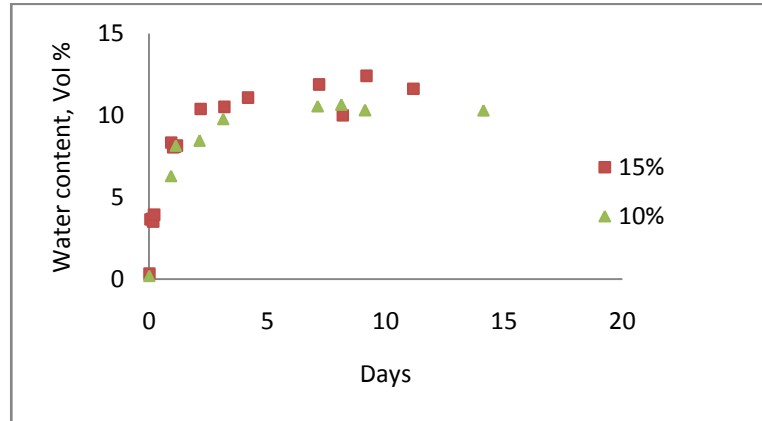
Fig.137. Variation of water uptake profiles for PANI-PU 10% and 15% estimated by FFISY
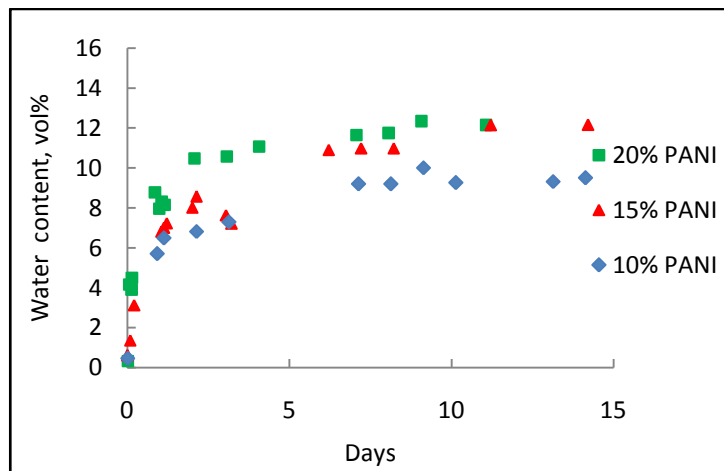
Fig.138. Variation of water uptake profiles for coated PANI-PU 10%, 15% and 20% estimated by EISY
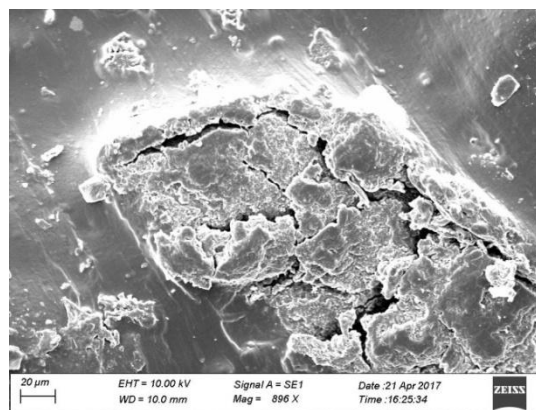
Fig 139. Micro cracks in PU-PANi encapsulants at X 500 magnification

The water uptake order indicates that, on addition of PANi, more pores are created in the coating and there is no sufficient wetting between PU and PANi. This

statement was supported by the presence of micro cracks in the encapsulant (Fig. 139).

7.6. Conclusion

The water uptake in the encapsulants was estimated by the change in capacitance due to water ingress. The intention of the study was to develop FFISY as a tool for the estimation of water uptake in encapsulant. Hence the measured results were compared with that of widely accepted EISY. For that, electrochemical impedance spectroscopy of encapsulants was measured in similar conditions. The water uptake was calculated from the change in capacitance of the encapsulant due to water ingress by applying widely accepted B-K equation.

Water uptake calculated from EIS and FFIS has 2 % difference if the encapsulant thickness is within the penetration depth of the FEF sensor. If encapsulant thickness was beyond the penetration depth of the sensor, water content estimated from the two techniques differ more than 5 %.

The water uptake estimated from capacitance technique was higher than gravimetric technique. Brasher-Kingsburry attributed the reason for this to the uneven distribution of water in the encapsulant. If water is distributed as columns perpendicular to the surface of the encapsulant, a higher water content value will be obtained. Also, uneven distribution of water can happen due to the presence of voids in the encapsulants. Water clogging in and around the micro voids may result in uneven water distribution. However the SEM does not show any presence of micro voids.

It is also observed that, as the encapsulant thickness increases, the deviation increases. A homogenous material shows closer water content values estimated from both the technique as reported by many authors. Thinner encapsulants are expected to have a more homogenous microstructure compared to that of a thick coating. It may be the reason that, the thicker coatings show a larger deviation from gravimetric technique than thinner encapsulants. In spite of this deviation, it has been shown that the capacitance method is valid for comparing the barrier effect of different coating or encapsulant formulations.

Fillers like CB and PANi in PU causes capacitance based water content to deviate largely from gravimetric value compared to unfilled PU. This was due to the presence of voids that may cause water clogging and hence results in uneven distribution of water. A slight decrease (0.2 %) in the water uptake of PU-silica encapsulant on addition of silica nano particles was observed. Water uptake of CB and nano silica loaded PU estimated by FFISY has similar values as that of EISY technique and variation lies in ± 2 %. Water uptake estimated for PANi filled PU by EISY and FFISY differ more than 10 % due to non-uniformity of the samples prepared in the techniques. The non-uniformity has happened due to the poor dispersion of PANi in PU which was confirmed by the SEM micrographs showing the presence of micro cracks in the PU-PANi encapsulants.

Neoprene encapsulant shows better performance than other encapsulants since it is less prone to water ingression and has higher impedance retention compared to others during the study period. The water uptake of the encapsulant decreased on addition of nano silica whereas on addition of other fillers like PANi and carbon black, the water uptake increases.

CHAPTER – 8

Estimation of Electrical Degradation

8.1. Objective

a) Estimation of electrical degradation of underwater encapsulants by fringing field impedance spectra and compare the results with that of electrochemical impedance spectra.

8.2. Introduction

The electrical resistance of the polymeric coating decreases with time during its exposure to saline water [3,4]. According to Mayne [120], water and ions penetrate into the coating in the areas with lower crosslink density in the first stage. Following that, an ion exchange process takes place, by which the ions from the electrolyte become attached to the polymer network. Consequently, the electrical resistance of the coating decreases.

The electrical resistance of the encapsulant can be estimated from the fringing field impedance spectrum by fitting the spectrum in the appropriate equivalent circuit (Fig.24). The percentage of electrical degradation was calculated and was compared with that obtained from EISY technique.

8.3. Comparison of electrical degradation estimated by FFISY and EISY

The electrical resistance is computed from the fringing field impedance spectra measured at regular intervals in chapter 5 and the change in value was plotted against time. The percentage of electrical degradation was calculated by comparing the instant value of electrical resistance with the virgin value, mathematically represented as;

$$Electrical\ degradation, \% = 100 - \left(\frac{R_{instant}}{R_{virgin}} * 100 \right) \qquad (18)$$

The electrical degradation is calculated from the ratio of instant EIS electrical resistance to the initial EIS electrical resistance obtained by fitting the EIS (100 Hz – 100 KHz) similar to FFISY. The electrical resistance variation estimated from FFIS and EIS were compared for selected samples of same material and thickness. The electrical resistance variation of PU and epoxy encapsulant samples in 3.5 wt % NaCl aqueous solution for two months were compared in the following sections.

8.3.1. Thin encapsulants

8.3.1.1. Polyurethane encapsulants

Electrical resistance of a 410 ± 10 μm thick encapsulant estimated from FFIS is plotted with time in Fig. 140. Electrical resistance decreased continously and reached a steady value after 40 days. The electrical resistance estimated from EIS also decreased with time and reached a steady value (Fig.141).
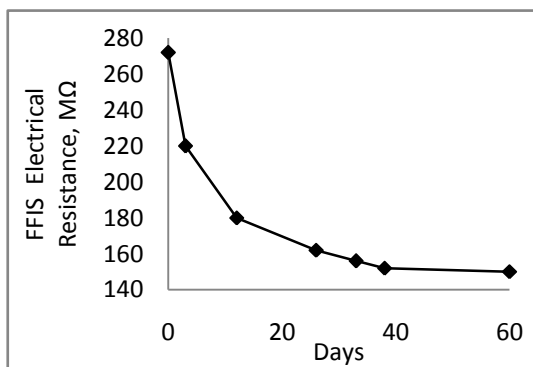
Fig. 140. Variation of electrical resistance with time of 410 μm thick PU encapsulant in saline water by FFISY
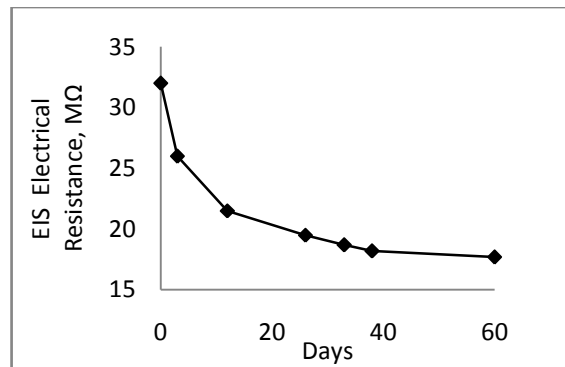
Fig.141. Variation of electrical resistance with time of 401 μm thick encapsulant in saline water by EISY

The estimated percentage of electrical resistance variation were comparable for both techniques. Around 40 % of the electrical degradation was occurred in the encapsulant during the evaluation period (Fig. 142). For a good coating, water uptake is the first step of electrical degradation process; this process causes the opening of conductive pathways in the coating, allowing the ions to pass through the coating [120]. It is reported in many EISY studies, pore resistance of the coating has decreased by 3 to 4 order when soaked in saline water for more than one week depending on the type of coating [132,135,136]. Here, EIS electrical resistance computed from EIS spectra (100 Hz to 100 kHz) were used for comparison with FFIS spectra of same frequency range.
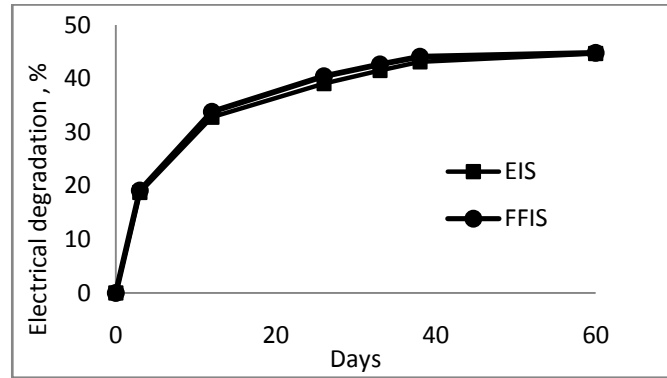
Fig.142. Comparison of percentage of electrical resistance variation of 410 μm thick PU encapsulant measured by FFISY & EISY

8.3.1.2. Epoxy encapsulants

The percentage of electrical degradation profile of fresh and aged epoxy encapsulants were compared. The initial resistance of two types of encapsulants was different as understood from Fig.143 (a) & (b). This may be due to the moisture attack during thermal oxidation on the aged encapsulant before immersing in 3.5 wt% NaCl aqueous solution.
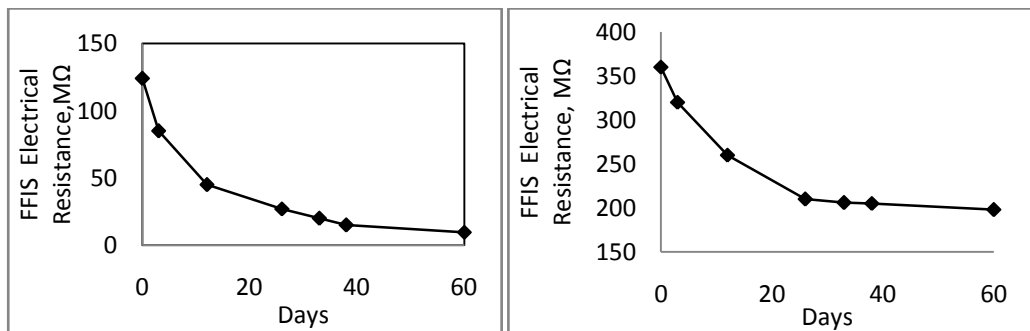
Fig. 143. Variation of electrical resistance with time of 410 μm thick epoxy encapsulant in saline water (a) aged epoxy and (b) fresh epoxy

The electrical resistance decreased in fresh and aged epoxy encapsulants. Electrical degradation of fresh and age epoxy encapsulant was 90 % and 40 % respectively. It is reported that thermal oxidation of Bisphenol-A diglycidyl ether based epoxy leads to carbonyl and amide formation with subsequent chain scission[133]. Glass transition temperatures (Tg) of the polymer decreases and sol fraction increases due the thermal oxidation [134]. After thermal oxidation, the polymer is expected to absorb more water due to the formation of degradation products of hydrophilic nature.The water and ions will ingress easily into the aged encapsulant due to more number of hydrophilic sites and results in a drastic reduction of electrical resistance. More than 80 % percentage of electrical

degradation was observed for aged encapsulant and 40 % percentage of electrical degradation was observed for fresh epoxy encapsulant of same thickness (Fig.144).
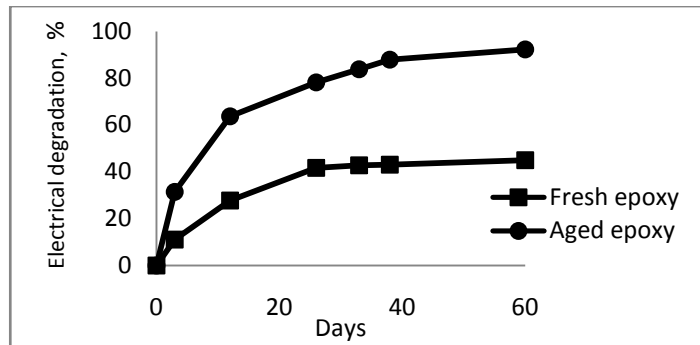
Fig.144. Comparison of percentage of electrical resistance variation of aged and fresh epoxy encapsulant measured by FFISY

8.3.2. Thick encapsulants

8.3.2.1. Polyurethane encapsulants

Electrical degradation profile of 2±0.1 mm thick PU encapsulant in 3.5 wt % NaCl aqueous slution were compared in similar fashion. The electrical resistance estimated from FFISY and EISY were shown in Fig. 145 (a) & (b). A 23 % decrease in FFIS electrical resistance was observed during the two months evaluation period comparable with percentage decrease of EIS electrical resistance (Fig. 146). As in the case of thin encapsulants, the decrease in resistance was due to the water attack in the low molecular weight or low cross linked sites (hydrophilic sites) [120].
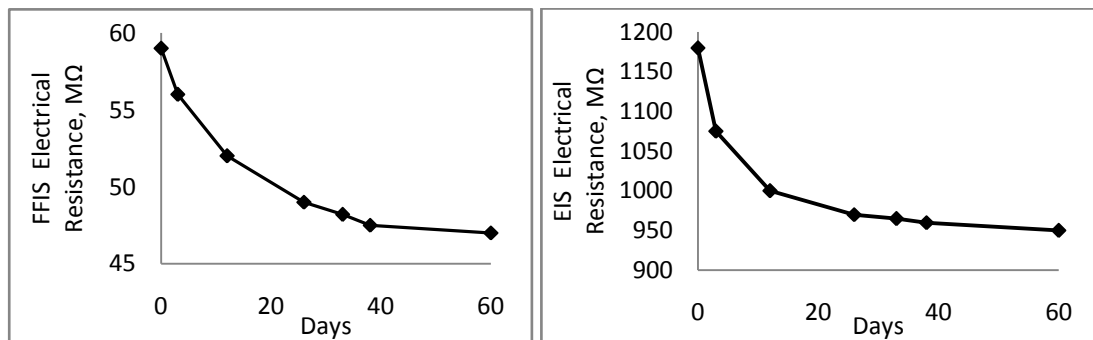
Fig.145. Variation of electrical resistance of 2 mm thick PU encapsulant with time (a) FFISY & (b) EISY

It is to be noticed that, the percentage of decrease is less in thick encapsulants compared to thin ones. This may be due to the number of 'hydrophilic sites' in the encapsulant exposed to water was same for both thick and thin

encapsulants as both have same exposure area. The underneath part of the encapsulant is yet to be attacked by water molecules during the 60 days evaluation period.
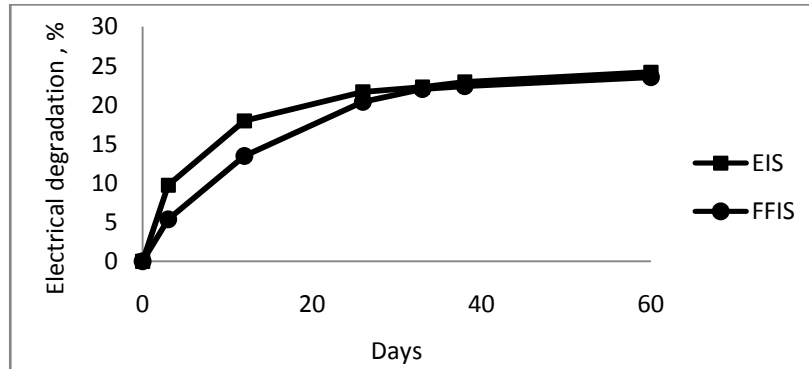
Fig.146. Comparison of electrical degradation profile of 2mm thick PU encapsulant measured by FFISY & EISY

8.3.2.2. Epoxy encapsulants

FEF sensor could record the electrical degradation profile of 1± 0.1 mm thick aged epoxy encapsulant during immersion in saline water. The decrease in electrical resistance value determined by EISY and FFISY technique are shown in Fig. 147 (a) & (b).
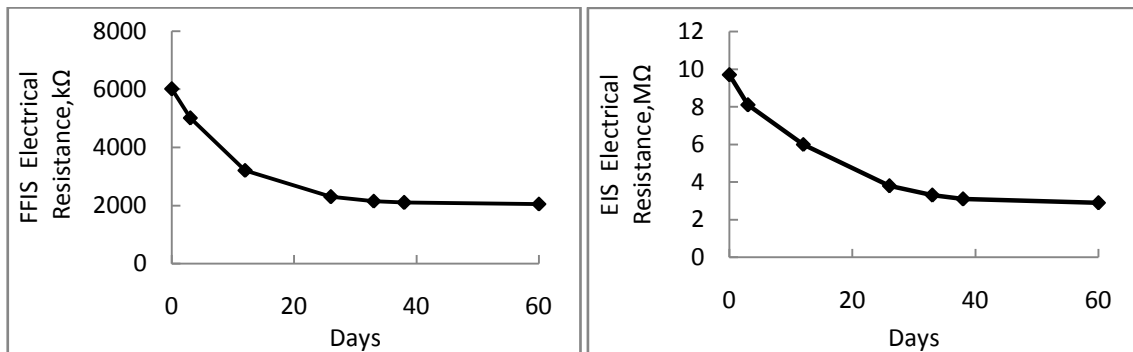
Fig.147. Variation of electrical resistance of an aged epoxy encapsulant with time (a) FFISY & (b) EISY

The FFISY and EISY shows a comparable electrical degradation profile estimated to ~70% (Fig. 148). The reason for selecting an aged epoxy encapsulant was to infuse considerable percentage of electrical degradation in the encapsulant during the evaluation period. Water ingress starts from the surface layer and go deeper in the encapsulant with time. The water attacks all the hydrophilic sites on the surface first and starts to move inside with time. A period of 60 days caused more than 80 % electrical degradation in thin encapsulant. Water ingress occurred

in the thick encapsulant from surface of same exposed area as that of thin encapsulants. As the encapsulant was thicker, water could not reach to entire thickness during 60 days of evaluation period so that only ~70 % electrical degradation happened in the encapsulant.
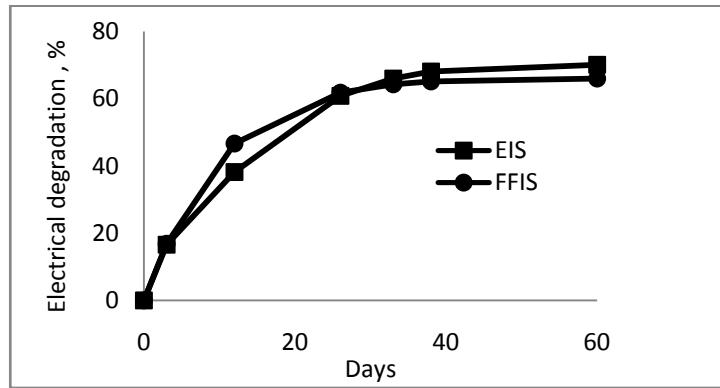
Fig.148. Comparison of percentage of electrical resistance variation profile of aged epoxy encapsulant measured by FFISY & EISY

8.3.2.3. Polychloroprene encapsulants

FFISY measured the decrease in electrical resistance of a 2 mm thick CR encapsulant immersed in 3.5 wt % NaCl solution for a period of 60 days (Fig.149 (a)). The electrical resistance measured by FFISY technique decreases from 70 MΩ to ~42 MΩ and saturates. The EIS electrical resistance decreases from 2.95 GΩ to 1.5 GΩ and saturates in a similar fashion (Fig.149 (b)). The electrical degradation profile obtained from FFIS and EIS shows a comparable pattern (Fig.150). The Electrical degradation of CR formulation has comparable with that of PU.
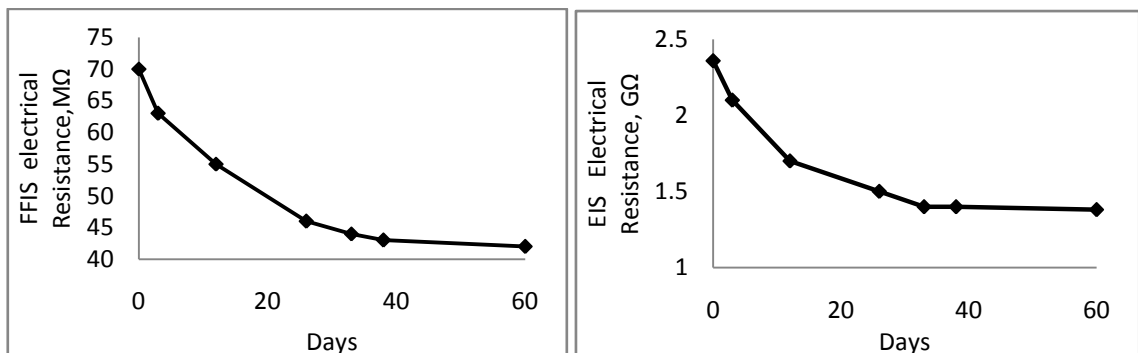
Fig.149. Variation of electrical resistance of 2 mm thick CR encapsulant immersed in 3.5 wt % NaCl solution measured by (a) FFISY & (b) EISY
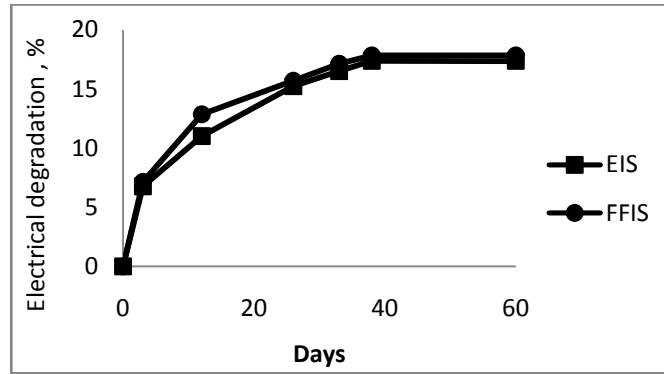
Fig.150. Comparison of percentage of electrical resistance variation profile of CR encapsulant measured by FFISY & EISY

8.3.2.4. Filled polyurethane encapsulants

Electrical degradation of filled encapsulants were estimated by FFISY. The electrical degradation of PU loaded with carbon black, nano silica and PANi were estimated by FFISY for 60 days. The results were compared with that of EISY technique.

8.3.2.4.1. Carbon black loaded polyurethane

Electrical degradation profile of 1 mm thick PU encapsulant loaded with 2% CB was compared with that obtained from EISY technique. It is observed that electrical resistance estimated by FFISY technique, decreases with time as in the previous cases (Fig.151 (a)). The EIS electrical resistance of the encapsulant was also decreasing with time as shown in Fig. 151 (b). Electrical degradation profile estimated by these techniques was comparable (Fig.152)
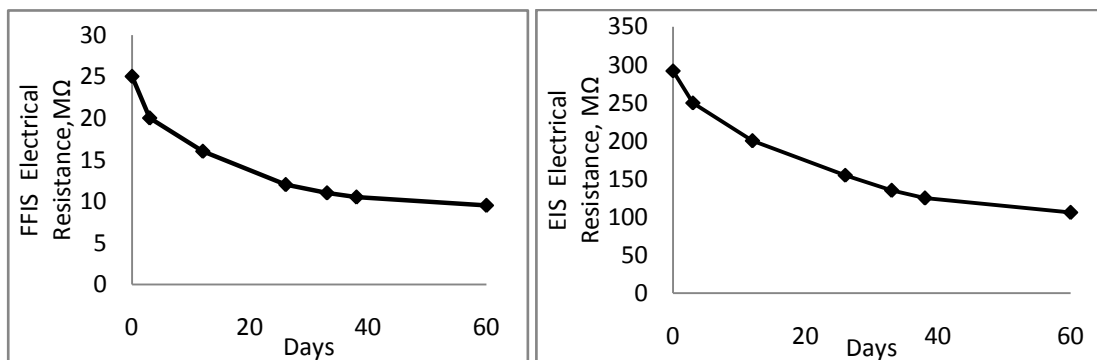
Fig.151. Variation of electrical resistance of 1 mm thick PU-CB 2% encapsulant immersed in 3.5 wt % NaCl aqueous solution (a) FFISY & (b) EISY

It was observed that CB powder was not properly wetted by PU resin during mixing. Poor adhesion between carbon black and PU create voids or even macroscopic defects in the PU-filler interface. It is reported that, the presence of macroscopic defects due to poor adhesion between pigment and binder would accelerate the electrical degradation [123, 139].
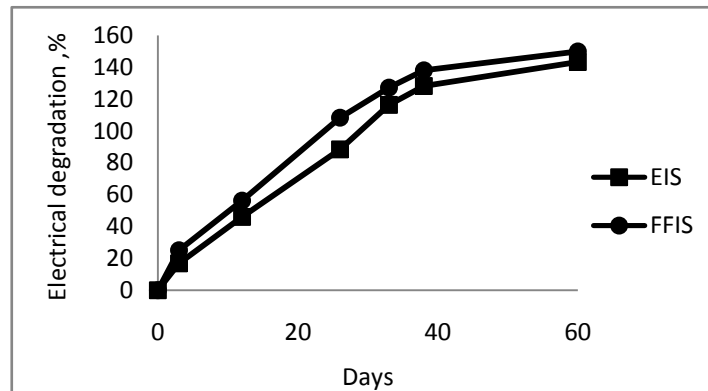
Fig.152. Comparison of percentage of electrical resistance variation profile of 1 mm thick PU-CB 2% encapsulant measured by FFISY & EISY

8.3.2.4.2. Nano silica loaded polyurethane

Electrical degradation profile of 1 mm thick PU encapsulant loaded with 4% silica in 3.5 wt% NaCl aqueous solution was estimated by FFISY and EISY (Fig.153 (a) & (b)). The electrical resistance decreases during 60 days of evaluation. The electrical degradation of the encapsulant was ~40 % which is lower than that of CB loaded PU (Fig.152). It indicates that, nano silica has better compatibility with PU than CB. The percentage of electrical degradation profile estimated by EISY supports this data.
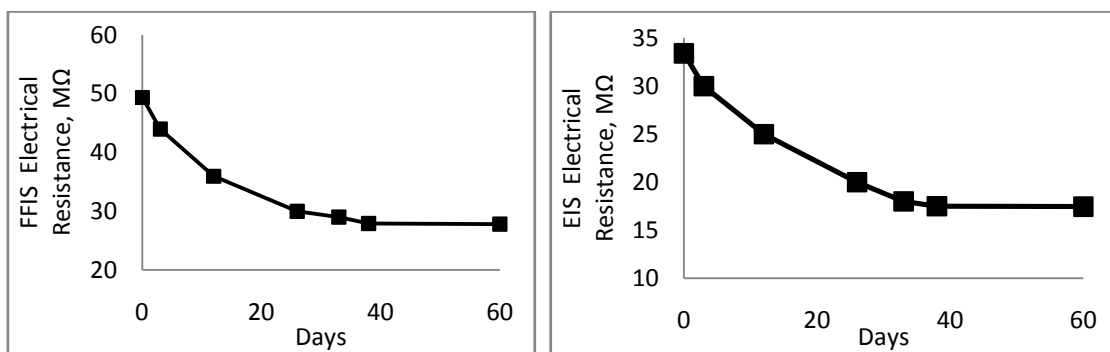
Fig.153. Comparison of percentage of electrical resistance variation profile of 1 mm thick PU-silica 4% encapsulant measured by (a) FFISY & (b) EISY
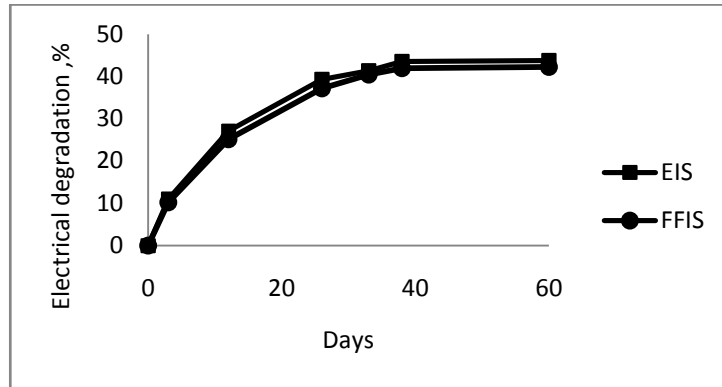
Fig.154. Comparison of percentage of electrical degradation of 1 mm thick PU-silica 4% encapsulant measured by FFISY & EISY

8.3.2.4.3. PANi loaded polyurethane

The electrical degradation profile of PU loaded with PANi was estimated by EISY. A decrease in electrical resistance for 10 wt%, 15 wt% and 20 wt% PANi encapsulants was observed immediately on exposure to saline water (Fig.155). The initial decay of electrical resistance of the system is fast and slows down after a few hours for all the three systems, indicating that water uptake occurs through the surface pores of the encapsulant in the initial hours.

The percentage of electrical degradation of the three encapsulants show same trend and stabilizes after a few hours (Fig.156). The study was done for two weeks as the saturation occurs within a few days. PU was not able to wet the PANi and it resulted in macro defects in the encapsulant as clear from the SEM images given in last chapter (Fig.139). This resulted in an accelerated electrical degradation in PANi loaded PU encapsulant.
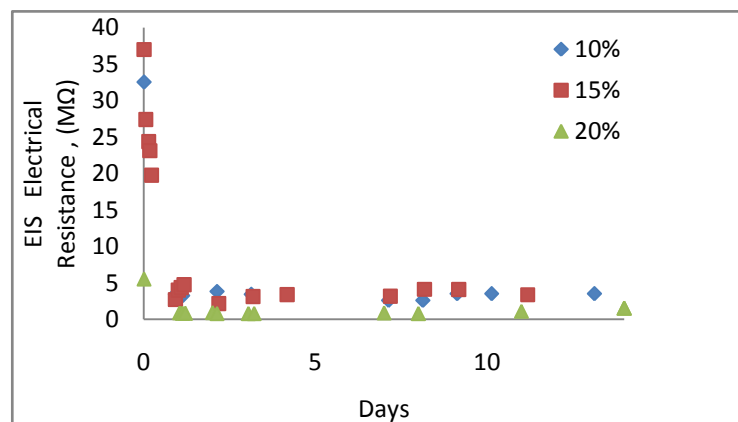
Fig. 155. Variation of electrical resistance of PU-PANi encapsulant with time
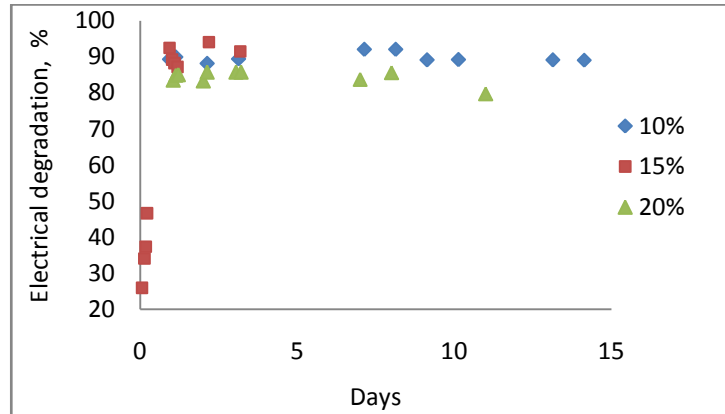
Fig.156. Percentage of electrical degradation PU- PANi encapsulant with time.

8.4. Conclusion

Electrical degradation profile of PU, epoxy and CR encapsulants was estimated by FFISY technique and EISY. The measured electrical resistance variation was comparable for both the techniques with values within ± 2 %.

The reason for the electrical degradation of the encapsulant in saline water was explained based on reported literature. For a good coating, water ingress in the encapsulant is the first step of electrical degradation process. Water uptake occurs due to the attack of water molecules in the inherent microscopic regions of encapsulants. These regions are 'hydrophilic' as they contain low molecular weight or low cross linked materials. Interconnection of these microscopic regions forms a conductive pathways for the ions. As a result, the electrical resistance of the encapsulant decreases.

Non compatible fillers create macroscopic defects and this accelerates the electrical degradation of the encapsulant. Hence non compatible fillers like carbon black and PANi enhances the water uptake and accelerates electrical degradation. At the same time, nano silica slows down the electrical degradation by improving the water barrier property. The percentage of electrical degradation profile estimated by FFISY and EISY techniques for the filled PU encapsulants was also comparable.

FFISY and EISY of aged epoxy encapsulant was measured to monitor large scale percentage of electrical degradation in a shorter period. A thick aged epoxy encapsulant succumbed to 70 % electrical degradation in less than 40 days and the results were comparable with that of EISY.

CHAPTER – 9

Development of a Portable FFIS Measuring System

9.1. Objective

The objective is to develop a prototype of a portable FFISY system for the field evaluation of underwater encapsulants. In order to achieve this, the following objectives were set;

(a) Development of a probe with FEF sensor and its characterization.

(b) Implementation of a measuring electronics for portable system.

(c) Measurement of FFIS of encapsulants using the probe and compare the estimated water uptake and electrical degradation with EIS.

9.2. Introduction

The water uptake and degradation profile of encapsulants can be monitored by FEF sensor as understood in previous chapters. However, the studied sensor needs to be converted into a system suitable for field measurement. A hand held probe mounted with FEF sensor and a portable measuring electronics, forms the parts of a portable system.

9.3. Development of probe

The portable FFIS system has a probe named as 'impedance probe' carrying the sensor at one end. The probe was designed to be held in hand and kept over the encapsulant for measurement. The sensor is projected out of probe structure for better contact with encapsulant during measurement. Fig. 157 shows the schematic of cross-section of impedance probe.

The FEF sensor is connected to a measuring circuit by a flexible cable. The sensor and the cable are housed in a Delrin body. Delrin housing has a diameter of 35 mm and length 10 cm. The probe is capped with a high density material such as steel for providing sufficient weight to the probe. The total weight of the probe is 520 gm. This facilitates an intact contact between sensor and the encapsulant during measurement without holding the probe, improves repeatability of readings.
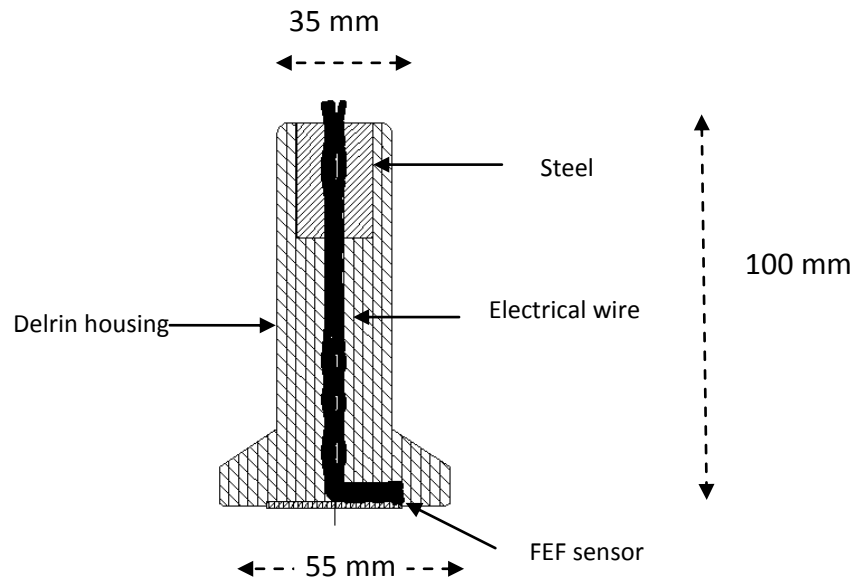
Fig. 157.Schematic of impedance probe (Patent pending- application No. No.201711004301)

9.3.1. Modification of FEF sensor

The developed FEF sensor for the evaluation of thin encapsulants was modified to insert on the probe. The contact area of FEF sensor was increased to enhance the sensitivity without modifying electrode width and spacing between electrodes. Enhancement of area improves the sensitivity by increasing the capacitance of the sensor. The area of the sensor was increased from 93 mm^2 to 10 cm^2. Fig.158 shows the modified sensor and Fig. 159 is the 500 times magnified image of the sensor electrodes. Electrical leads are taken from the back side of the sensor near the edge.
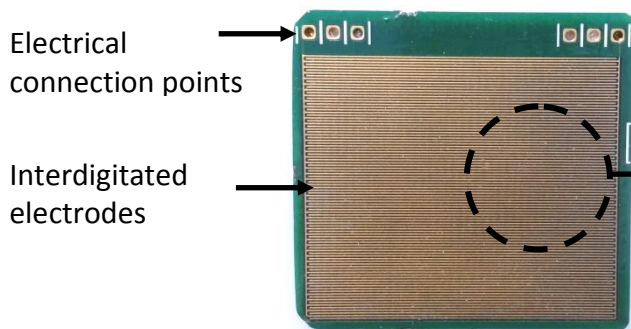
Fig.158. Modified FEF sensor
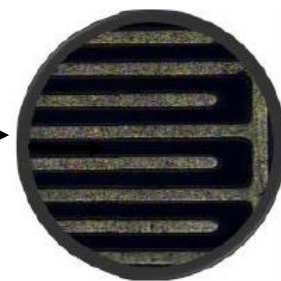
Fig.159. Electrodes of FEF sensor with interdigitated electrodes with 500 times magnification seen through optical microscope.

9.3.2. Passivation of modified FEF sensor

Passivation is generally defined as a technique of rendering a substance inactive or inert by chemical action. In this study, the sensor surface is coated with a thin layer (~10-25 μm) of polymer and the process is called as passivation of sensor. Passivation of sensors offers the following advantages;

1. Passivation avoids chances of electrical shorting between closely spaced metal electrodes by any conductive micro particles.
2. Passivation helps to minimize the air film between sensor and the material under test i.e. encapsulant. An air free contact during measurement provides repeatability in measurement readings.
3. Environmental protection-stability and life of sensor improves.

Fig.160 shows schematic lay out of the passivated sensor. Passivated sensor (Fig.161) has a flat surface so that an intimate contact will be maintained between sensor and the test sample.
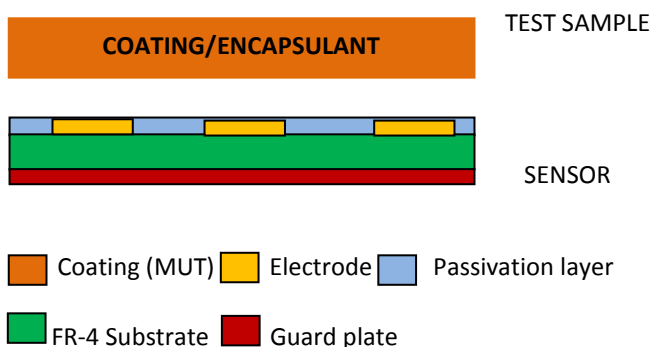
Fig.160. Schematic -Cross-section of passivated sensor   Fig.161. Passivated sensor
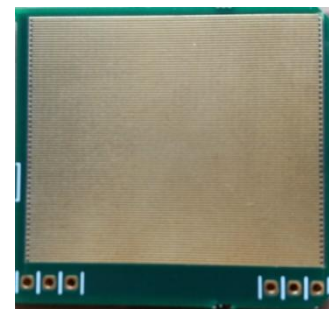
9.3.2.1. Passivation process

An ultra low viscosity epoxy resin was selected for passivation process to wet the sensor thoroughly including the narrow spaces between the electrodes. An embedding resin (EPON epoxy embedding kit) was selected as it has low viscosity (~130cP) and excellent adhesion characteristics. The sensor was immersed in sonicated resin bath for 30 minutes and then after allowed to spin in a spin coater for 2 minutes. A film having thickness 14 μm, was formed over the sensor and allowed to cure in room temperature (27 ± 1° C) for 48 hours.

9.3.2.2. Effect of passivation on sensor characteristics

The capacitance spectra of all the sensors in selected liquids (A.R grade), were measured from 100 Hz to 10 MHz using LCR bridge (model: Wayken) before (Fig.162) and after passivation (Fig.163). The dielectric constants of selected liquids are given in the bracket; Hexane (ε_r=1.88), Ethyl acetate (ε_r=6.02), Isopropyl alcohol (ε_r=19.92), Ethanol (ε_r=24.6), water (ε_r=78.3).
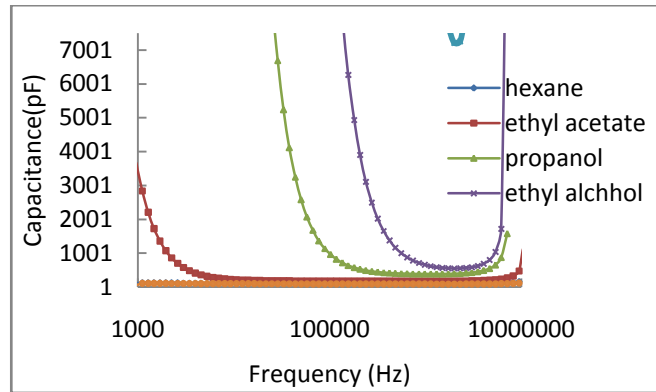
Fig.162.Capacitance-frequency spectra of impedance probe FEF sensor before passivation
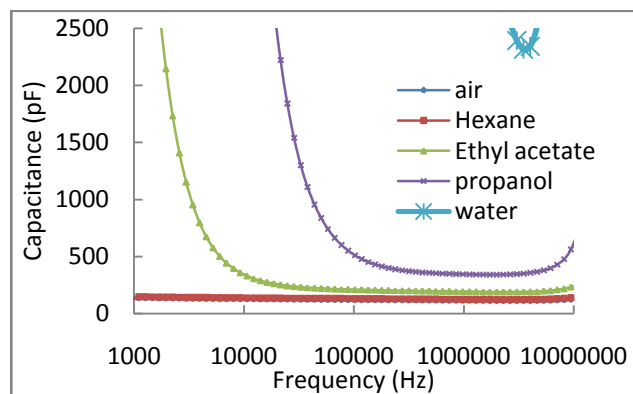
Fig.163. capacitance frequency spectra of impedance probe FEF sensor after passivation
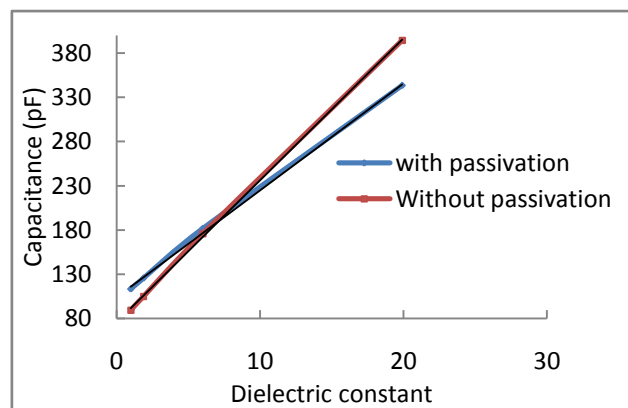
Fig 164. Effect of passivation on the sensitivity of the impedance probe FEF sensor

The sensitivity of the sensor decreased due to passivation (Fig.164). The sensitivity decreases from 16.05 pF/dielectric constant to 12.07 pF/dielectric constant. Also it is interesting to note that, the frequency at which the linear relationship between capacitance and dielectric constant came down after passivation. The sensor response was non-linear at 88 kHz before passivation as shown in Fig.165. However, sensor shows a good linear response at 88 kHz after passivation (Fig. 166).
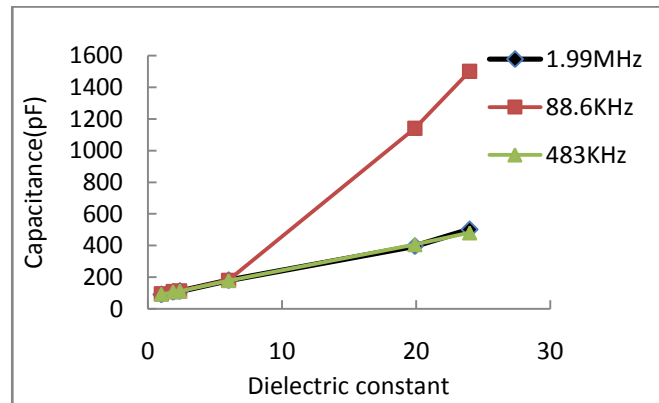
Fig 165. The frequency at which the impedance probe FEF sensor shows linearity before passivation
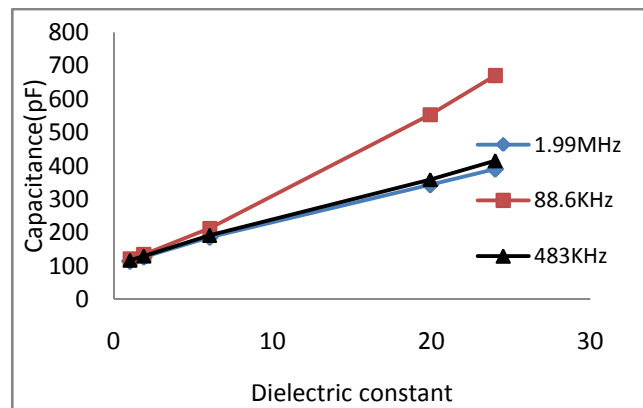
Fig 166. The frequency at which the impedance probe FEF sensor shows linearity after passivation
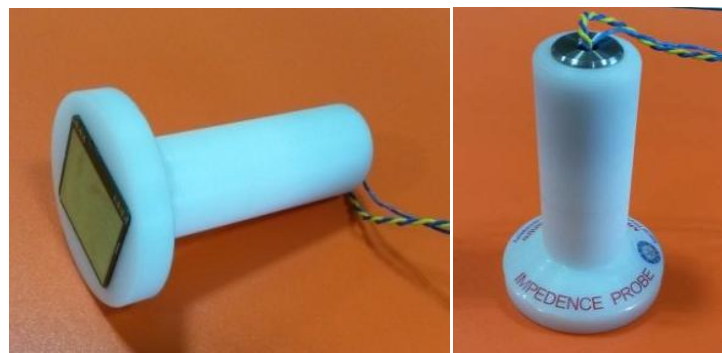
Fig.167. Photographs of fabricated fringing electric field impedance probe

Fig.167 shows the developed impedance probe. The probe was placed over the encapsulant test sample and voltage was applied through two electrical leads and an additional electrical wire is connected to the guard plate (back plate) of the sensor for grounding.

9.4. Measuring circuit development

It was proved that FEF sensor could measure the electrical resistance and capacitance changes in the encapsulant due to water ingress. All the sensor readings were measured by the impedance analyzer in the laboratory. A measuring circuit (Application Specific Integrated Circuit-ASIC) was developed with the help of a professional circuit designer in order to make the system portable to facilitate field evaluation. The probe was connected to the measuring circuit (Fig.168) which has a potentiostat with frequency response analyzer (FRA). The probe on contact with the surface of the coating measures the FFIS from 100 Hz to 100 kHz on applying specified sinusoidal voltage. The impedance and phase measured by the sensor was compared with that measured using impedance analyzer. The measured impedance spectrum of the encapsulant was fitted to the equivalent circuit to get encapsulant capacitance and resistance.

Fig.168. Fabricated measuring circuit.

9.4.1. Circuit calibration

ASIC was calibrated with a standard impedance analyser (Waynker) in the designed frequency range. The impedance spectrum of the impedance probe FEF sensor was measured by ASIC in air and the measured spectrum is compared with the spectrum measured by the standard impedance analyser (Fig.169 & 170).

The error was calculated in the measurement readings by ASIC, assuming that the reading obtained from impedance analyser is a true value. The error is calculated as the ratio of the difference in measured value of ASIC and impedance

analyser to the value of impedance analyzer. The percentage of error in impedance and phase measurement were less than 2 % and 3 % respectively (Fig.171).
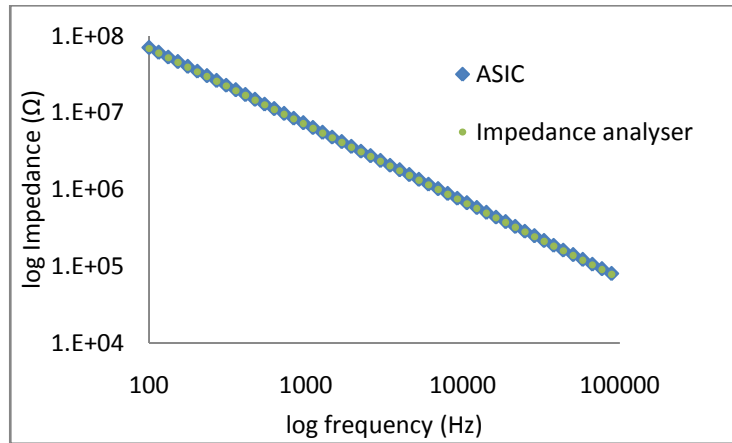
Fig.169. Comparison of impedance spectra of impedance probe FEF sensor measured by ASIC and impedance analyser
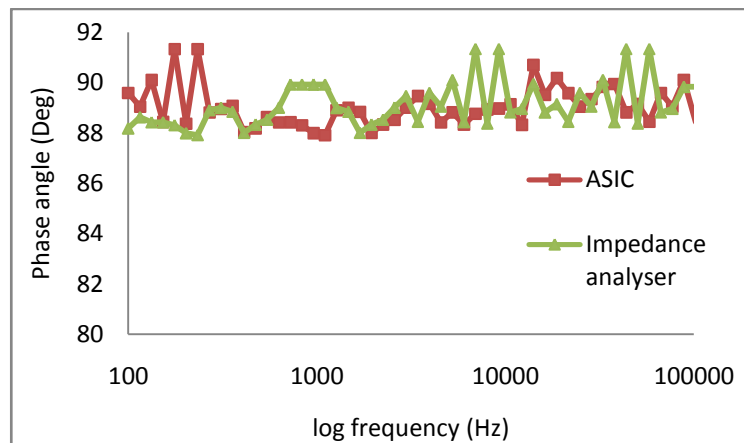
Fig.170. Comparison of phase angle spectra of impedance probe FEF sensor measured by ASIC and impedance analyser
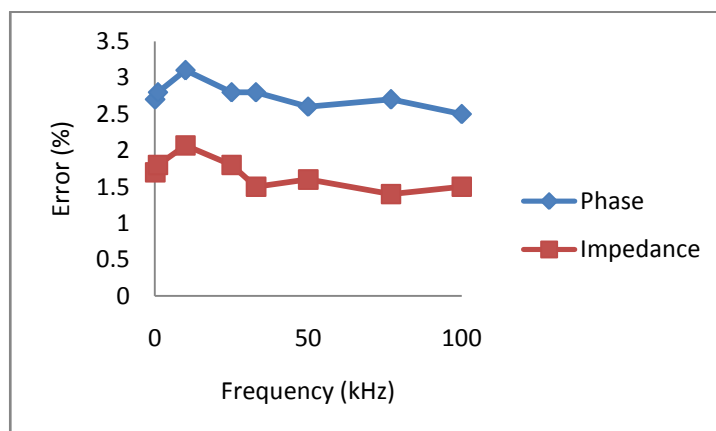
Fig.171. Error in measurement of impedance and phase of impedance probe FEF sensor by ASIC

9.5. Measurement of impedance spectra by impedance probe

Impedance spectra of PU and CR encapsulant test sample were measured by impedance probe.

9.5.1. Polyurethane encapsulants

PU sheet samples of 10x10 cm dimension having thickness 405 ± 30 μm were immersed in 3.5 wt% NaCl aqueous solution. The samples were taken out of saline water and carefully wiped the surface of the sample using a filter paper before each measurement. The impedance probe was placed over the dry surface of PU encapsulant test sample for the measurement of FFIS. The dimension of PU sample was larger than FEF sensor area to avoid any edge effects in measurement (Fig.172). The probe was connected to the ASIC and measurements were taken at different time intervals. The measurement was taken at the same place on the surface of PU sample to avoid error in reading due to change of measurement place.
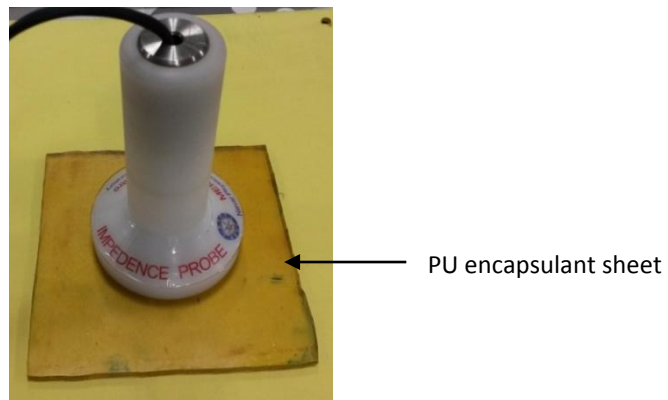
Fig.172. Evaluation of PU encapsulant sheet using impedance probe.
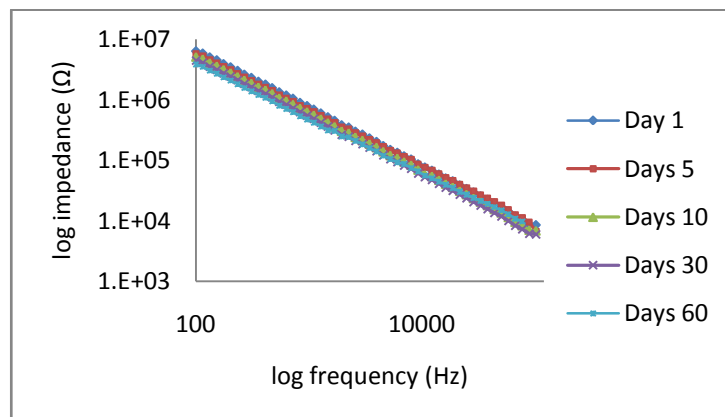
Fig.173. Fringing feild Impedance spectra of 405 μm thick PU encapsulant measured by impedance probe.

Fringing field impedance spectra of PU sheet exposed to saline water is shown in Fig.173. The impedance decreased from ~6.3 MΩ to 3.8 MΩ after 60 days of immersion in saline water. The recorded FFIS spectra were used to estimate the water uptake profile. EIS spectra of another PU sample of same thickness (± 30 μm) were taken to estimate the same. Capacitance–time profile of   PU encapsulant of same thickness measured by EISY and FFISY were shown in Fig.174 (a) & (b). Even though capacitance values were different for different techniques, the profile remains same. The water uptake profile estimated using Brasher Kingsbury equation was within 2% difference (Fig.175).
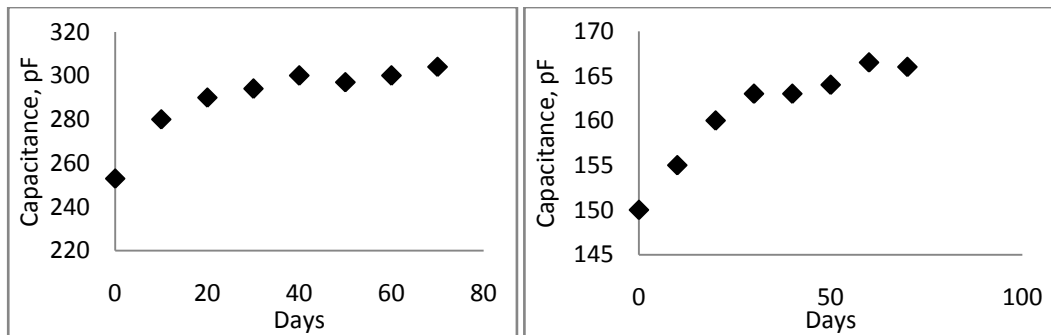
Fig.174: Capacitance variation of 398 μm PU encapsulant in 3.5 wt% NaCl aqueous solution measured by (a) EIS & (b) impedance probe
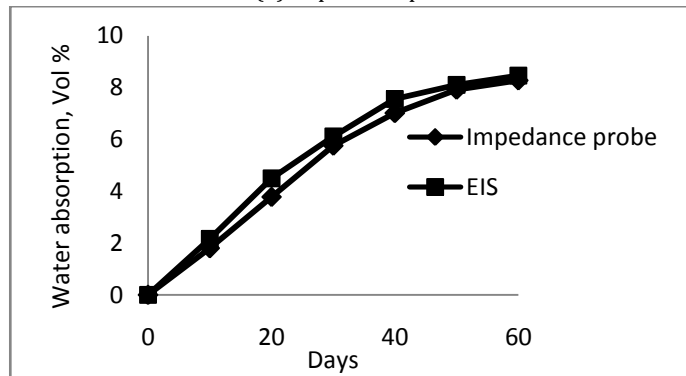
Fig.175: Water uptake profile of PU encapsulant in 3.5 wt% NaCl aqueous solution measured by impedance probe & EISY

Electrical resistance of the encapsulant decreases with time as revealed by FFIS and EIS (Fig. 176 (a) & (b)). The electrical resistance values were different for FFISY and EISY techniques. However the percentage of electrical degradation was comparable (Fig.177).
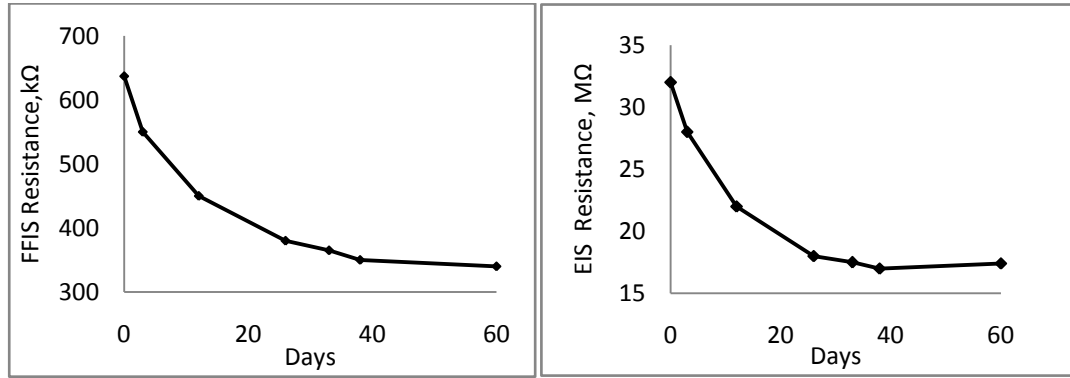
Fig.176. Variation of electrical resistance of PU encapsulant measured by (a) impedance probe & (b) EISY
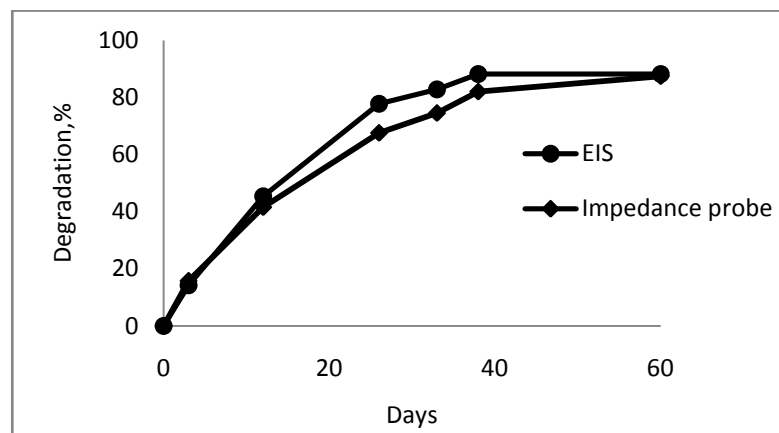
Fig.177. Comparison of degradation profile of PU measured by impedance probe & EISY

9.5.2. Polychloroprene encapsulants

CR encapsulant samples of 100 x100x1.5 mm dimension was immersed in 3.5wt% NaCl aqueous solution. Fringing field Impedance spectra of CR encapsulants were measured by impedance probe. The samples were taken out of saline water and carefully wiped all water drops from the surface of the sample using a filter paper before each measurement. The impedance probe was placed over the rubber and measured the FFIS (Fig.178).

CR encapsulant sheet
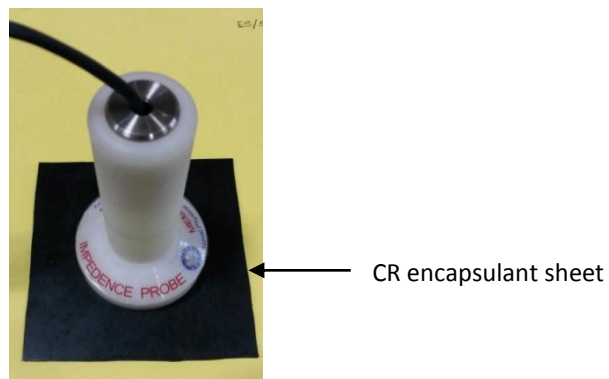
Fig.178. Evaluation of CR encapsulant sheet using impedance probe.

The probe connected to the impedance analyzer and the measurement was taken at regular intervals. The measurement was taken at the same place of the rubber sheet to avoid error in reading due to change of measurement place. Fringing field impedance spectra of CR encapsulant sheet exposed to saline water is shown in Fig.179.
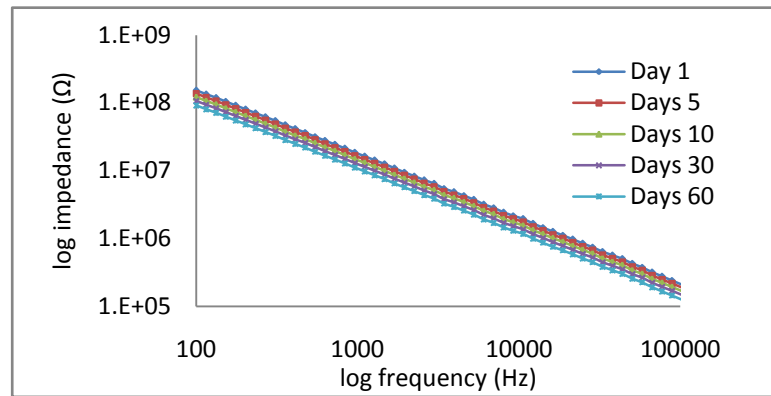
Fig.179. FFIS of CR encapsualnt sheet of 1.5 mm thickness measured by impedance probe.

The capacitance changes during water uptake was calculated by FFIS and EIS (Fig.180 (a)& (b)). The estimated water uptake calculated from capacitance changes has comparable profile (Fig.181).
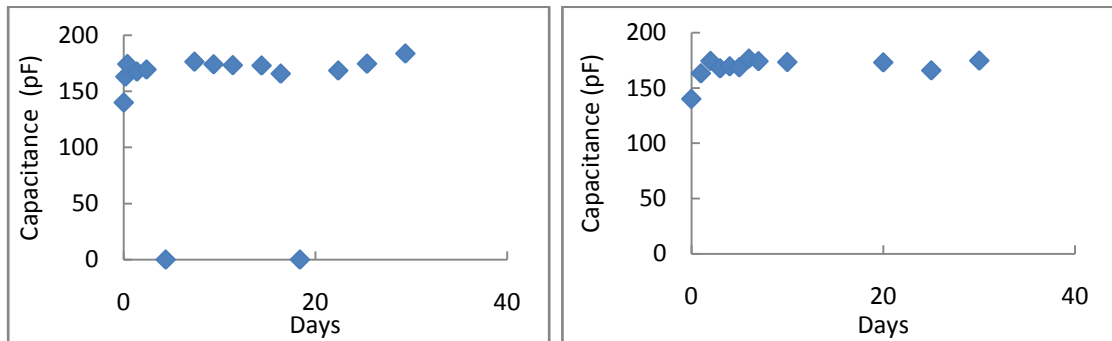
Fig.180: Capacitance variation of 1.5 mm CR encapsulant in 3.5 wt% NaCl aquous solution, measured (a)by EISY & (b) impedance probe
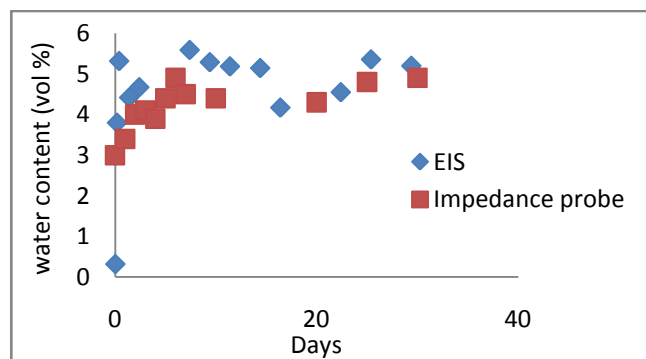
Fig.181: Water uptake profile of CR encapsulant in 3.5 wt% NaCl aqueous solution measured by impedance probe & EISY

The decrease in electrical resistance of CR encapsulant was estimated by impedance probe is shown in Fig.182 (a). The electrical resistance decreases with time and saturates after 40 days. The EIS electrical resistance of the CR encapsulant was plotted in Fig.182 (b). The FFIS electrical resistance and EIS electrical resistance change has similar trend even though the values were different. The degradation percentage calculated based on decrease in FFIS & EIS electrical resistance has comparable values (Fig.183). The electrical degradation percentage was below 2.5% during the 60 days of evaluation, for both the techniques.
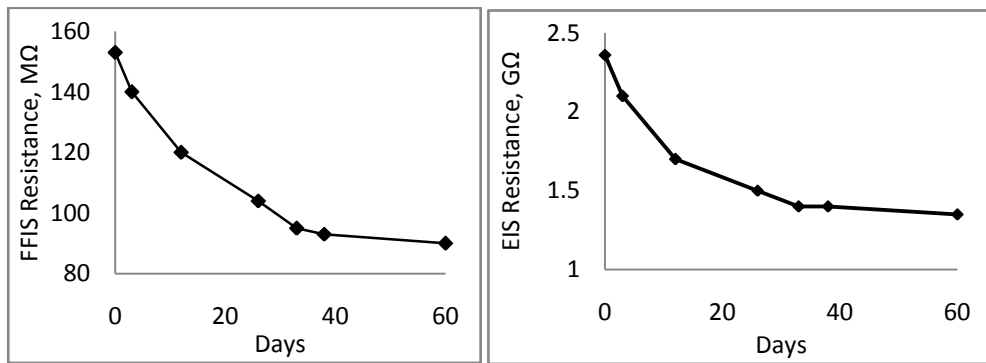
Fig.182. Variation of electrical resistance of CR encapsulant in 3.5 wt% NaCl aqueous solution with time measured by (a) impedance probe & (b) EISY
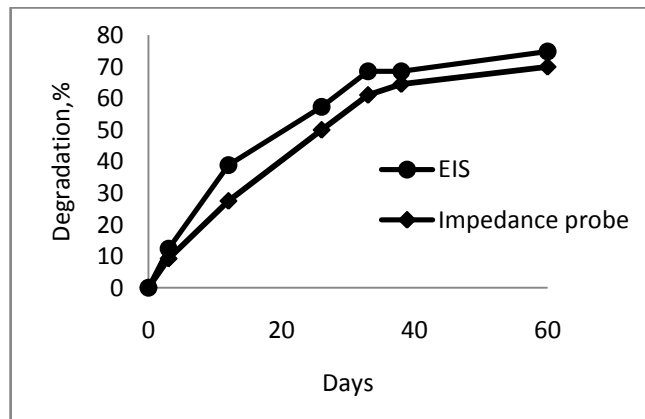
Fig.183. Comparison of electrical degradation profile of CR encapsulant in 3.5 wt% NaCl aqueous solution with time, measured by impedance probe & EISY

9.6. Estimation of electrical resistivity from FFIS electrical resistance

Estimation of electrical degradation of encapsulant materials is based on the change in electrical resistance of that material. Hence, the estimation of absolute value of electrical resistance (electrical resistivity) is not essential for the calculation of electrical degradation. However, electrical resistivity can be calculated by calibrating the sensor with standard samples. The resistance (R_{coat}) of

the encapsulant is related to its resistivity (ρ_{coat}) by the cell constant K_{Cell} [70] as described by eqn.7 & 8.
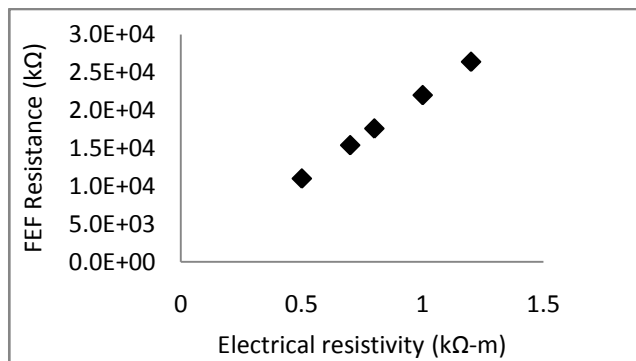
Fig.184. Calibration chart of impedance probe FEF sensor for measuring electrical resistivity

The electrical resistance of FEF sensor was measured when immersed in standard KCl solutions of known electrical resistivity as per ASTM D1125-91. Cell constant of the FEF impedance probe sensor was calculated by Eqn.8 or from the slop of the curve (Fig.184). The calibrated probe was used for measuring the electrical resistivity of the unknown samples. The cell constant of the sensor was 0.045 cm^{-1}.

9.7. Conclusion

A portable evaluation system with hand held probe and a portable measuring circuit were developed for the field evaluation of underwater encapsulants. Measuring circuit was validated with a standard impedance analyzer. The FFIS of PU and CR encapsulant samples in 3.5 wt % NaCl aqueous solution were recorded using the probe named as FEF impedance probe. The water uptake profile and electrical degradation of encapsulant samples were comparable with that from EISY. It is also observed that, the data obtained during calibration and testing were less noisy compared to the impedance probe measurement on the exposed encapsulant. This may be due to the intact contact of the sensor with the coating during calibration.

The technical data sheet of impedance probe is given below;

a. Water content estimation (or dielectric constant estimation)

   i. Sensitivity: 12.1pF / dielectric constant

   ii. Accuracy : ± 0.1 %

   iii. Range: 1-10 dielectric constant

    b. Electrical resistance measurement

      i. Sensitivity: ± 0.05%

     ii. Accuracy: ± 0.1 %

    iii. Range: 10 GΩ to 1 MΩ

The water uptake and electrical degradation profile estimated from FFIS were very well comparable with EIS. This technique can be used for the non destructive measurement of water uptake and electrical degradation of underwater encapsulants.

CHAPTER – 10

Summary & Suggestions for Future Studies

10.1. Summary

A non destructive technique is developed in this study for measuring the water uptake and electrical degradation of encapsulants. The technique developed is a novel application of fringing field impedance spectroscopy and the intellectual property right of this technique is protected by filing an Indian patent (Application No.201711004301 dated 30 March 2017).

Fringing electric field (FEF) sensor is the essential part of fringing field impedance spectroscopy. A FEF sensor which can measure changes in capacitance and electrical resistance of encapsulants during water ingress, is developed in this thesis work. Sensitivity and penetration depth (measurement depth) were identified as the main sensor parameters to be optimized during design process. Following conclusions were made on the design of FEF sensor.

- Sensor area, width of sensor electrodes and gap between sensor electrodes are the important dimensions that determine the sensitivity and penetration depth of FEF sensor.

- The sensitivity of the FEF sensor for determining water uptake can be increased by four times by one unit increase in sensor contact area.

- As the gap between electrodes decreases, sensitivity of the sensor to measure the water uptake in the encapsulant increases and the effect is exponential below 50 μm electrode gap.

- As the electrode width increases, sensitivity of the sensor to measure the water uptake in the encapsulant increases.

- The sensor sensitivity for water uptake measurement is largely depend on electrode gap than electrode width and it is six times more for electrode gap below 50 μm.

- For the electrodes having gap 10 μm and width 300 μm, 1 vol % of water uptake by the encapsulant resulted in increase of 0.47 pF unit capacitance.

- Penetration depth of the FEF sensor and sensitivity for capacitance variation are inversely proportional.

- Penetration depth of the FEF sensor and sensitivity for electrical resistance variation are directly proportional.

- These relations were quantified theoretically and further verified experimentally.

- An optimum sensitivity is observed for both capacitance and electrical resistance measurement near to penetration depth of 500 μm. Hence FEF sensor with penetration depth ~500 μm were selected for encapsulants having thickness up to 500 μm.

- It is concluded from analytical studies that, sensors with different penetration depth are required for different encapsulant thicknesses for maximizing the sensitivity.

Two types of FEF sensor designs having penetration depths 500 μm and 2 mm, were selected for fabrication for measuring encapsulants having thickness varying from 100 μm to 2 mm.

The above sensors were fabricated by a cost effective method using PEN mask. Cost effective method and materials (FR-4 PCB) selected for the fabrication of PCB make this sensor very economical.

Water uptake of encapsulants and its resultant electrical degradation in saline water was monitored by continuously measuring the fringing field impedance spectra by the FEF sensor. This was done by following the increase in capacitance and decrease in electrical resistance of encapsulants due to water ingress.

The measured water uptake and percentage of electrical degradation were comparable with the values estimated from electrochemical impedance spectroscopy.

The measured water uptake was compared with the value estimated by gravimetry and found higher. The difference between the values of two techniques increased as the thickness of encapsulant increased. This variation is attributed to the two different method of measurement adopted, capacitance method and gravimetric method and explained based on literature citation.

Finally, a prototype hand held sensor probe and a portable measuring circuit were developed in this thesis work. The FEF sensor which is to be fitted in the probe, is modified by enhancing the contact area and giving a passivation layer over the sensor. The measuring circuit is validated with standard impedance analyser. The water uptake profile and electrical degradation percentage were estimated by the probe and the readings were comparable with the values from EISY.

From the above studies, it is concluded that FFISY technique can be employed as a non destructive technique for measuring water uptake and electrical degradation of encapsulant.

10.2. Suggestions for future studies

1. The experiments in this research work were conducted in controlled temperature ($27 \pm 1°C$). Effect of temperature on the measurements needs to be estimated in future studies.

2. Similarly, the effect of humidity on the sensor measurements needs to be estimated.

3. A sensor with multiple level of penetration depth is proposed as future work, so that different sensors may not be required for different encapsulant thickness. This can be achieved by placing sensor electrodes physically as close as possible and by implementing programmable measuring circuit.

4. A sensor with soft contact surface is proposed for encapsulant with rough surface to achieve an intact contact between sensor and encapsulant.

5. Analytical studies have done for the encapsulant below 100 μm and corresponding sensor needs to be developed suitable for thin coatings below 100 μm.

6. A FEF sensor for dielectric mapping of encapsulant is proposed for detecting voids in encapsulants.

7. A flexible FEF sensor is proposed which can be conformal to any curved surface so that encapsulants having curved surfaces can be evaluated.

REFERENCES

1. C. H. Sherman, J. Butler, Transducers and arrays for underwater sound, Springer Science (2007) Newyork.

2. D. Stansfield, Underwater electroacoustic transducers: a handbook for users and designers, Bath University Press (1991)

3. G. K. van der Wela and O. C. G. Adan, Moisture in organic coatings-a review, Progress in Organic Coatings, 37 (1999)1.

4. A. Amirudin, D. Thierry, Application of electrochemical impedance spectroscopy to study the degradation of polymer-coated metals, Progress in Organic Coatings, 26(1995)1.

5. J. M. McIntyre, H. Q. Pham, Electrochemical impedance spectroscopy; a tool for organic coatings optimizations, Progress in organic coatings, 27(1996)201.

6. K. S. Rajan, L. Byrd II, and A. V. Mamishev, Moisture content estimation in paper pulp using fringing field impedance spectroscopy, IEEE Sensors Journal, 4(2004) 378.

7. K. S. Rajan, L. Byrd and A. V. Mamishev, Measuring moisture, fiber and titanium dioxide in pulp with impedance spectroscopy, TAPPI Journal, 4(2005)23.

8. R. B. McIntosh and M. E. Casada, Fringing field capacitance sensor for measuring the moisture content of agricultural commodities, IEEE Sensors Journal, 8(2008) 240.

9. A .D. Waite, Sonar for Practising Engineers, Third Edition, John Wiley & Sons (2002)

10. D. M. Brasher and A. H. Kingsbury, Electrical measurements in the study of immersed paint coatings on metal. I. Comparison between capacitance and gravimetric methods of estimating water uptake, Journal of Applied Chemistry, 4 (1954)62.

11. G. W. Walter, The application of impedance methods to study the effects of water uptake and chloride ion concentration on the degradation of paint films—I. Attached films, Corrosion Science, 32(1991)1059.

12. V. B.Miskovic-Stankovic, M. D. Maksimovic, Z. Kacarevic-Popovic and J. B. Zotovic, The sorption characteristics and thermal stability of epoxy coatings

electrodeposited on steel and steel electrochemically modified by Fe–P alloys, Progress in Organic Coatings, 33(1998)68.

13. V. B. Miskovic-Stankovic, M. R. Stanic and D. M. Drazic, Corrosion protection of aluminium by a cataphoretic epoxy coating, Progress in Organic Coatings, 36 (1999)53.

14. V. B.Miskovic-Stankovic, D. M. Drazic and M. J. Teodorovic, Electrolyte penetration through epoxy coatings electrodeposited on steel, Corrosion Science, 37(1995)241.

15. V. B. Miskovic-Stankovic, D. M. Drazic and Z. Kacarevic-Popovic, The sorption characteristics of epoxy coatings electrodeposited on steel during exposure to different corrosive agents, Corrosion Science, 38(1996)1513.

16. R. A. Nelson, The determination of moisture transitions in cellulosic materials using differential scanning calorimetry, Journal of Applied Polymer Science, 21 (1977)645.

17. L. Rodriguez-Pardoa, A. Cao-Paza, J. Farinaa, A. Covelob, X. R. Nóvoab and C. Pérezb, Water uptake kinetics in anti-corrosion organic films with a high resolution microbalance oscillator sensor, Sensors and Actuators B, 144(2010) 443.

18. L. V. S. Philippe, S. B. Lyon, C. Sammon, J. Yarwood, Validation of electrochemical impedance measurements for water sorption into epoxy coatings using gravimetry and infra-red spectroscopy, Corrosion Science, 50(2008)887.

19. T. Nguyen, E. Byrd, D. Bentz and C. Lin, In situ measurement of water at the organic coating/ substrate interface, Progress in Organic Coatings, 27(1996)181.

20. S. Castela and A. M. Simões, Assessment of water uptake in coil coatings by capacitance measurements, Progress in Organic Coatings, 46(2003)55.

21. Z. Kolek, Characterization of water penetration inside organic coatings by capacitance measurements, Progress in Organic Coatings, 30(1997)287.

22. Mingcheng SUN, Fuchun LIU, Hongwei SHI and Enhou HAN, A study on water absorption in freestanding polyurethane films filled with nano-TiO2 pigments by capacitance measurements, Acta Metallurgica Sinica(English Letters), 22(2009) 27.

23. N. J. W. Reuvers, H. P. Huininka, O. C. G. Adana, S. J. Garciac and J. M. C. Mol, Water uptake in thin nylon 6 films as measured by electrochemical impedance spectroscopy and magnetic resonance imaging, Electrochimica Acta, 94(2013) 219.

24. S. R. Taylor, Assessing the moisture barrier properties of polymeric coatings using electrical and electrochemical methods, IEEE Transactions on Electrical Insulation, 24(1989)5.

25. L. Hartshorn, N. J. L. Megson and E. Rushton, The structure and electrical properties of protective films, Journal of the Society of Chemical Industry, 56 (1937)266.

26. C. V. Lacombre, G. Bouvet, D. Trinh, S. Mallarino and S. Touzain, Water uptake in free films and coatings using the Brasher and Kingsbury equation: a possible explanation of the different values obtained by electrochemical Impedance spectroscopy and gravimetry, Electrochimica Acta, 231(2017)162.

27. F. S. A. Lindqvist, Theory of dielectric properties of heterogeneous substances applied to water in a paint film, Corrosion, 41(1985)69.

28. A. S. Castela and A. M. Simoes, An impedance model for the estimation of water absorption in organic coatings.Part I: A linear dielectric mixture equation, Corrosion Science, 45(2003)1631.

29. A. S. Castela and A. M. Simoes, An impedance model for the estimation of water absorption in organic coatings. Part II: A complex equation of mixture, Corrosion Science, 45(2003)1647.

30. B. F. N. Leonardo, Water Transport in organic coatings, Corrosion, 49(1993)235.

31. J. M. Sykes, A variant of the Brasher–Kingsbury equation, Corrosion Science, 46 (2004)515.

32. G. W. Walter, The application of impedance methods to study the effects of water uptake and chloride ion concentration on the degradation of paint films—II. Free films and attached/free film comparisons, Corrosion Science, 32(1991)1085.

33. R. K. Hiremath, M. K. Rabinala and B. G. Mulimani, Simple setup to measure electrical properties of polymeric films, Review of scientific instruments, 77 (2006)126106.

34. S. S. Azim, S. Sathiyanarayanan and G. Venkatachari, Anticorrosive properties of PANI–ATMP polymer containing organic coating, Progress in Organic Coatings, 56 (2006)154.

35. R. Y. Wang, T. Zhang, Q. Bao and D. M. Rawson, Study on fish embryo responses to the treatment of cryoprotective chemicals using impedance spectroscopy, European Biophysics Journal, 35(2006)224.

36. T. E. Kerner, K. D. Paulsen, A. Hartov, S. K. Soho and S. P. Poplack, Electrical impedance spectroscopy of the breast: clinical imaging results in 26 subjects, IEEE Trans.Medical Imaging, 21(2002)638.

37. A. D. Bauchot, F. R. Harker and W. M. Arnold, The use of electrical impedance spectroscopy to assess the physiological condition of kiwifruit, Postharvest Biology and Technology, 18(2000)9.

38. R. L. Smith, A. V. Bray, and D. K. Coates, Impedance spectroscopy as a technique for monitoring aging effects in nickel hydrogen and nickel-metal hydride batteries, IEEE 35th International Power Sources Symposium, (1992).

39. C. A. Witt, Thermionic insulator testing (AC impedance spectroscopy), Proceedings of the 24th Intersociety Energy Conversion Engineering Conference, (1989).

40. G. González , E. S. Kolosovas-Machuca , E. López-Luna ,H. Hernández-Arriaga and F. J. González, Design and fabrication of interdigital nanocapacitors coated with HfO_2, Sensors, 15(2015)1998.

41. E. Barsoukov and J. R. Macdonald, Electrical impedance spectroscopy: Theory, experiment and application, John Wiley & Sons, (2005).

42. L. Calleogar, Electrical Impedance: Principles, measurement, and applications (Series in Sensors) CRC press, A Taylor & Francis publications, (2012) .

43. A. J. B. Larry and R. Faulkner, Electrochemical methods: Fundamentals and applications, John Wiley & Sons, (2001).

44. E. P. M. Van Westing, G. M. Ferrari and J. H. W. De Wit, The determination of coating performance with impedance measurements--II. Water uptake of coatings, Corrosion Science, 36(1994)957.

45. J. J. Santana, J. E. González, J. Morales, S. González and R. M. Souto, Evaluation of ecological organic paint coatings via electrochemical impedance spectroscopy, International journal of electrochemical science, 7(2012)6489 .

46. J. R. Scully and S. T. Hensley, Lifetime prediction for organic coatings on steel and a magnesium alloy using electrochemical impedance methods, Corrosion, 50 (1994)705.

47. E. P. M. van Westing, G. M. Ferrari, and J. H. W. de Wit, The determination of coating performance with impedance measurements-I. Coating polymer properties, Corrosion Science, 34(1993)1511.

48. M. C. S. S. Macedo, I. C. P. Margarit-Mattos, F. L. Fragata, J. B. Jorcin, N. P´eb`ere, and O. R. Mattos, Contribution to a better understanding of different behaviour patterns observed with organic coatings evaluated by electrochemical impedance spectroscopy, Corrosion Science, 51(2009)1322.

49. F. Geenen, Characterization of organic coatings with impedance measurements, Ph.D. Thesis, Technische Universiteit Delft, (1991).

50. P. Sanguino, T. Monteiro, F. Marques, C. J. Dias, R. Igreja, and R. Franco, Interdigitated capacitive immunosensors with PVDF immobilization layers, IEEE Sensors and Journal , 14(2014)1260.

51. Z. Zou, J. Kai, M. J. Rust, J. Han and C. H. Ahn, Functionalized nano interdigitated electrodes arrays on polymer with integrated microfluidics for direct bio-affinity sensing using impedimetric measurement, Sensors and Actuators A, 136(2007) 518.

52. F. Deflorian, L. Fedrizzi, S. Rossi and P. L. Bonora, Organic coating capacitance measurement by EIS: ideal and actual trends,Electrochimica Acta, 44 (1999) 4243.

53. Yinghua WEI, Lixin ZHANG and Wei KE, Determination of water sorption in freestanding epoxy film by capacitance method using EIS, Journal of Material science & technology, 22(2006)108.

54. A. S. Castela and A. M. Simões, Water sorption in freestanding PVC films by capacitance measurements, Progress in Organic Coatings, 46(2003)130.

55. A. S. Castela and A. M. Simões, Assessment of water uptake in coil coatings by capacitance measurements, Progress in Organic Coatings,46(2003)55.

56. Z. Kolek, Characterization of water penetration inside organic coatings by capacitance measurements, Progress in Organic Coatings, 30(1997)287.

57. C. P. Wong, Application of polymer in encapsulation of electronic parts, Advances in Polymer Science- Springer publications, 84(2005)63 .

58. G. D. Davis and C. Dacres, Portable, hand- held, in-situ electrochemical sensor for evaluating corrosion and adhesion on coated or uncoated metal structures, US patent 6054038(2000) .

59. B. Tom, buter Sibo, Electrochemical cell for EIS, Europian patent EP2068139A1 (2007).

60. J. G. Victoria, Electrochemical impedance spectroscopy and system, US patent 0027070(2009).

61. A. D. Zdunek, P. Vanecek, A. Eugene and Kernerman, Method of measuring coating quality, US patent 6106693(2000).

62. G. D. Davis, C. Dacres, In-situ electrochemical based moisture sensor in composite and bonded structures, US patent 6313646(2001).

63. J. N. Murray, Coating evaluation system, US patent 5746905(1998).

64. G. D. Davis, R. C. Dunn and R. A. Robert, Coating monitor for evaluating the effectiveness of protective coatings, US patent 0081136A1(2012).

65. K. S. Rajan, A. V. Mamishev and M. Zahn, Fringing electric and magnetic field sensors, Encyclopedia of Sensors, 10(2006)1.

66. M. F. Azman, A. Yahya and H. Purwanto, Effect of numbers of fringing electric field (FEF) fingers on the performance of sensor for water content in soil, International Journal of Materials, Mechanics and Manufacturing, 1(2013)46.

67. V. Markevicius, D. Navikas, A. Valinevicius, D. Andriukaitis and M. Cepenas, The soil moisture content determination using interdigital sensor, Elektronika IR Elektrotechnika, ISSN 1392-1215, 18(2012)25.

68. A. V. Mamishev, K. S. Rajan, F. Yang, Yanqing Du and M. Zahn, Interdigital sensors and transducers, Proceedings of the IEEE ,92(2004)808.

69. A. S. Abu-Abed and R. G. Lindquist, Capacitive interdigital sensor with homogeneous nematic liquid crystal film, Progress In Electromagnetics Research B, 7(2008)75.

70. W. Olthuis, W. Streekstra, P. Bergveld, Theoretical and experimental determination of cell constants of planar-interdigitated electrolyte conductivity sensors, Sensors and Actuators B, 24(1995)252.

71. W. Laureyna,D. Nelisa, P. V. Gerwena,K. Baerta, L. Hermansa, R. Magnéeb, J. J. Pireauxb and G. Maesc, Nanoscaled interdigitated titanium electrodes for impedimetric biosensing, Sensors and Actuators B: Chemical, 68(2000)360.

72. R. N. Dean, A. Rane, M. Baginski, Z. Hartzog and D. J. Elton, Capacitive fringing field sensors in printed circuit board technology, IEEE transactions on instrumentation and measurement, 61(2012)1105.

73. A. V. Mamishev, B. C. Lesieutre, and M. Zahn, Optimization of multi-wavelength interdigital dielectrometry instrumentation and algorithms, IEEE Transactions on Dielectrics and Electrical Insulation, 5(1998)408.

74. A. Fuchs, M. J. Moser, H. Zangl and T. Bretterklieber, Using capacitive sensing to determine the moisture content of wood pellets – investigations and application , International Journal on Smart Sensing and Intelligent Systems, 2(2009)293.

75. N. Angkawisittpan and T. Manasri, Determination of sugar content in sugar solutions using interdigital capacitor sensor, Measurment Science Review, 12 (2012)8.

76. A. K. Sen and J. Darabi, Modeling and optimization of a microscale capacitive humidity sensor for HVAC applications, IEEE Sensors Journal, 8(2008)333.

77. C. M. Thompson and W. L. Heimer II, Relationship between acoustic properties and structure of polyurethanes, Journal of the Acoustical Society of America, 77 (1985)1229.

78. G. M. Stack, J. M. Miller, E. Y. Chang, Development of seawater-resistant polyurethane elastomers for use as sonar encapsulants, Journal of Applied Polymer Science, 42(1991)911.

79. C. Hapburn, Polyurethane elastomers' Second Edition, Elsevier and applied science (1992) London.

80. V. B. Pillai, Studies on rubber compositions as passive acoustic materials in underwater electroacoustic transducer technology and their ageing characteristics, Thesis, Cochin University of Science and Technology (2003).

81. R. N. Capps, Influence of carbon black fillers on acoustic properties of polychloroprene (neoprene) elastomers, Journal of the Acoustical Society of America, 78(1985)406.

82. Shuangkou Chen, Jianfang Zhu,Taigang Zhou, Bai He, Wenzhang Huang , Bochu Wang, Preparation and properties study of polyaniline conductive anti-fouling coating , International Journal of Electrochemical Science, 7(2012)8170 .

83. V. Rajasekharan, T. Stalin, S. Viswanathan and P. Manisankar, Electrochemical evaluation of anticorrosive performance of organic acid doped polyaniline based coatings, International Journal of Electrochemical Sciencent, 8(2013)11327 .

84. D. G. Aggelis and A. S. Paipetis, Monitoring of resin curing and hardening by ultrasound, Construction and Building Materials, 26(2012)755.

85. J. Simitzis, D. Triantou, S. Soulis, G. Tsangaris, L. Zoumpoulakis and E. Manolopoulos, Influence of backbone rigidity on the curing and the dielectric relaxations of unsaturated polyesters, Journal of Applied Polymer Science, 120 (2011)1984.

86. C. E. Corcione and M. Frigione, Characterization of nanocomposites by thermal analysis, Materials, 5(2012)2960.

87. W. Stark, H. Goering, U. Michel and H. Bayerl, Online monitoring of thermoset postcuring by dynamic mechanical thermal analysis DMTA, Polymer Testing, 28 (2009)561.

88. F. Lionetto and A. Maffezzoli, Relaxations during the postcure of unsaturated polyester networks by ultrasonic wave propagation, dynamic mechanical analysis and dielectric analysis, Journal of Polymer Science /part B-Polymer Physics, 43 (2005)596.

89. G. M. Maistros and I. K. Partridge, Monitoring autoclave cure in commercial carbon fibre/epoxy composites , Composites Part B: Engineering, 29(1998)245.

90. C. E. Corcione and A. Maffezzoli, Transport properties of graphite/epoxy composites: Thermal, permeability and dielectric characterization, Polymer Testing, 32(2013)880.

91. G. Nikolic,S. Zlatkovic, M. Cakic, S. Cakic, C. Lacnjevac and Z. Rajic, Fast fourier transform IR characterization of epoxy GY systems crosslinked with aliphatic and cycloaliphatic EH polyamine adducts, Sensors, 10(2010)684.

92. E. Dessipri, E. Minopoulou, G. D. Chryssikos, V. Gionis, A. Paipetis and C. Panayiotou, Use of FT-NIR spectroscopy for on-line monitoring of formal dehyde-based resin synthesis, European Polymer Journal , 29(2003)1533.

93. I. Alig, D. Lellinger, S. Agarwal and H. Oehler, Monitoring of photopolymerization kinetics and network formation by combined real-time near-infrared spectroscopy and ultrasonic reflectometry, Reactive and Functional Polymers, 73 (2013)316.

94. L. Merad, M. Cochez, S. Margueron, F. Jauchem, M. Ferriol, B. Benyoucef and P. Bourson, In situ monitoring of the curing of epoxy resins by Raman spectroscopy, Polymer Testing,28(2009)42.

95. P. J. Schubel, R. J. Crossley, E. K. G. Boateng and J. R. Hutchinson, Review of structural health and cure monitoring techniques for large wind turbine blades, Renewable Energy, 51(2013)113.

96. C. K. Alexander and M. N. O. Sadiku, Fundamentals of Electric Circuits, McGraw Hill, (1999)608.

97. A. Guadarrama-Santanaa, A. Garcıa-Valenzuelaa, F. Perez-Jimeneza and L. Polo-Paradab, Interdigitated capacitance sensors in the mm scale with sub-femtoFarad resolution suitable for monitoring processes in liquid films, Revista Mexicana de Fısica, 60(2014)451.

98. Y. Wei, L. Zhang and W. Ke, Determination of water absorption in freestanding epoxy film by capacitance method using EIS, Journal of Material Science and Technology, 22(2006)108.

99. M. C. S. S. Macedo, I. C. P. Margarit-Mattos, F. L. Fragata, J. B. Jorcin, N. Pébère and O. R. Mattos, Contribution to a better understanding of different behaviour patterns observed with organic coatings evaluated by electrochemical impedance spectroscopy, Corrosion Science, 51(2009)1322.

100. A. Alabbasi, S. Liyanaarachchi, M. B. Kannan, Polylactic acid coating on a biodegradable magnesium alloy: An in vitro degradation study by electrochemical impedance spectroscopy,Thin Solid Films, 520(2012)6841.

101. M. Hattori, A. Nishikata and T. Tsuru, EIS study on degradation of polymer coated steel under ultraviolet radiation, Corrosion Science, 52 (2010)2080.

102. B. P. Sahoo, K. Naskar and D. K. Tripathy, Conductive carbon black-filled ethylene acrylic elastomer vulcanizates:physico-mechanical, thermal, and electrical properties, Journal of Material Science, 47(2012)2421

103. M. A. Deyaba, G. Meleb, A. M. Al-Sabagha, E. Bloiseb, D. Lomonacoc, S. E. Mazzettoc and C. D. S. Clementec, Synthesis and characteristics of alkyd resin/M-Porphyrins nanocomposite for corrosion protection application, Progress in Organic Coatings, 105(2017)286.

104. J. Laconte, V. Wilmart, J. P. Raskin and D. Flandre, Capacitive humidity sensor using a polyimide sensing film, symposium on design, test, integration and packaging of MEMS/MOEMS, (2003)223.

105. A. V. Mamishev, K. S. Rajan, F. Yang, Yanqing Du and M. Zahn, Interdigital sensors and transducers, Proceedings of the IEEE, 92(2004)808.

106. T. T. Ngo, H. Shirzadfar, D. Kourtiche and M. Nadi, A planar interdigital sensor for bio-impedance measurement: Theoretical analysis, optimization and simulation, Journal of Nano and Electronic Physics, 6(2014)01011.

107. H. Wang and A. V. Mamishev, Measurement of coating thickness and loading using concentric fringing electric field sensors, IEEE Sensors Journal, 14(2014) 68.

108. X. Li, G. Rower, V. Inclan and A. V. Mamishev, Nondimensiolaized parametric modeling of fringing electric field sensors, IEEE Sensors Journal, 6(2006)1602.

109. G. Grundmeier, W. Schmidt and M. Stratmann, Corrosion protection by organic coatings: electrochemical mechanism and novel methods of investigation, Electrochimica Acta, 45(2000)2515.

110. F. Dolatzadeh, S. Moradian, M. M. Jalili, Effect of nano silica on moisture absorption of polyurethane clear Coats as studied by EIS and Gravimetric methods, Progress in color Colorants and coatings, 3(2010)92.

111. C. L. Pen, C. Lacabanne and N. Pébère, Characterisation of water-based coatings by electrochemical impedance spectroscopy, Progress in Organic Coatings,46 (2003)77.

112. X. Zhang, F. Wang and Y. Du, Protective performance of epoxy resin modified with coal tar coating studied by electrochemical impedance spectroscopy,Progress in Organic Coatings, 53(2005)302.

113. X. Yuan, Z. F. Yue, X. Chen, S. F. Wen, L. Li and T. Feng, EIS study of effective capacitance and water uptake behaviors of silicone-epoxy hybrid coatings on mild steel, Progress in Organic Coatings, 86(2015)41.

114. X. B. Li, S. D. Larson, A. S. Zyuzin, and A. V. Mamishev, Design principles for multicuhannel fringing flectric field Sensors, IEEE Sensors Journal,6(2006) 406 .

115. P. V. Gerwen, W. Laureyn, G. Huyberechts, M. O. D. Beeck, K. Baert, J. Suls, W. Sansen, P. Jacobs, L. Hermans and R. Mertens, Nanoscaled interdigitated electrode arrays for biochemical sensors, Sensors and Actuators B, 49(1998)73.

116. D. Loveday, P. Peterson and B. Rodgers, Evaluation of organic coating with electrochemical impedance spectroscopy,Part 1: Fundamental of electrochemical impedance spectroscopy, Journal of Coating Technology, 1(2004)48.

117. D. Loveday, P. Peterson, B. Rodgers, Evaluation of organic coating with electrochemical impedance spectroscopy, Part 2: Application of EIS to coating, Journal of Coating Technology, 1(2004)88.

118. D. Loveday, P. Peterson, B. Rodgers, Evaluation of organic coating with electrochemical impedance spectroscopy Part 3: Protocols for testing Coating with EIS, Journal of Coating Technology, 2(2005)22.

119. F. Rezaei, F. Sharif, A. A. Sarabi, S. M. Kasiriha, M. Rahmanian, E. Akbarinezhad, Evaluating water transport through high solid polyurethane coating using the EIS method, Journal of Coating Technology and Research, 7(2010)209.

120. J.E.O. Mayne, The mechanism of protective action of paints, Corrosion vol. 2, Corrosion Control: L.L. Shreir et al. (Ed.), Butterworth, London, (1976).

121. F. Delor-Jestin, D. Drouin, P.-Y. Cheval and J. Lacoste, Thermal and photochemical ageing of epoxy resin; Influence of curing agents,Polymer Degradation and Stability,91(2006)1247

122. G.W. Walter,The application of impedance spectroscopy to study the uptake of sodium chloride solution in painted metals, Corrosion Science, 32(1991)1041.

123. T.Nguyen, J.B.Hubbard and J.M. Pommersheim, Unified model for the degradation of organic coating on steel in a neutral electrolyte, Journal of Coatings Technology, 68(1996)45

124. H.Kim and K. Char, Dielectric changes during the curing of epoxy resin based on the diglycidyl ether of bisphenol A (DGEBA) with diamine, Bullettin of Korean Chemical Society, 20(1999)1329.

125. S. Zhou,L.Wu, J. Sun, W. Shen, The Change of the Properties of Acrylic-Based Polyurethane Via Addition of Nano-Silica, Progress in Organic coatings, 45(2002)33.

126. M. Sangermano, G. Malucelli, E. Amerio, A. Priola, E. Billi, G. Rizza, Photopolymerization of Epoxy Coatings Containing Silica Nanoparticles, Progress in Organic coatings, 54(2005)134

127. H. Shi, F. Liu, L. Yang, E. Han, Characterization of Protective Performance of Epoxy Reinforced with Nanometer-Sized TiO2 and SiO2, Progress in Organic coatings, 62(2008)359.

128. S. González, F. Cáceres, V. Fox, R.M. Souto, Resistance of metallic substrates protected by an organic coating containing aluminum powder,Progress in Organic Coatings, 46(2003)317.

129. A.Ghasemi-Kahrizsangi, H. Shariatpanahi, J.Neshati, E.Akbarinezhad, Corrosion behavior of modified nano carbon black/epoxy coatingin accelerated conditions, Applied Surface Science,331(2015)115.

130. http://www.princetonappliedresearch.com/ZSimpWin

131. C.H. Hare, Water permeability in pigmented films, Journal of Protective Coatings and linings, 1410(1997)77.

132. H. Xiao and F. Mansfeld, Evaluation of coating degradation with electrochemical impedance spectroscopy and electrochemical noise analysis, Journal of Electrochemical Society, 141(1994)2332.

133. Y. Zahraa,F. Djouani, B. Fayollea, M. Kuntz and J. Verdua, Thermo-oxidative aging of epoxy coating systems, Progress in Organic Coatings, 77(2014)380.

134. E. Ernault, E.Richaud, B.Fayolle, Thermal oxidation of epoxies: Influence of diamine hardener, Polymer Degradation and Stability, 134(2016)76.

135. Q.Zhou, Y. Wang, Comparisons of clear coating degradation in NaCl solution and pure water, Progress in Organic Coatings, 76(2013)1674.

136. D. E. Khaled, N.N. Castellano, J.A. Gázquez, A. J. Perea-Moreno,F.Manzano-Agugliaro, Dielectric spectroscopy in biomaterials: Agrophysics, Materials 9(2016)310.

137. J.Yu, C.Liu, Microfabricated thin film impedance sensor & ac impedance measurements, Sensors, 10(2010)5845.

138. http://www.huntsman.com/advance_materials/Media%20Library/global/files /APAC_Literature_coating_Epoxy

139. F.Li, L. Qi,J. Yang, M. Xu, X. Luo, D. Ma,Polyurethane/Conducting Carbon Black Composites: Structure, Electric Conductivity, Strain Recovery Behavior, and Their Relationships, Journal of Applied Polymer Science, 75(2000)68.

PUBLICATIONS & PATENT

1. K. A. Thomas, Shiny Nair, A. V. Ramesh Kumar,V. Natarajan, Reji John, 'Application of fringe field capacitance sensor for the study of water permeation in organic coatings' *Journal of coating technology and research*, *13 (5) 829–835, 2016* .

2. K. A. Thomas, Shiny Nair, R. Rajeswari, A.V. Ramesh kumar, V. Natarajan, T. Mukundan, Reji John, 'Electrochemical behaviour of PANI/Polyurethane antifouling coating in salt water studied by electrochemical impedance spectroscopy' *Progress in Organic Coatings, 89 267–270,2015*

3. K. A. Thomas, V. Natarajan, Method and device for determining degradation of coating of a substrate, *Indian patent (Application No.201711004301 dated 30 March 2017)*

4. K A Thomas, Shiny Nair, V.Natarajan, Reji John, ' A novel method for the detection of degradation in polyurethane coating in wet environment' *Proceedings of International conference on Advances in Polymer Technology, APT -16, February 25-26, 2016, Kochi, India*

5. K.A.Thomas, Shiny Nair, Shanavas. A , Reji John, V.Natarajan, 'Determination of curing profile of polymer resins by miniature interdigital capacitor sensor', *Proceedings of ISSS National Conference on MEMS Smart Materials, Structures and Systems, September 23-25, 2015, Kochi, India.*

6. Akhil Nath, K.A.Thomas, A. V. Ramesh Kumar and Reji John, 'Electrochemical studies on PU Nanocomposite underwater sensor encapsulate' *Nanotech Insights Vol.5 Issue 3&4, 42-45, 2014*